Evidence for a Reversible, Redox-Mediated Component to Eccentric Contraction-Induced Force Loss in Dystrophin-Deficient Skeletal Muscle

A DISSERTATION
SUBMITTED TO THE FACULTY OF
UNIVERSITY OF MINNESOTA
BY

John Theodore Olthoff

IN PARTIAL FULFILLMENT OF THE REQUIREMENTS
FOR THE DEGREE OF
DOCTOR OF PHILOSOPHY

Advisor: James M. Ervasti, Ph.D.

April, 2018

Acknowledgements

I would like to thank my thesis advisor Jim Ervasti for being a magnificent mentor. He has helped me progress as a scientist towards my career goals through his expertise, guidance, and patience.

I would like to thank the members of the Ervasti Lab, both past and present. The collaboration, discussions of science, and goofing off that takes place in lab has made it such a wonderful place to work. Thank you Ben Perrin, Joe Belanto, Dana Talsness, Jackie McCourt, Alli O'Rourke, Chris Chamberlain, Xiaobai Patrinostro, D'anna Nelson, Tung Nguyen, and Preston McCourt.

I would like to thank our long-time collaborator Dawn Lowe and the rest of her research lab, especially Angus Lindsay. The muscle physiology presented in my dissertation would not have been possible without their unique expertise and hard work.

I would like to thank my committee members, Laure Gammill, Meg Titus, Michael Kyba, Dawn Lowe, and Gant Luxton. They have provided much appreciated advice, criticism, and mentorship over my graduate school years.

I would like to thank George Rodney, Kristen Nowak, Nigel Laing, and Daniel Garry for providing transgenic and knockout mice for these studies. I am also grateful of George's lab for performing myofiber stretch-induced ROS measurements.

I would like to recognize the Murine Genetics Core at The Scripps Research Institute for generation of transgenic mice.

I would like to thank the University of Minnesota Center for Mass Spectrometry and Proteomics for performing the iTRAQ screen and helping with analysis.

I would like to thank Dave Thomas, director of the NIH Minnesota Muscle training grant (AR007612) along with Deborah Ferrington and LaDora Thompson, co-directors of the NIA Functional Proteomics of Aging training grant (AG029796) for supporting my graduate career.

I thank Rolf Turk for introducing me to science with his captivating mentorship.

I would like to thank my friends from Iowa, Minnesota, the MCSB Program, and elsewhere for all the good times over the years. I also thank my family, Craig, Nancy, Jeff, and Jamie for their unrelenting support to follow my dream of being a scientist. Lastly, I could not have gotten this far without the support from the love of my life, Stephanie Kendall.

Dedication

This dissertation is dedicated to John Irvin Olthoff (Pa).

Abstract

Duchenne muscular dystrophy (DMD) is one of the most common and severe forms of muscular dystrophy. To better understand eccentric contraction-induced force loss in dystrophic muscle, we used iTRAQ proteomics to identify proteins that were differentially expressed in *mdx* mice overexpressing nonmuscle γ_{cyto}-actin (*mdx*/Actg1-TG), which we have previously shown to significantly protect *mdx* muscle against force loss. We identified peroxiredoxin-2 (PrxII) as significantly decreased in *mdx* muscle compared to WT but restored to WT levels in *mdx*/Actg1-TG muscle. We show that increased sarcolemmal NADPH Oxidase 2 (NOX2)-dependent ROS production contributes to eccentric contraction-induced force loss while causing hyperoxidation and subsequent proteasomal degradation of PrxII in *mdx* muscle. Interestingly, ablation of PrxII exacerbated force loss in *mdx* muscle, while overexpression of PrxII led to a dose-dependent protection of force loss. We also establish the contribution of myoglobin to force loss in *mdx* muscle through the production of hydroxyl radicals. Finally, we demonstrate that oxidation-sensitive cysteine 272 unique to γ_{cyto}- and β_{cyto}-actins is required to protect *mdx* muscle from force loss through inhibition of NOX2-dependent ROS production. Together, the data presented in this dissertation suggest that eccentric contractions may induce a rapidly reversible, redox-mediated inhibition of contractility, thus acting as a "circuit breaker" to protect *mdx* muscle from more disastrous structural damage during subsequent high force contractions.

Table of Contents

List of Tables

List of Figures

Chapter 1: Introduction

Skeletal Muscle

Muscles are the cellular machines that drive every movement within our bodies, from allowing us to blink to powering our legs while walking. The three types of muscle – cardiac, smooth, and skeletal – have each evolved to play specific roles within the body. Cardiac muscle allows the heart to continuously pump blood that carries oxygen to all tissues throughout the lifetime of an organism. Smooth muscles involuntarily contract in a rhythmic manner called peristalsis to move food through the digestive tract and blood through capillaries (Huizinga, 1999). Skeletal muscles may power movements involuntarily, such as breathing via contraction of the diaphragm, and voluntarily, such as curling a dumbbell with your biceps. Though their cellular functions vary considerably, all three types of muscles produce force using the same mechanism, utilizing chemical energy in the form of ATP to generate mechanical energy in the form of contractile force (Rayment et al., 1993).

Of the three types of muscles, skeletal muscle is by far the most abundant in humans, accounting for 32-40% of our average body mass (Janssen et al., 2000). The structure of skeletal muscle is best described as a series of hierarchical bundling (Figure 1-1). The muscle tissue itself is comprised of bundles of fascicles which are surrounded by connective tissue called the perimysium. Each fascicle is composed of a bundle of myofibers, the cellular units of the skeletal muscle, each surrounded by a plasma membrane called the

sarcolemma (Figure 1-1A). The myofiber is an extremely unique cell type, being excitable, highly elongated, and containing hundreds to thousands of peripheral nuclei due to the fusion of many myoblasts during embryonic development (Bentzinger et al., 2012). Each myofiber contains bundles of myofibrils, the contractile unit of skeletal muscle (Figure 1-1B). Each myofibril consists of a series of sarcomeres, which are the functional units of contraction composed mainly of actin thin filaments and myosin thick filaments. Depending on intracellular calcium concentration and ATP hydrolysis, the thick and thin filaments of many sarcomeres will slide past each other, resulting in sarcomere shortening and contractile force production (Ebashi and Endo, 1968).

Duchenne Muscular Dystrophy

There are more than 30 forms of muscular dystrophy resulting from mutations in various genes encoding proteins critical for muscle cell integrity and function (Cohn and Campbell, 2000). Of these disorders, Duchenne muscular dystrophy (DMD) is the most prevalent, affecting approximately 1 of every 4,000 live male births (Mendell et al., 2012). Unfortunately for these patients, DMD is also one of the most severe forms of muscular dystrophy (Emery, 2002).

The French neurologist Duchenne de Boulogne, from whom the disease was named, was one of the first to describe the clinical symptoms of DMD in the mid 1800's (Duchenne, 1855). Early symptoms of DMD may appear as early as 3 to 5 years of age and include skeletal muscle hypertrophy (especially seen in calf muscles), decreased ability to perform otherwise normal activities, weakness of the proximal muscle groups, and elevated serum creatine kinase levels (Cros et al., 1989; Percy et al., 1979). Another early manifestation of DMD has been described as the Gower's maneuver (Figure 1-2), in which young patients rely heavily on their upper body to raise themselves up from a sitting to a standing position due to weakened leg muscles (Gowers, 1886). Because of the progressive nature of muscle weakness and deterioration, patients typically become non-ambulatory in their early teens, thus confined to a wheel chair. In their late twenties to early thirties, patients succumb to fatal cardiac arrest or respiratory failure (Rall and Grimm, 2012). Although ventilatory support and the

use of corticosteroids help to manage symptoms and improve quality of life (Angelini, 2007; Ricotti et al., 2013), there remains to be a cure for DMD.

In 1987, Kunkel, Worton, and colleagues discovered the gene mutated in DMD (Burghes et al., 1987; Koenig et al., 1987). The aptly named *DMD* gene was found to be positioned on the X chromosome, explaining the X-linked recessive genetics of the disorder. The *DMD* gene is the largest known gene found in nature, spanning over 2.4 megabases of DNA. Due to the vast size of the *DMD* gene, it is statistically more prone to *de novo* mutation, which accounts for nearly a third of all DMD cases (Chamberlain, 1992; Flanigan, 2014; Verma et al., 2010). The remaining two thirds of DMD cases result from heritable mutations from female carriers who are usually asymptomatic (Flanigan, 2014).

The *DMD* gene contains multiple promoters in which several tissue-specific transcripts can be produced (Byers et al., 1993; Górecki et al., 1992; Nudel et al., 1989; Pillers et al., 1993), but its full-length transcript is comprised of 79 exons (Muntoni et al., 2003). The full length transcript encodes the protein dystrophin, which is predominately expressed in skeletal muscle (Hoffman et al., 1987). Deleterious mutations in the *DMD* gene that render either non-functional forms or complete absence of dystrophin protein cause DMD. Lack of dystrophin is characteristically caused by chromosomal rearrangement, large deletions/insertions, or nonsense mutations. Some mutations in the *DMD* gene lead to a milder form of the disease called Becker muscular dystrophy (BMD). The mutations found in BMD patients typically produce in-frame deletions,

resulting in an internally truncated, partially functional dystrophin protein (Koenig et al., 1989; Monaco et al., 1988).

Dystrophin and the Dystrophin-Glycoprotein Complex

Dystrophin is a large, 427 kDa cytoplasmic protein expressed predominately in striated muscle. It has an overall rod-like structure, consisting of an N-terminal globular domain, a central rod domain, a cysteine-rich globular domain, and a C-terminal domain (Koenig et al., 1988). The N-terminus contains tandem calponin homology (CH) domains which cooperatively bind filamentous actin and thus are named actin binding domain 1 (ABD1) of dystrophin (Norwood et al., 2000). The central rod region is the largest domain in dystrophin and is comprised of 24 spectrin-like repeats, each with a triple helical structure (Muthu et al., 2012; Pascual et al., 1997). Also present in the central rod region are four interspersed, proline-rich “hinge” domains, which are thought to allow flexibility to the rod-like protein (Koenig and Kunkel, 1990). A second actin binding domain (ABD2) was found in the central rod region at spectrin repeats 11-17, suggesting that dystrophin may bind laterally along actin filaments (Amann et al., 1998; Rybakova et al., 1996). The cysteine-rich domain of dystrophin contains WW, EF-hand, and ZZ domains, all of which are required for interaction with β-dystroglycan at the sarcolemma (Bork and Sudol, 1994; Hnia et al., 2007; Ponting et al., 1996). Finally, the C-terminal domain of dystrophin displays known interactions with α-dystrobrevin and α-syntrophin.

In striated muscle, dystrophin is localized to the sarcolemma and enriched at lattice-like structures called costameres (Porter et al., 1992; Straub et al.,

1992; Zubrzycka-Gaarn et al., 1988). The costamere consists of a cluster of proteins located at the Z-disk of peripheral myofibrils extending out to the sarcolemma (Figure 1-3), thereby coupling the forces produced by the sarcomere to the plasma membrane of the myofiber (Ervasti, 2003). At the costamere, dystrophin forms two important interactions, one with the cortical actin cytoskeleton and the other with a membrane-bound glycoprotein complex, each necessary for membrane stability (Ervasti, 2007; Ervasti and Campbell, 1993; Levine et al., 1990). At its N-terminus, dystrophin utilizes its two actin binding domains to form a mechanically strong connection to filamentous γ_{cyto}-actin, linking dystrophin to peripheral myofibers (Rybakova et al., 2000). At its C-terminus, dystrophin binds directly to the integral membrane protein β-dystroglycan (Suzuki et al., 1992), which links dystrophin to several membrane-bound glycoproteins, forming what is called the dystrophin-glycoprotein complex (DGC).

The DGC was first discovered by Campbell and colleagues when dystrophin was seen to be enriched from the sarcolemma via wheat germ agglutinin chromatrography, which binds strongly to glycosylated proteins (Campbell and Kahl, 1989; Ervasti et al., 1990). The complex was discovered to contain 10 major constituents: dystrophin, α- and β-dystroglycan, sarcospan, the sarcoglycans (α-, β-, γ-, and δ-isoforms), dystrobrevin, and syntrophin (Figure 1-4) (Ervasti and Campbell, 1991). α- and β-dystroglycan are transcribed from a single mRNA but are post-transcriptionally cleaved to form two separate

polypeptide chains (Ibraghimov-Beskrovnaya et al., 1992). β-dystroglycan is a transmembrane protein with both an extracellular interaction with α-dystroglycan and an intracellular interaction with dystrophin. Extracellular α-dystroglycan is heavily glycosylated, which is required for its interactions with extracellular matrix proteins, notably laminin (Ervasti and Campbell, 1993).

The DGC is necessary for muscle cell stability during contraction, and this is most evident from the fact that mutations in many of the proteins making up the DGC cause various forms of muscular dystrophy (Cohn and Campbell, 2000; Rahimov and Kunkel, 2013). Mutations in the dystroglycan gene lead to limb girdle muscular dystrophy, while mutations in genes required for proper α-dystroglycan glycosylation cause several types of congenital muscular dystrophies (Godfrey et al., 2011; Hara et al., 2011; Michele et al., 2002). Mutations in the sarcoglycan isoforms lead to limb girdle muscular dystrophies 2C-F (Laval and Bushby, 2004; Ozawa et al., 2005). Furthermore, genetic knock-out of α-dystrobrevin, α1-syntrophin, and sarcospan all present a unique muscular dystrophy in mice (Bunnell et al., 2008; Grady et al., 1999; Kameya et al., 1999; Lebakken et al., 2000). Although mutations in several genes that constitute the DGC produce variable muscle phenotypes, the loss of dystrophin alone leads to a destabilization of the entire DGC, suggesting it is an essential component to the complex.

The *mdx* Mouse Model of DMD

The use of animal models of DMD has greatly increased our mechanistic understanding of this disease and has led to the development of therapeutic strategies. There are numerous models of DMD, from small invertebrates to larger mammals. Non-mammalian dystrophin-deficient animal models include *Caenorhabditis elegans*, *Drosophila melanogaster*, and zebrafish (Chamberlain and Benian, 2000; Kunkel et al., 2006; Lloyd and Taylor, 2010). Larger mammalian models include the newly developed rat and pig DMD models (Hollinger et al., 2014; Klymiuk et al., 2013; Nakamura et al., 2015), along with the well-characterized golden retriever muscular dystrophy (GRMD) model which has been used in pre-clinical testing of DMD therapies (Cooper et al., 1988; Kornegay et al., 1988; Valentine et al., 1986). However, the most widely used animal model of DMD to date is the naturally-occurring *mdx* mouse model (Bulfield et al., 1984).

The *mdx* mouse contains a nonsense mutation in exon 23 of the *DMD* gene, rendering the mouse dystrophin-deficient (Sicinski et al., 1989). Although the *mdx* mouse has been a critical resource in elucidating mechanisms of DMD, the dystrophic phenotype is relatively mild compared to DMD patients (Partridge, 2013; Tanabe et al., 1986). The milder phenotype of *mdx* mice has, in part, been credited to the compensatory upregulation of utrophin, the fetal homologue of dystrophin (Blake et al., 2002; Dowling et al., 2002; Matsumura et al., 1992).

Evidence for this compensatory protection include a more severe phenotype seen in the dystrophin/utrophin double knockout mouse model (Deconinck et al., 1997; Grady et al., 1997) and nearly-full rescue of the dystrophic phenotype upon utrophin overexpression (Tinsley et al., 1998). An enhanced myofiber regenerative capacity compared to humans may also explain the milder phenotype in *mdx* mice. When *mdx* mice are bred onto the DBA/2J genetic background, which is known to have decreased regenerative capacity, the dystrophic phenotype is more severe (Fukada et al., 2010; Rodrigues et al., 2016).

While the *mdx* mouse displays an overall mild phenotype compared DMD patients, several aspects of the disease are recapitulated in the model. In the absence of dystrophin, *mdx* mice exhibit significant reduction of other DGC components at the sarcolemma (Ervasti et al., 1990; Ohlendieck and Campbell, 1991). The disruption of the DGC likely causes the sarcolemmal instability seen in *mdx* mice, evident through increased uptake of membrane-impermeable dyes within the myofibers (Matsuda et al., 1995) and elevated levels of serum creatine kinase which is normally sequestered in the cytoplasm (Glesby et al., 1988). Furthermore, the histopathology seen in *mdx* skeletal muscle is commensurate with that seen in DMD patients, displaying central nucleation of myofibers (indicating degeneration and subsequent regeneration), decreased and variable myofiber size, and increases in fibrosis, fatty deposition, and inflammation (Briguet et al., 2004). Physiological parameters measured in *mdx* mice indicate

an increased muscle weakness, with reductions in grip strength and whole-body tension (Connolly et al., 2001), along with substantial inactivity following mild exercise (Kobayashi et al., 2008). Lastly, *mdx* mice display remarkable sensitivity to eccentric contraction-induced force loss (discussed in detail later).

Actin Isoforms in Skeletal Muscle

Actin is the most abundant protein in the majority of eukaryotic cells, serving as a fundamental component in a wide variety of cellular processes. Important roles for actin include cell shape maintenance, cell division, maintaining membrane integrity, vesicular trafficking, transcriptional regulation, cell migration, and force production in muscle cells (Bunnell et al., 2011; Dominguez and Holmes, 2011; Pollard and Cooper, 2009; Tondeleir et al., 2012). Many of these processes attributed to actin are made possible by actin's unique ability to transition from monomeric (G-actin) to filamentous (F-actin) states. Reversible polymerization of 42 kDa G-actin to F-actin occurs under ionic conditions and in the presence of monovalent or divalent ions found within the cell (Selden et al., 1983). Polymerization of actin occurs at different rates at each end of the filament due to the innate polarity of actin filaments (Pollard and Borisy, 2003). The rate of actin polymerization and depolymerization also varies depending on the concentration of ions, the availability of ATP/ADP, and the presence of actin binding proteins (Carlier and Pantaloni, 1997; Pollard et al., 2000). One of the most notable acting binding protein is the molecular motor protein myosin, whose interaction with actin filaments is required for vesicular trafficking, cell shape and mobility, and production of force within the sarcomere of muscle cells (Clarke and Spudich, 1977).

Although widely referred to as a single entity, actin exists as six different isoforms encoded by six separate genes. The actin isoform gene family consists of two main groups: the cytoplasmic actins and the muscle actins (Figure 1-5). The two cytoplasmic actins, β_{cyto}- and γ_{cyto}-actin, are expressed in all cell types. The four muscle actins, $\alpha_{skeletal}$-, $\alpha_{cardiac}$-, α_{smooth}-, and γ_{smooth}-actin, are expressed in skeletal, cardiac, and smooth muscle cells, respectively. All six actin isoforms share a high degree of sequence homology, and the modest sequence changes that do exist are remarkably conserved form birds to mammals (Rubenstein, 1990). In particular, the cytoplasmic actins differ only by 4 biochemically similar amino acids at the N-terminus (Figure 1-5), while all six actin isoforms share no less than 93% identity (Perrin and Ervasti, 2010). However, the functional significance of maintaining six highly-conserved actin isoforms is not fully understood.

Both cytoplasmic actins are the predominate actin species during myogenesis, when muscle cell precursors called myoblasts migrate to future sites of skeletal muscle and fuse with other myoblasts to form nascent myofibers called myotubes (Duan and Gallagher, 2009; Lloyd et al., 1992; Nowak et al., 2009b; Peckham, 2008). When myotubes are formed, the cell undergoes an actin “isoform switch”, where β_{cyto}- and γ_{cyto}-actin become downregulated while $\alpha_{skeletal}$-actin becomes upregulated (Schwartz and Rothblum, 1981). In mature skeletal muscle, $\alpha_{skeletal}$-actin is the predominate isoform and it comprises the thin filaments of the myofibril. β_{cyto}- and γ_{cyto}-actin levels remain low in adult muscle,

accounting for only 1/4,000 of the total actin pool (Hanft et al., 2006). Both cytoplasmic actins are localized to the costamere, where it constitutes the cortical actin cytoskeleton that interacts with dystrophin at the DGC (Craig and Pardo, 1983; Otey et al., 1988; Rybakova et al., 2000). β_{cyto}- and γ_{cyto}-actin also localize to the neuromuscular junction, the myotendinous junction, and the peri-Z-disk region (Gokhin et al., 2010; Hall et al., 1981; Kee et al., 2004; Papponen et al., 2009). Muscle-specific genetic ablation of both β_{cyto}- and γ_{cyto}-actin results in a mild but progressive myopathy, demonstrating that cytoplasmic actins play an important role in muscle cell maintenance (Prins et al., 2011; Sonnemann et al., 2006). Interestingly, γ_{cyto}-actin is upregulated nearly 10-fold in *mdx* skeletal muscle compared to WT (Hanft et al., 2006). To understand whether this upregulation was compensatory or maladaptive, γ_{cyto}-actin was both ablated and overexpressed in *mdx* skeletal muscle (Baltgalvis et al., 2011; Jaeger et al., 2009; Prins et al., 2008). While knockout of γ_{cyto}-actin neither rescued nor exacerbated the dystrophic phenotype (Prins et al., 2008), γ_{cyto}-actin overexpression protected *mdx* muscle from eccentric contraction-induced force loss (Baltgalvis et al., 2011). These studies indicate that although expressed at significantly lower levels than $\alpha_{skeletal}$-actin, both β_{cyto}- and γ_{cyto}-actin play an essential role in muscle function.

Eccentric Contraction-Induced Force Loss

There are three types of muscle contraction: isometric, concentric, and eccentric. An isometric contraction generates tension without changing length, while a concentric contraction produces enough force to overcome the load while the muscle shortens. Eccentric contractions generate force that is insufficient to overcome the load, and the myofibers lengthen as they contract. Eccentric contractions occur in most muscle groups, and act to decelerate the joint at the end of a movement rather than pull a joint in the direct of contraction as seen with concentric contractions (Faulkner, 2003). Though eccentric training may be used to increase strength in healthy muscle (Colliander and Tesch, 1990), dystrophin-deficient muscles are extremely sensitive to eccentric contraction-induced force loss (Lovering and Brooks, 2014).

Groundbreaking studies by Sweeney (Petrof et al., 1993), Moens (Moens et al., 1993), and collaborators demonstrated that *mdx* muscles were particularly susceptible to rapid force loss during eccentric contractions (ECC). Variations of these studies include isolation of extensor digitorum longus (EDL) muscles from control and *mdx* mice and placement in an *ex vivo* Krebs bathing medium. EDLs are typically lengthened 10% of the muscles length during electrically-stimulated contractions to produce ECCs. While WT mice do not display any drop in force production during ECC, *mdx* mice lose more than 80% of their force production over 10 ECCs (Figure 1-6). Interestingly, *mdx* mice are resistant to force loss

following isometric or concentric contractions (Call et al., 2013). ECC force loss in *mdx* mice has been validated in laboratories around the world as a highly reproducible phenotype, and has since been utilized as an important quantitative read-out for the development of DMD therapies (Grounds et al., 2008; Willmann et al., 2012). However, the molecular mechanisms underlying ECC force loss in *mdx* muscle remain elusive.

ECC force loss in *mdx* muscle is often attributed to “injury” or “damage”, implying that some slowly reversible structural impairment has occurred that would take days to recover. Initially, it was thought that membrane damage contributed mostly to ECC force loss in *mdx* muscle (Petrof et al., 1993). However, membrane instability was only seen in ~20% of myofibers following ECC, and likely could not explain the 80% force loss seen. Other studies have implicated neuromuscular junction impairment as contributing to ECC force loss (Pratt et al., 2013), as well as failure of action potential propagation (Call et al., 2013). Recently, highly-reversible signaling pathways have been implicated in ECC force loss in dystrophin-deficient muscle, including Akt kinase, calcium, and ROS signaling cascades (Allen et al., 2010; Blaauw et al., 2008; Millay et al., 2009; Powers and Jackson, 2008a). Involvement of these reversible signaling events corroborates studies that show reversibility of ECC force loss in *mdx* that takes on the order of minutes, not days (Han et al., 2011; Roy et al., 2016). Together, these recent studies suggest that, in addition to slowly reversible

structural damage, highly reversible molecular signaling contributes to ECC force loss in dystrophin-deficient skeletal muscle.

Potential Therapies for DMD

There is currently no cure for DMD; however, numerous therapeutic approaches are presently under investigation. Genetic methods in animal models of DMD have shown magnificent promise in pre-clinical studies, while those currently in clinical trials display variable success. Therapies for DMD include gene therapy, protein therapy, nonsense read-through, exon skipping, and gene editing.

Gene therapy methods of replacing mutated *DMD* genes have focused on the use of adeno-associated virus (AAV). However, this has been problematic given the limited capacity of AAV vectors and that the cDNA of dystrophin is nearly 14 kb. Therefore, studies have focused on generating miniaturized dystrophins (called “mini-“ or “micro-dystrophins”) with large internal deletions in the central rod domain (Gregorevic et al., 2004; Watchko et al., 2002). These miniaturized dystrophin constructs can be packaged into AAV, and systemic delivery of these vectors into dystrophin-deficient animals have shown efficacy (Lai et al., 2009, 2013, Wang et al., 2000, 2007). However, possible immune responses to the foreign protein in patients have hindered the advancement of this therapy. In one clinical trial, a mini-dystrophin packaged in rAAV was found to elicit a T cell response to the transgene (Mendell et al., 2010). Improved constructs with more appropriate promoters are currently being tested (Chamberlain and Chamberlain, 2017).

Protein therapy has also been utilized as an approach to treat DMD. Since gene replacement therapies have resulted in immune responses to foreign dystrophin, several studies have focused on using utrophin, the homolog of dystrophin, for protein therapy. Utrophin is remarkably similar in structure to dystrophin, but its expression is confined to the neuromuscular and myotendinous junctions of mature skeletal muscle (Blake et al., 2002; Tinsley et al., 1992). Utrophin has been shown to functionally replace dystrophin in mice, as transgenic overexpression of utrophin in *mdx* muscle rescues the dystrophic phenotype (Rybakova et al., 2002; Tinsley et al., 1998, 1996). However, utrophin may not replace every function of dystrophin since it lacks microtubule and nNOS binding activity (Belanto et al., 2014; Li et al., 2010). Yet, efforts have been made to deliver exogenous utrophin protein to rescue the dystrophic phenotype. The lysine-rich transduction domain of the HIV-1 TAT protein was fused to the N-terminus of a truncated micro-utrophin, allowing for cellular entry of the entire protein (Sonnemann et al., 2009). Intraperitoneal injection of TAT-utrophin localized to the sarcolemma where it restored the DGC, leading to significant histological and physiological improvements. Additionally, small molecule upregulation of endogenous utrophin have shown efficacy in *mdx* mice, with one utrophin modulator currently used in a clinical trial (Ricotti et al., 2016; Tinsley et al., 2011).

A significant portion of mutations that cause DMD are nonsense mutations, which lead to a premature stop codon. This causes nonsense-

mediated decay of the mRNA, or if transcribed, produces a truncated protein minimally lacking the C-terminal domain necessary for β-dystroglycan binding. Early studies have shown that the antibiotic gentamicin could bind to 18S rRNA causing the ribosome to skip over or “read-through” a stop codon, inserting another amino acid at random in its place (Palmer et al., 1979). Administration of gentamicin to *mdx* mice, a nonsense mutation model itself, led to proper dystrophin expression and localization (Barton-Davis et al., 1999). While the efficacy of gentamicin treatment in human patients was unclear (Malik et al., 2010), these findings prompted high throughput screening aimed at finding nonsense mutation read-through drugs to better treat DMD. One drug, Ataluren, has been used in a clinical trial but failed to display clinical efficacy (Bushby et al., 2014). However, other read-through drugs are currently being developed and moved into clinical trials (Guiraud and Davies, 2017; Reinig et al., 2017). Drawbacks to this type of therapy include lifetime and therefore costly drug administration, and that only 10-15% of patients have nonsense mutations (Bladen et al., 2015), so most DMD patients would not benefit from read-through therapy.

Another therapeutic approach involves restoring the endogenous reading frame of the *DMD* gene in patients with out-of-frame deletions using exon-skipping technologies. This method involves creating oligonucleotides or phophorodiamidate morpholino oligomers with antisense sequences to a region of dystrophin pre-mRNA (Aartsma-Rus et al., 2009; Alter et al., 2006; van

Deutekom et al., 2007; Kinali et al., 2009). The antisense oligonucleotide then binds to nascent dystrophin transcript, causing the splicing machinery to skip over the exon which is targeted. This technology has shown efficacy in the *mdx* mouse model, where exon 23 was targeted for skipping using morpholinos (Yin et al., 2009). Treatment of *mdx* mice with the morpholinos led to expression of sarcolemmal dystrophin and rescued several parameters of dystrophy including histopathology and elevated serum CK levels. The drug eteplirsen was recently approved to treat a subset of DMD patients by skipping exon 51 (Aartsma-Rus and Krieg, 2017). A disadvantage to this personalized approach is that exon skipping produces small truncations in dystrophin protein, so this treatment may only render a Becker-like phenotype instead of a full recovery.

Recent advancements in gene editing technology have opened the door for the use of CRISPR/Cas9 to correct mutations in the *DMD* gene (Mendell and Rodino-Klapac, 2016). The therapeutic approaches using CRIPSR/Cas9 involve AAV-mediated delivery of Cas9 and specific guide RNAs (gRNAs) and transplantation of gene-edited human induced pluripotent stem cells (iPSCs). Several groups have recently demonstrated the efficacy of AAV-mediated delivery of Cas9 and gRNAs targeting the nonsense mutation found in *mdx* mice, displaying partial dystrophin restoration and improvements in the dystrophic phenotype (Bengtsson et al., 2017; Long et al., 2016; Nelson et al., 2016; Tabebordbar et al., 2016; Xu et al., 2016). Using CRISPR/Cas9 in DMD-derived human iPSCs, one study described the ability to restore out-of-frame deletions

applicable to nearly 60% of DMD patient mutations (Young et al., 2016). The pre-clinical studies using genome editing with CRISPR/Cas9 delivered by AAV look promising, and this therapy may soon be utilized in a clinical setting.

Questions Addressed by This Thesis

The most highly robust and reproducible phenotype of the *mdx* mouse is its sensitivity to precipitous loss of contractile force after performing eccentric contractions. Although the measurement of eccentric contraction-induced force loss in *mdx* muscle and its rescue towards WT is widely accepted as an important proof-of-concept in the development of new therapeutic approaches for DMD, the molecular mechanisms underlying force loss remain poorly understood.

This dissertation aims to expand the field of knowledge on eccentric contraction-induced force loss in dystrophin-deficient muscle. The force lost in *mdx* muscle is often referred to as contraction-induced “damage” or “injury”, suggesting the myofiber has endured some form of slowly-reversible structural damage that would take on the order of days to recover. However, it is known that rapidly-reversible signaling pathways play a role in eccentric contraction-induced force loss in dystrophin-deficient muscle, such as calcium, Akt/PKB kinase, and ROS pathways. *These studies are incompatible with structural damage and bring into question the contribution of myofiber injury to eccentric contraction-induced force loss in mdx muscle.*

To better understand the mechanisms underlying eccentric contraction-induced force loss, we employed iTRAQ proteomics to identify proteins that were differentially expressed in *mdx* mice overexpressing nonmuscle γ_{cyto}-actin

(*mdx*/Actg1-TG), which our lab has previously shown to significantly protect *mdx* muscle against force loss (Baltgalvis et al., 2011). Using this method initially, work in this dissertation set out to answer an important answer in the field: **What are the molecular mechanisms that contribute to eccentric contraction-induced force loss in dystrophin-deficient skeletal muscle?**

Figures

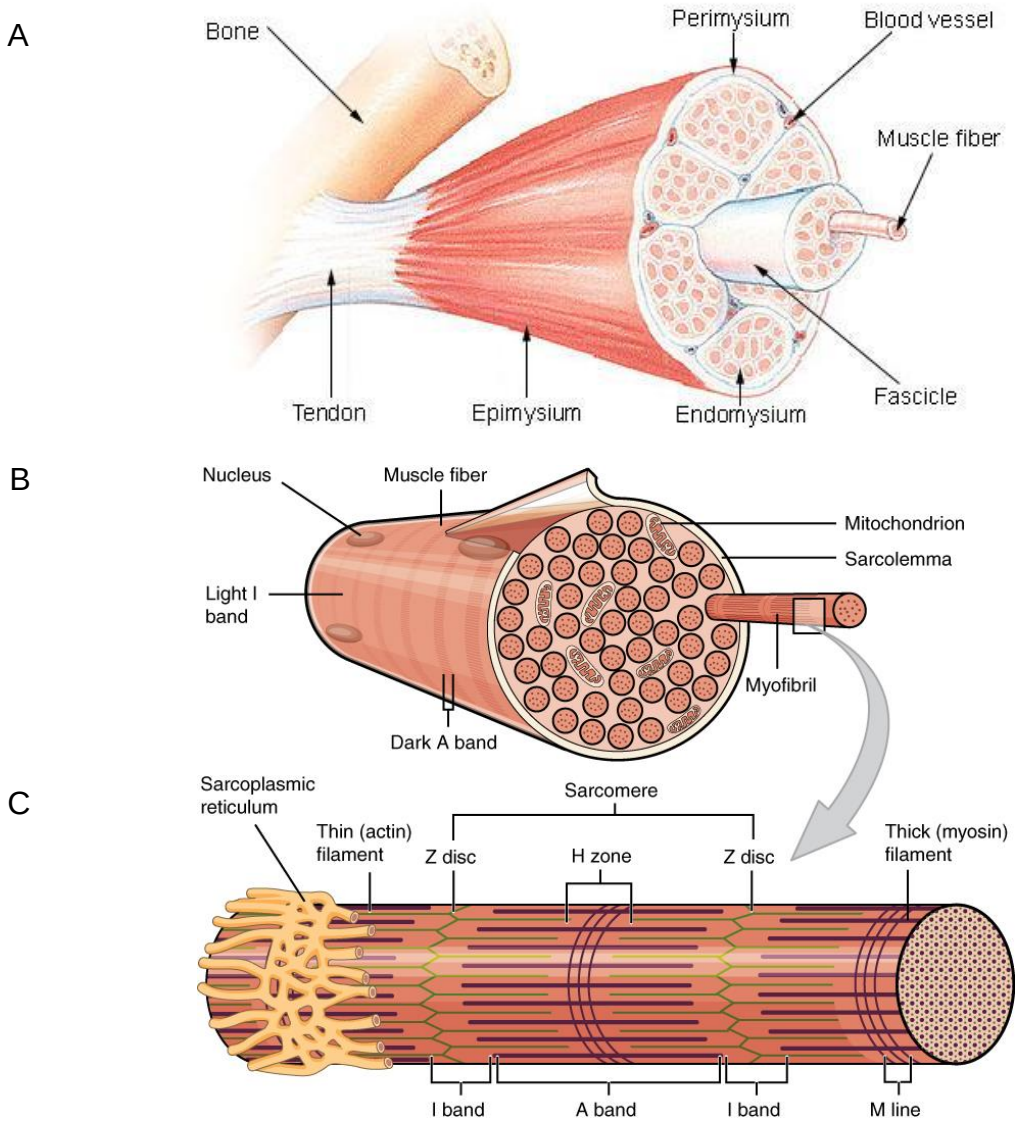

Figure 1-1. Hierarchical Organization of Skeletal Muscle. (A) Skeletal muscle organization includes bundles of fascicles, each containing bundles of myofibers. (B) Myofiber organization includes bundles of myofibrils, the contractile unit of muscle. (C) Myofibrils are comprised of a repeated series of sarcomeres containing thin (actin) and thick (myosin) filaments. (A - from Pearson, 2009; B & C - from OpenStax, Anatomy & Physiology, 2016)

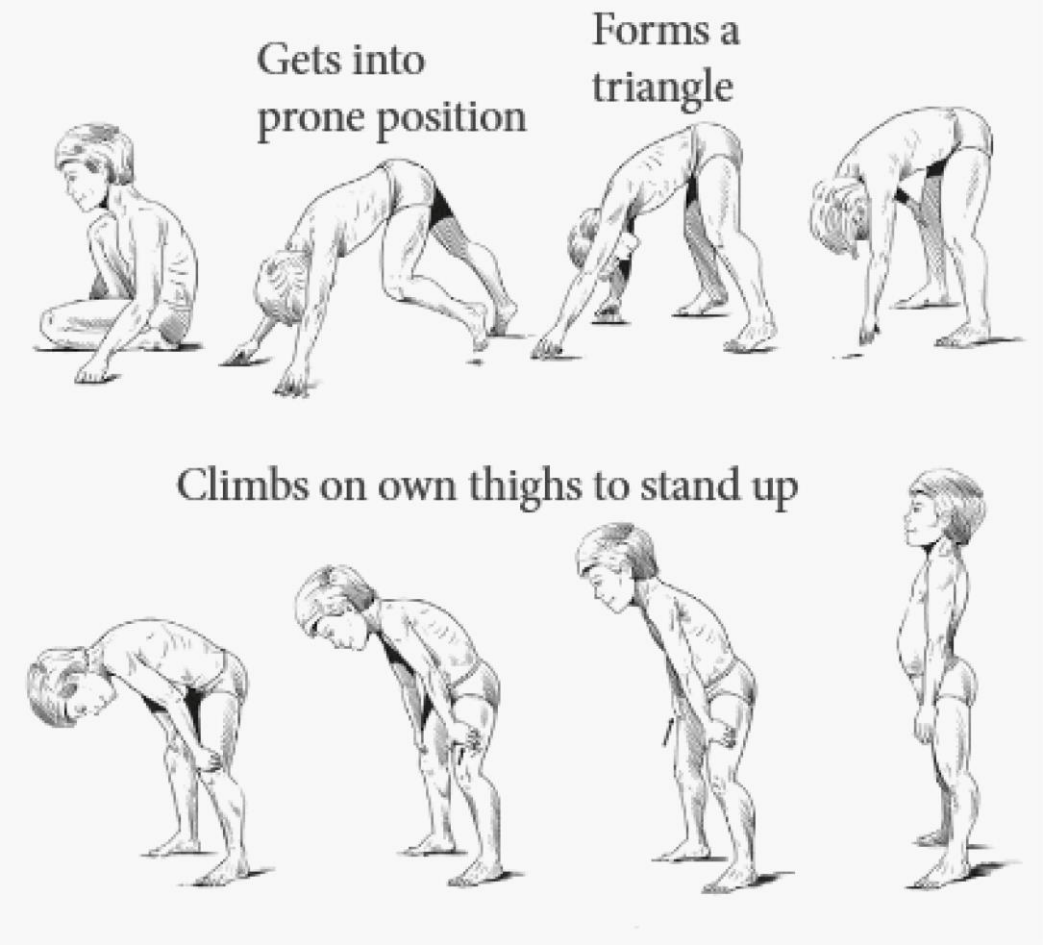

Figure 1-2. Gower's Maneuver. The Gower's maneuver is an early clinical sign that indicates weakness of the proximal muscles in young patients with DMD. The patient is seen using their upper limbs to raise themselves to a standing position. (modified from Epomedicine, 2016)

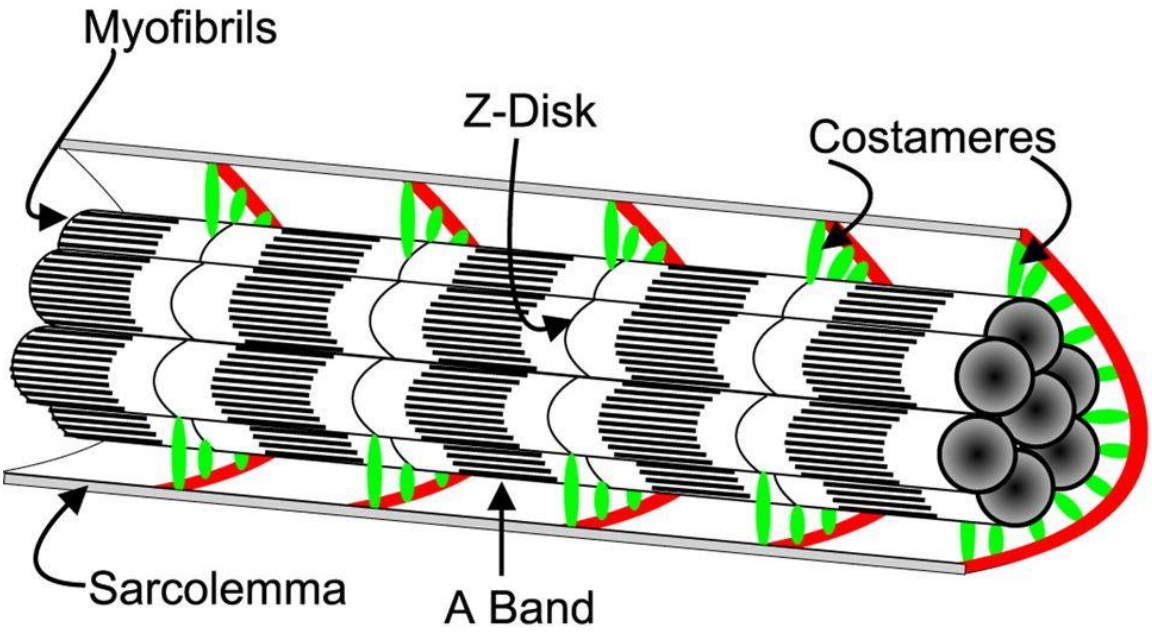

Figure 1-3. Localization of costameres in skeletal muscle fibers. Costameres (shown in green) are the circumferential elements that physically link peripheral myofibrils (composed of $\alpha_{skeletal}$-actin) to the sarcolemma in register with the Z-disk. Dystrophin and the cortical actin cytoskeleton (composed of γ_{cyto}- and β_{cyto}-actins) are highly enriched at costameres. Through interactions with a membrane-bound glycoprotein complex (shown in red), dystrophin links cortical actin with the extracellular matrix. (From Ervasti, 2003)

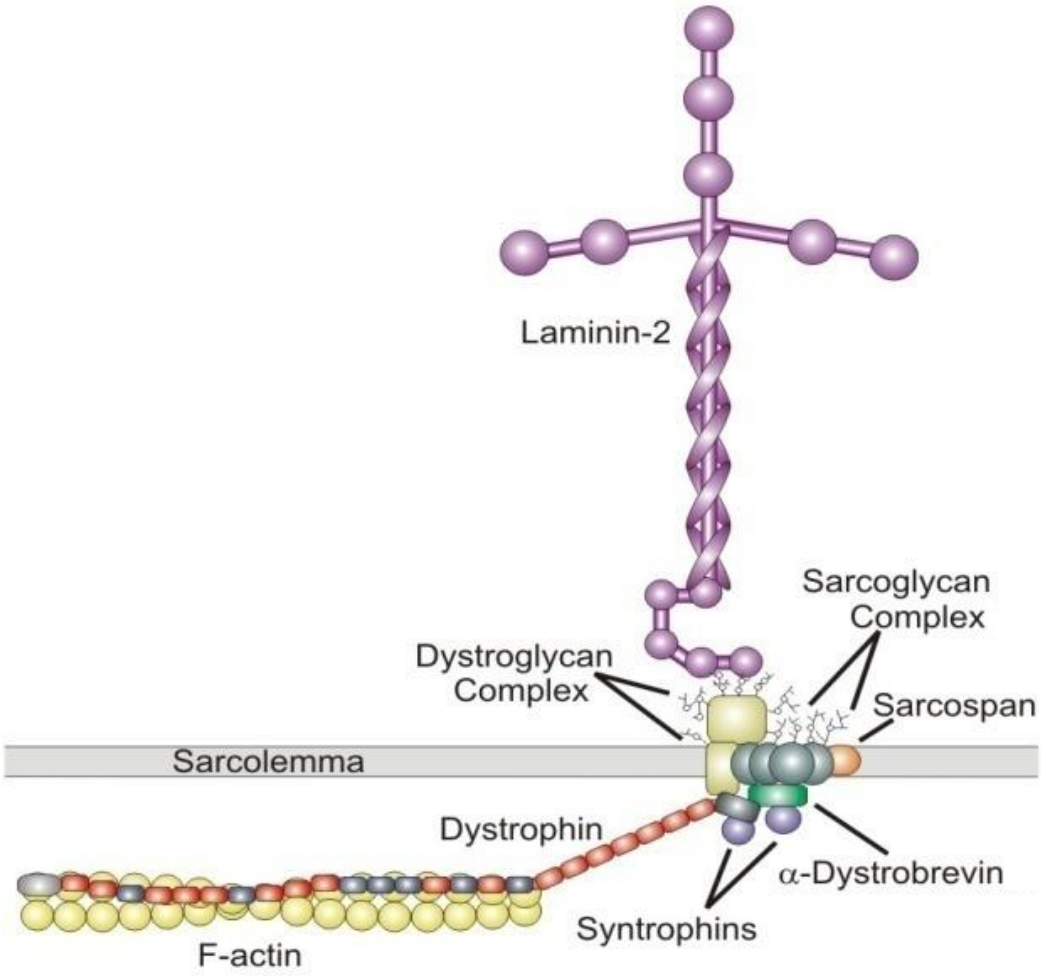

Figure 1-4. The Dystrophin-Glycoprotein Complex (DGC). Diagram of the core members of the dystrophin-glycoprotein complex located at the sarcolemma of skeletal muscle. The cytosolic integral membrane proteins are dystrophin, syntrophins, and α-dystrobrevin. The integral membrane proteins are β-dystroglycan, sarcospan, and the sarcoglycan complex (α-, β-, γ-, and δ-isoforms). The extracellular peripheral membrane proteins are α-dystroglycan and laminin-2.

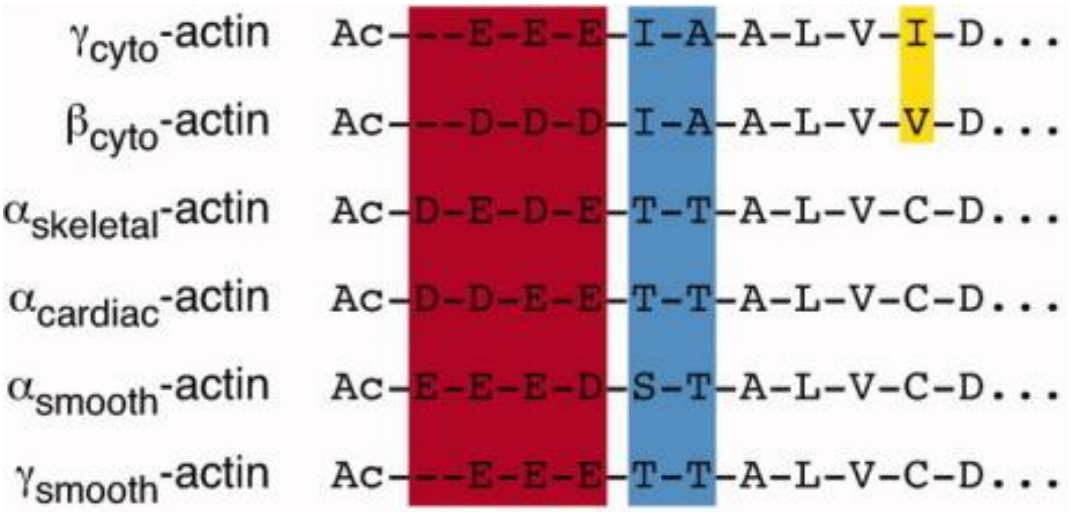

Figure 1-5. The Six-Member Family of Actin Isoforms. Alignment of the N-terminal ends of the six mammalian actin isoforms. Sequence differences are highlighted. (modified from Perrin and Ervasti, 2010)

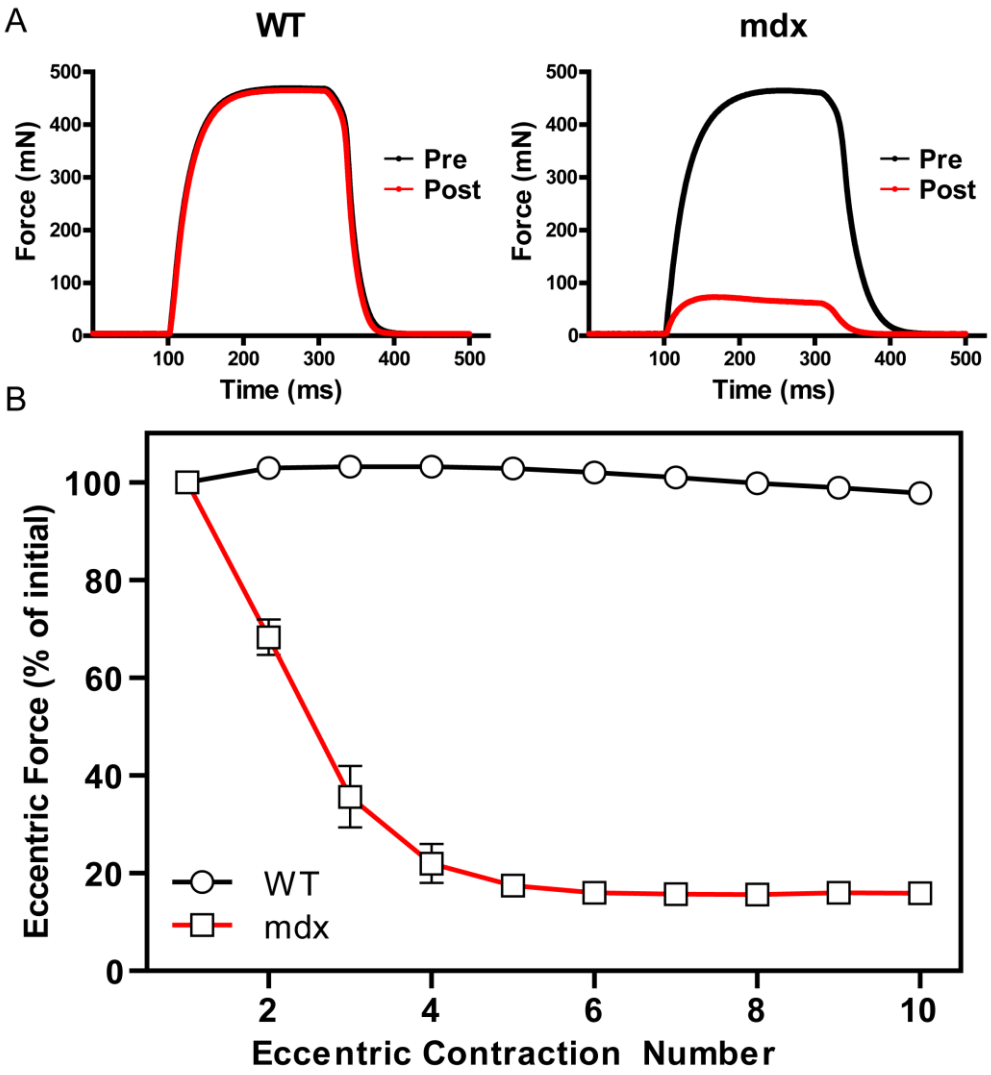

Figure 1-6. Eccentric Contraction-Induced Force Loss in *mdx* skeletal muscle. (A) Isometric force tracings of isolated WT and *mdx* EDL muscles before (Pre) and after (Post) performing 10 eccentric contractions *ex vivo*. (B) EDLs isolated from WT and *mdx* were subjected to 10 eccentric contractions and the force produced at each contraction expressed as a percentage of the force produced during the first contraction.

Chapter 2: Loss of peroxiredoxin-2 exacerbates ROS-mediated force loss in dystrophin-deficient muscle

Angus Lindsay assisted in *ex vivo* EDL physiology experiments (Figures 2-5C, 2-7B, 2-8B, 2-9D, 2-11A & B, and 2-14C). Reem Abo-Zahrah performed single myofiber stretch-induced ROS measurements (Figure 2-14D). Kristen Baltgalvis performed *mdx* ECC recovery experiments (Figure 2-1). Xiaobai Patrinostro and Joseph Belanto aided in the molecular cloning necessary to generate *mdx*/C272A-TG and *mdx*/Actb-TG transgenic mice (used in Figures 2-13 and 2-14. Dawn Lowe measured ECC force loss in *mdx*/Actg1-TG and *mdx*/Coco transgenic mice (Figure 2-2C & F). All other experiments were performed by John T. Olthoff.

Summary

Force loss in skeletal muscle exposed to eccentric contraction is often attributed to injury. We show that EDL muscles from dystrophin-deficient *mdx* mice recover 65% of lost force within 120 minutes of eccentric contraction and exhibit minimal force loss when the interval between contractions is increased from 3 to 30 minutes. A proteomic screen of *mdx* muscle identified an 80% reduction in the antioxidant peroxiredoxin-2, likely due to proteolytic degradation following hyperoxidation by NADPH Oxidase 2. Eccentric contraction-induced force loss in *mdx* muscle was exacerbated by peroxiredoxin-2 ablation, and improved by peroxiredoxin-2 overexpression or myoglobin knockout. Finally, overexpression of γ_{cyto}- or β_{cyto}-actin protects *mdx* muscle from eccentric contraction-induced force loss by blocking NADPH Oxidase 2 through a mechanism dependent on cysteine 272 unique to cytoplasmic actins. Our data suggest that eccentric contraction-induced force loss may function as an adaptive “circuit breaker” that protects *mdx* muscle from injurious contractions.

Introduction

Duchenne muscular dystrophy (DMD) is an X-linked recessive disease caused by deleterious mutations in the *DMD* gene, rendering non-functional forms or complete absence of the protein dystrophin (Hoffman et al., 1987). Dystrophin is normally enriched at subsarcolemmal structures known as costameres, where it links the cortical actin cytoskeleton to the extracellular matrix through interactions with a membrane-bound glycoprotein complex (Ervasti, 2003; Ervasti and Campbell, 1991). DMD is one of the most common and severe forms of muscular dystrophy, affecting ~1:4,000 boys (Mendell et al., 2012). Dystrophin-deficiency leads to progressive weakness and deterioration of skeletal muscle beginning at 3 to 5 years of age. DMD patients typically become non-ambulatory by 12 years of age, with death ensuing by the second or third decade due to cardiac or respiratory failure (Rall and Grimm, 2012). Although several treatments exist, including ventilatory support and use of corticosteroids (Angelini, 2007; Ricotti et al., 2013), there is no cure for DMD.

Much of the mechanistic understanding of DMD has been elucidated in the dystrophin-deficient *mdx* mouse model, which encodes a nonsense mutation in exon 23 of the *DMD* gene ablating dystrophin protein expression (Bulfield et al., 1984; Sicinski et al., 1989). Although the *mdx* mouse presents a milder phenotype compared to DMD patients (Partridge, 2013), several aspects of the disease are recapitulated in the model, including pervasive muscle weakness

(Pastoret and Sebille, 1995), substantial histopathology due to repetitive rounds of muscle degeneration and regeneration (DiMario et al., 1991), and elevated serum creatine kinase levels (Glesby et al., 1988). Landmark studies by Sweeney (Petrof et al., 1993), Moens (Moens et al., 1993), and colleagues demonstrated that *mdx* skeletal muscles are particularly sensitive to precipitous loss of contractile function after performing eccentric contractions (ECC). With validation by many laboratories around the world as a highly robust and reproducible phenotype of murine dystrophy, the measurement of force loss induced by ECC in *mdx* mice has emerged as an important quantitative readout for the efficacy of potential DMD therapies (Grounds et al., 2008; Willmann et al., 2012). However, the molecular mechanism by which ECC force loss occurs in *mdx* muscle is poorly understood.

ECC force loss in *mdx* muscle is frequently referred to as contraction-induced “injury” or “damage”, implying that some form of slowly reversible damage has occurred within the myofiber that would take days to fully recover (Allen et al., 2016). Recent studies suggest that morphological defects at the neuromuscular junction (Pratt et al., 2013), loss of sarcolemmal excitability (Call et al., 2013), and myofibrillar dysfunction (Blaauw et al., 2010) all contribute to ECC force loss in *mdx* muscle. Several signaling mechanisms have also been implicated, including calcium (Allen et al., 2010; Millay et al., 2009), Akt/PKB kinase (Blaauw et al., 2008), neuronal nitric oxide synthase (Rebolledo et al., 2016), and redox pathways (Powers and Jackson, 2008b). The effect of reactive

oxygen species (ROS) on ECC force loss is particularly interesting considering recent discoveries of aberrant stretch-activated ROS in *mdx* skeletal muscle (Khairallah et al., 2012; Shkryl et al., 2009; Ward et al., 2014; Whitehead et al., 2010).

In this study, we demonstrate that isolated *mdx* skeletal muscle recovers 65% of lost force production within 120 minutes of ECC and loses minimal force if the interval between eccentric contractions is increased from 3 to 30 minutes. To gain a mechanistic understanding of ECC force loss, we employed iTRAQ proteomics to identify proteins that were differentially expressed in skeletal muscle of *mdx* mice overexpressing nonmuscle γ_{cyto}-actin (*mdx*/Actg1-TG), which we have previously shown are significantly protected against ECC force loss (Baltgalvis et al., 2011). We identified the antioxidant enzyme peroxiredoxin-2 (PrxII) as significantly decreased in *mdx* muscle compared to WT, but restored to WT levels in *mdx*/Actg1-TG mice. We verify that hyperactive NADPH oxidase 2 (NOX2)-dependent ROS production contributes to ECC force loss and likely causes proteolytic degradation of hyperoxidized PrxII. Ablation of PrxII exacerbated ECC force loss in *mdx* muscle, while overexpression of PrxII led to a dose-dependent protection against ECC force loss. We also demonstrate that myoglobin participates in ECC force loss in *mdx* muscle, likely through the production of hydroxyl radicals via Fenton chemistry. Finally, we show that oxidation-sensitive cysteine 272 unique to γ_{cyto}- and β_{cyto}-actin is required to protect *mdx* muscle from ECC force loss while blocking NOX2-mediated ROS

production. Together, these data suggest that ECC may drive a transient, redox-based inhibition of contractility that protects dystrophin-deficient muscle from more catastrophic structural damage caused by subsequent high force contractions.

Results

Rapid recovery of ECC force loss in *mdx* skeletal muscle

Our standard ECC protocol incorporates a 3 minute interval between the 10 ECC to eliminate fatigue, which is corroborated by the lack of force loss when isolated *mdx* extensor digitorum longus (EDL) muscles perform 10 more energy consumptive isometric contractions (Bigland-Ritchie and Woods, 1976; Woledge et al., 1985) (Figure 2-1A). Imposing 10 ECC on the contralateral EDL resulted in the expected 90% drop in force; however, we observed 65% recovery of lost force production within 2 hours (Figure 2-1A). More surprising, the ECC force loss measured in *mdx* EDL muscles was significantly attenuated when the interval between ECC was increased from 3 to 30 minutes (Figure 2-1B). These data demonstrate that dystrophin-deficient *mdx* muscle can rapidly recover from the perturbation imposed by one or multiple ECC.

Overexpression of γ_{cyto}-actin specifically protects *mdx* muscle from ECC force loss

We previously generated a mouse model that overexpresses γ_{cyto}-actin specifically in skeletal muscle (Actg1-TG) to levels that replace 40% of α_{sk}-actin in myofibrils (Figures 2-2A and 2-2B; Jaeger et al., 2009) and which significantly

protects *mdx* muscle from ECC force loss (Figure 2-2C; Baltgalvis et al., 2011). To address whether protection of *mdx* muscle from ECC force loss depends specifically on the γ_{cyto}-actin isoform, we crossed transgenic mice (Coco) that overexpress alpha-cardiac actin (α_{ca}-actin) specifically in skeletal muscle (Nowak et al., 2009a) onto the *mdx* background (*mdx*/Coco). Similar to the robust expression of γ_{cyto}-actin in *mdx*/Actg1-TG (Figures 2-2A and 2-2B), muscles from *mdx*/Coco animals all showed high α_{ca}-actin expression that was uniformly distributed throughout the muscle fibers (Figures 2-2D and 2-2E). In contrast to *mdx*/Actg1-TG mice (Figure 2-2C), however, EDL muscles from *mdx*/Coco animals were not significantly protected from ECC force loss (Figure 2-2F). These data lead us to conclude that some feature specific to γ_{cyto}-actin is necessary to protect *mdx* muscles from ECC force loss.

Overexpression of γ_{cyto}-actin restores peroxiredoxin-2 levels in *mdx* muscle

To begin to understand how γ_{cyto}-actin overexpression protects *mdx* muscle from ECC force loss, we performed 8-plex isobaric tags for relative and absolute quantification (iTRAQ)-based mass spectrometry analysis (Wiese et al., 2007) on tibialis anterior (TA) muscles lysates isolated from 4 *mdx*/Actg1-TG mice controlled against 4 non-transgenic *mdx* littermates. The iTRAQ screen initially identified 1,963 proteins representing all major protein constituents of adult myofibers in both *mdx* and *mdx*/Actg1-TG muscle. After applying a 99%

false discovery rate to the initial protein list, 144 high-confidence proteins survived, with only two proteins demonstrating significantly different levels between *mdx* and *mdx*/Actg1-TG muscles. One differentially-expressed protein was γ_{cyto}-actin, upregulated 28-fold in *mdx*/Actg1-TG over *mdx*, while the second protein, peroxiredoxin-2 (PrxII) was significantly upregulated 3.75-fold in *mdx*/Actg1-TG over *mdx*. In addition to confirming the iTRAQ result, western blot analysis with PrxII-specific antibodies demonstrated that PrxII is significantly decreased in *mdx* muscle compared to WT and restored to WT levels in *mdx*/Actg1-TG mice (Figures 2-3A and 2-3B). In contrast, PrxII levels in *mdx*/Coco muscle overexpressing α_{ca}-actin were not different from *mdx* muscle (Figures 2-3A and 2-3B). PrxII is one member in a family of six sulfhydryl-dependent cellular peroxidases that reduce endogenous hydrogen peroxide (H_2O_2) (Rhee, 2016). Western blot analyses for the other five family members revealed that PrxI, PrxIII, and PrxVI levels were not different between WT, *mdx*, and *mdx*/Actg1-TG muscles, while PrxIV and PrxV were substantially elevated in *mdx* and *mdx*/Actg1-TG compared to WT (Figure 2-3C). Thus, PrxII was the only peroxiredoxin significantly altered in *mdx* muscle (decreased) and restored to its WT level in *mdx*/Actg1-TG (Figure 2-3C).

NOX2 ablation rescues PrxII levels and attenuates ECC force loss in *mdx* muscle

PrxII mRNA levels were not different between WT, *mdx*, and *mdx*/Actg1-TG muscles (Figures 2-4A and 2-4B), suggesting the loss of PrxII protein in *mdx* muscle is post-transcriptional. Recovery of PrxII levels in *mdx*/Actg1-TG muscle does not seem to involve a direct interaction between PrxII and γ_{cyto}-actin, as PrxII did not bind to F- or G-actin *in vitro* (Figure 2-4C-E) or *in vivo* (Figure 2-4G). Peroxiredoxins are known to undergo irreversible hyperoxidation at conserved peroxidatic cysteine residues leading to inactivation (Rhee, 2016; Rhee et al., 2005) and degradation via the 20S proteasome (Cho et al., 2014). Therefore, we performed western blot analysis on WT, *mdx*, and *mdx*/Actg1-TG muscle lysates using antibodies specific to hyperoxidized peroxiredoxin (Woo et al., 2003). Relative to total PrxII protein (PrxII), the level of hyperoxidized PrxII was significantly increased in *mdx* muscle compared to WT, and was partially restored to WT levels in *mdx*/Actg1-TG muscle (Figure 2-5A). While hyperoxidized PrxII can be reactivated by sulfiredoxin-catalyzed reduction (Chang et al., 2004), we did not detect expression of sulfiredoxin in skeletal muscle (Figure 2-6B).

Three groups recently demonstrated increased expression of NADPH oxidase 2 (NOX2) subunits in *mdx* muscle, which were shown to produce significantly more reactive oxygen species (ROS, ultimately in the form of H_2O_2) in response to mechanical stretch (Khairallah et al., 2012; Shkryl et al., 2009; Whitehead et al., 2010). Because inhibition of NOX2 by apocynin was also shown to protect *mdx* muscle from ECC force loss (Khairallah et al., 2012), we

performed experiments to elucidate the relationship between NOX2 and PrxII in *mdx* muscle. We first confirmed that several NOX2 subunits (gp91^{phox}, p67^{phox}, p22^{phox}, and Rac1) were increased in *mdx* muscle and remained elevated in *mdx*/Actg1-TG muscle (Figure 2-6A). We next compared PrxII protein levels in WT, *mdx*, and *mdx*/p47$^{-/-}$ muscle, which is ablated for the p47^{phox} subunit necessary for NOX2 activity (Pal et al., 2014). PrxII was restored to WT levels in *mdx*/p47$^{-/-}$ muscle (Figure 2-5B), supporting a role for NOX2-dependent ROS production in the loss of PrxII from *mdx* muscle. Finally, *mdx*/p47$^{-/-}$ muscle was significantly protected from ECC force loss compared to *mdx* muscle (Figure 2-5C). Collectively, these data suggest that aberrant NOX2-dependent ROS signaling leads to PrxII hyperoxidation and degradation in *mdx* muscle.

Myoglobin knockout protects *mdx* muscle from ECC force loss

In skinned WT rodent EDL myofibers, prolonged exposure to extremely high concentrations of H_2O_2 is required to cause significant decrements in Ca^{2+}-activated force, unless myoglobin is included in the bathing medium (Murphy et al., 2008). The effect of myoglobin is thought to be caused by hydroxyl radicals produced by the reaction of H_2O_2 with Fe^{2+} in myoglobin (Lamb and Westerblad, 2011). Given that *mdx* ECC force loss depends on an intact muscle fiber (Blaauw et al., 2008, 2010; Lynch et al., 2000), we investigated whether myoglobin mediates the inhibitory effect of ROS on the contractile function of

mdx muscle fibers exposed to ECC. We crossed myoglobin knockout mice ($mb^{-/-}$; Garry et al., 1998) onto the *mdx* background to generate *mdx*/$mb^{-/-}$ mice. In verifying the absence of myoglobin in *mdx*/$mb^{-/-}$ muscle by western blot analysis (Figure 2-7A), we also showed that myoglobin levels are significantly decreased in *mdx* muscle and significantly restored in *mdx*/$p47^{-/-}$ muscle. Most importantly, knockout of myoglobin significantly protected *mdx* muscle from ECC force loss to the same extent as treatment of *mdx* muscle with the antioxidant N-acetylcysteine (Figure 2-7B). These data suggest that myoglobin synergizes with ROS to effect ECC force loss in *mdx* muscle.

PrxII ablation exacerbates ECC force loss in *mdx* muscle

To further understand the role of PrxII in *mdx* ECC force loss, we crossed PrxII knockout mice ($PrxII^{-/-}$; Lee et al., 2003) onto the *mdx* background to generate *mdx*/$PrxII^{-/-}$ mice. Western blot analysis of $PrxII^{+/+}$, $PrxII^{+/-}$, and $PrxII^{-/-}$ muscle lysates verified PrxII antibody specificity (Figure 2-8A) and verified the absence of PrxII in *mdx*/$PrxII^{-/-}$ muscle (Figure 2-9A). H&E staining of muscle cryosections revealed that PrxII deletion resulted in a small, but significant exacerbation of histopathology in *mdx* muscle without an effect on WT muscle histology (Figures 2-9B and 2-9C). In our standard ECC protocol that imposes a 10% change in muscle length, $PrxII^{-/-}$ muscle was not susceptible to ECC force loss (Figure 2-8B), while ECC force loss in *mdx*/$PrxII^{-/-}$ tracked to that measured

in *mdx* (Figure 2-9D). However, *mdx*/PrxII$^{-/-}$ muscles showed significantly greater force loss than *mdx* muscle when exposed to ECC performed with a milder protocol utilizing a 5% length change that elicits lower eccentric force and thus a slower loss of force (Figure 2-9D). These data show that PrxII knockout increases the susceptibility of *mdx* muscle to ECC force loss.

PrxII overexpression protects *mdx* muscle from ECC force loss

Based on the detrimental effect of PrxII ablation on *mdx* muscle (Figure 2-9), we tested the hypothesis that PrxII overexpression would protect *mdx* muscle from ECC force loss. We generated 4 lines of transgenic mice that overexpress PrxII specifically in skeletal muscle and crossed each line onto the *mdx* background to obtain four distinct lines of *mdx*/PrxII-TG mice. Quantitative western blot analysis demonstrated PrxII overexpression to 1X, 12X, 58X and 112X over WT levels in the four lines (Figure 2-10A). In our standard ECC protocol, we observed a clear dose-dependent protection of *mdx* muscle from ECC force loss with the greatest effect measured when PrxII was overexpressed 58X over WT (Figures 2-11A and 2-11B). H&E staining of muscle cryosections from the 58X overexpressing *mdx*/PrxII-TG line revealed a small but significant decrease in the number of centrally nucleated fibers compared to *mdx* (Figures 2-11C and 2-11D). Because restoration of PrxII to 1X WT levels did not protect *mdx* muscle from ECC force loss (Figures 2-11A and 2-11B), the loss of PrxII

from *mdx* muscle is not the primary cause of ECC force loss in *mdx* muscle, but rather likely a consequence of excessive ROS produced by NOX2 in response to mechanical activation.

Protection of *mdx* muscle from ECC force loss by γ_{cyto}-actin requires Cys272

The protection of *mdx* muscle from ECC force loss by overexpression of γ_{cyto}-actin, but not α_{ca}-actin (Figure 2-2) led us to re-examine their highly homologous primary sequences. Interestingly, γ_{cyto}-actin and β_{cyto}-actin each contain 6 Cys while α_{sk}-actin and α_{ca}-actin only contain 5 Cys (Figure 2-12). The unique extra Cys in both γ_{cyto}-actin and β_{cyto}-actin is located at position 272 (Figure 2-12, green highlight, blue circle) and has been shown to be the most reactive with H_2O_2 (Lassing et al., 2007). To investigate the role of Cys272 of γ_{cyto}-actin in protecting *mdx* muscle from ECC force loss, we generated transgenic mouse lines overexpressing the C272A mutant of γ_{cyto}-actin (C272A-TG) as well as β_{cyto}-actin (Actb-TG) specifically in skeletal muscle and crossed the lines onto the *mdx* background to identify those that best match γ_{cyto}-actin overexpression in *mdx*/Actg1-TG (Figure 2-14A). In addition, recombinant γ_{cyto}-actin (for *mdx*/C272A-TG) and platelet actin (for *mdx*/Actb-TG) were used to generate standard curves for quantitative western blot analysis to verify equivalent expression of each actin transgene (Figure 2-13A-C). Uniformity of

C272A and β_{cyto}-actin overexpression were verified by immunofluorescence analysis (Figure 2-14B), while H&E staining revealed no obvious change in the histopathology of *mdx* muscle associated with overexpression of C272A or β_{cyto}-actin (Figure 2-13D). Most interestingly, β_{cyto}-actin overexpression protected *mdx* muscle from ECC force loss to the same extent as γ_{cyto}-actin, while ECC force loss in *mdx*/C272A-TG was not different from *mdx* (Figure 2-14C). Finally, we measured the rate of NOX2-dependent ROS production in response to cyclic stretch of single myofibers (Pal et al., 2014) isolated from WT, *mdx*, *mdx*/Actg1-TG, *mdx*/C272A-TG and *mdx*/Actb-TG (Figure 2-14D). Stretch-dependent, NOX2-mediated ROS signaling was significantly greater in *mdx* and *mdx*/C272A-TG compared to WT, *mdx*/Actg1-TG, or *mdx*/Actb-TG (Figure 2-14D). These data demonstrate that γ_{cyto}-actin and β_{cyto}-actin overexpression protects *mdx* muscle from ECC force loss by blocking the stretch-dependent NOX2-mediated production of ROS and show that Cys272 is necessary for inhibition.

Discussion

Our data best fit a model in which PrxII functions as an off switch to regulate stretch-activated NOX2 signaling in normal skeletal muscle (Kerr et al., 2015), but is lost from *mdx* muscle through hyperoxidation and proteolytic degradation effected by aberrant NOX2-mediated ROS production (Figure 2-15). PrxII is known to suppress redox-mediated growth factor signaling (Choi et al., 2005; Finkel, 2011; Kang et al., 2011), while NOX2 in *mdx* skeletal muscle has been demonstrated to produce significantly more ROS (Pal et al., 2014), particularly in response to mechanical stretch as occurs during ECC (Khairallah et al., 2012; Shkryl et al., 2009; Whitehead et al., 2010). Importantly, treatment with the NOX2 inhibitor apocynin (Khairallah et al., 2012), the non-specific antioxidant N-acetylcysteine (Whitehead et al., 2008), or catalase overexpression (Selsby, 2011) have been shown to protect *mdx* muscle from ECC force loss, mirroring the effect we observed in *mdx*/Actg1-TG (Figure 2-2C), *mdx*/p47$^{-/-}$ (Figure 2-5C), *mdx*/mb$^{-/-}$ (Figure 2-7C), *mdx*/PrxII-TG (Figure 2-11A), and *mdx*/Actb-TG EDL muscles (Figure 2-14C) (for more physiological parameters of all mouse lines, see Table 2-1).

Our stretch-activated ROS experiments with single myofibers from transgenic models overexpressing γ_{cyto}-actin, β_{cyto}-actin, or the C272A mutant of γ_{cyto}-actin (Figure 2-14D) suggest that cytoplasmic actin overexpression directly inhibits NOX2 activity in *mdx* skeletal muscle. *In vitro* binding experiments and

studies in nonmuscle cells have shown that actin can inhibit NOX2 activity by directly binding and sequestering the $p40^{phox}$, $p47^{phox}$, and/or $p67^{phox}$ regulatory subunits (Chen et al., 2007; Munnamalai et al., 2014). Alternatively, the additional redox-sensitive Cys272 unique to γ_{cyto}- and β_{cyto}-actins (Johansson and Lundberg, 2007; Lassing et al., 2007) may serve to shunt ROS-mediated oxidation away from conserved sulfhydryls necessary for contractile function. Future experiments will address both possibilities.

One poorly understood feature of ECC force loss in *mdx* muscle is its dependence on intact myofibers, because skinned fibers from *mdx* mice are no more susceptible to ECC than WT (Blaauw et al., 2008, 2010; Lynch et al., 2000). In studies of muscle fatigue, ROS in the form of H_2O_2 is thought to exert inhibitory effects on contractile proteins, yet extremely high concentrations of H_2O_2 are required to cause significant decrements in Ca^{2+}-activated force loss in skinned myofibers (Ferreira and Reid, 2008; Lamb and Westerblad, 2011). However, the concentration of H_2O_2 required to elicit force loss is greatly reduced when myoglobin is included in the bathing medium (Murphy et al., 2008; Lamb and Westerblad, 2011), which results in the production of highly reactive hydroxyl radicals through the reaction of H_2O_2 with Fe^{2+} in myoglobin (Lamb and Westerblad, 2011). Our experiments in *mdx*/$mb^{-/-}$ mice (Figure 2-7) suggest that myoglobin and H_2O_2 may catalyze similar Fenton chemistry in *mdx* muscle to cause ECC force loss with concomitant oxidative degradation of myoglobin.

While the ROS-based perturbations tested here by us and reported by others previously (Khairallah et al., 2012; Loehr et al., 2016; Selsby, 2011; Whitehead et al., 2008) all demonstrated significant protection of *mdx* muscle from ECC force loss, the measured protection is incomplete. Other studies have implicated elevated cytosolic calcium (Mázala et al., 2015; Morine et al., 2010; Yeung et al., 2005; Zanou et al., 2009), loss of neuromuscular junction or sarcolemmal membrane excitability (Call et al., 2013; Pratt et al., 2013), and Akt/PKB signaling (Blaauw et al., 2008) in *mdx* ECC force loss and our results are neither incompatible with or mutually exclusive of such mechanisms. For example, NOX2 negatively regulates Akt activation in skeletal muscle exposed to oxidative stress (De Figueiredo et al., 2015) while the activity of ion channels important for membrane excitability are sensitive to oxidation (Song et al., 2011). Although stretch-activated calcium channels are clearly one downstream effector of the ROS produced by NOX2 (Ward et al., 2014), it is not clear how an increase in cytosolic calcium could affect rapidly-reversible ECC force loss as reported here (Figure 2-1) and elsewhere (Han et al., 2011; Roy et al., 2016). Perhaps the rapidly-reversible component of ECC force loss, measured here over the course of two hours, is due to reversible oxidation of one or more proteins regulating muscle contraction, while the slowly-reversible component, or force loss that is recovered in the timeframe of several days (Brooks, 1998), is due to calcium-activated proteolysis of other muscle regulatory proteins. Alternatively, both the rapidly-reversible and slowly-reversible components of

ECC force loss in *mdx* muscle could result from oxidative stress. In some pathological states, peroxiredoxins (including PrxII) are subject to "over-oxidation" such that reversibly sulfenylated cysteine residues become irreversibly sulfinylated or sulfonylated (Finkel, 2011; Zhu et al., 2012). Such hyperoxidation may occur in proteins involved with contractility in *mdx* muscle, leading to their irreversible inactivation and contributing to the slowly-reversible component of ECC force loss.

As noted in the introduction, ECC force loss in *mdx* muscle is often referred to as "contraction-induced injury," or "contraction-induced damage," and muscle damage is operationally defined "as weakness which recovers very slowly after activity with a time course (4-8 days) similar to repair or regeneration" (Allen et al., 2016). We measured rapid recovery of force in isolated *mdx* EDL muscles exposed to ECC (Figure 2-1A). While our rapid recovery data are supported by other studies (Han et al., 2011; Roy et al., 2016), they are incompatible with the above definition of muscle damage. On the other hand, the rapidly-reversible component of ECC force loss fits well with a reversible ROS-mediated inhibition of contractile force. Rather than serving as a readout for muscle damage, ours and others' data collectively lead us to propose that ECC force loss may instead function as an adaptive "circuit breaker" that protects dystrophin-deficient muscle from potentially cell-lethal structural damage caused by continually repeated high force contractions.

Materials and Methods

Key Resources Table:

REAGENT or RESOURCE	SOURCE	IDENTIFIER
Antibodies		
Mouse monoclonal anti-γ_{cyto}-actin	Hanft et al., 2006	Clone 2-4
Mouse monoclonal anti-γ_{cyto}-actin	Hanft et al., 2006	Clone 1-17
Rabbit polyclonal anti-γ_{cyto}-actin	Hanft et al., 2006	Clone 7577
Mouse monoclonal anti-$\alpha_{cardiac}$-actin	Sigma-Aldrich	Cat #A9357
Rabbit polyclonal anti-PrxII	Sigma-Aldrich	Cat #R8656
Mouse monoclonal anti-Dystrophin	Leica Biosystems	Cat #NCL-DYS1
Mouse monoclonal anti-Utrophin	Santa Cruz Biotechnology	Cat #sc-33700
Mouse monoclonal anti-GAPDH	Sigma-Aldrich	Cat #G8795
Rabbit polyclonal anti-GAPDH	Sigma-Aldrich	Cat #G9545
Rabbit polyclonal anti-PrxI	Abcam	Cat #ab15571
Mouse monoclonal anti-PrxIII	Abcam	Cat #ab16751
Mouse monoclonal anti-PrxIV	Abcam	Cat #ab16943
Mouse monoclonal anti-PrxV	Abcam	Cat #ab16944
Rabbit polyclonal anti-PrxVI	Sigma-Aldrich	Cat #P0058
Rabbit polyclonal anti-PrxSO_3	Abcam	Cat #ab16830
Rabbit polyclonal anti-Myoglobin	Dako	Cat #A0324
Mouse monoclonal anti-β_{cyto}-actin	Sigma-Aldrich	Cat #A1978
Mouse monoclonal anti-β_{cyto}-actin (FITC)	Abcam	Cat #ab6277
Mouse monoclonal anti-gp91^{phox}	BD Biosciences	Cat #611414
Mouse monoclonal anti-p67^{phox}	BD Biosciences	Cat #610912
Rabbit polyclonal anti-p22^{phox}	Santa Cruz Biotechnology	Cat #sc-20781
Mouse monoclonal anti-Rac1	Cytoskeleton, Inc.	Cat #ARC03
Rabbit polyclonal anti-p47^{phox}	EMD Millipore	Cat #07-500
Rabbit polyclonal anti-p40^{phox}	EMD Millipore	Cat #07-501
Rabbit polyclonal anti-Sulfiredoxin	Proteintech	Cat #14273-1-AP
Rat monoclonal anti-Laminin	Sigma-Aldrich	Cat #L0663
Rabbit polyclonal anti-Laminin	Sigma-Aldrich	Cat #L9393
DyLight 680 Goat anti-Mouse IgG (H+L)	Cell Signaling Technology	Cat #5470S
DyLight 680 Goat anti-Rabbit IgG (H+L)	Cell Signaling Technology	Cat #5366S
DyLight 800 Goat anti-Mouse IgG (H+L)	Cell Signaling Technology	Cat #5257S
DyLight 800 Goat anti-Rabbit IgG (H+L)	Cell Signaling Technology	Cat #5151S
Alexa Fluor 488 Donkey anti-Mouse IgG (H+L)	ThermoFisher Scientific	Cat #A-21202
Alexa Fluor 488 Donkey anti-Rabbit IgG (H+L)	ThermoFisher Scientific	Cat #A-21206
Alexa Fluor 488 Goat anti-Rat IgG (H+L)	ThermoFisher Scientific	Cat #A-11006
Alexa Fluor 568 Donkey anti-Mouse IgG (H+L)	ThermoFisher Scientific	Cat #A-10037
Alexa Fluor 568 Goat anti-Rabbit IgG (H+L)	ThermoFisher Scientific	Cat #A-11011

Alexa Fluor 568 Goat anti-Rat IgG (H+L)	ThermoFisher Scientific	Cat #A-11077
Bacterial and Virus Strains		
DH5α Competent Cells	Invitrogen	Cat #18258012
DH10Bac Competent Cells	Invitrogen	Cat #10361012
Chemicals, Peptides, and Recombinant Proteins		
N-Acetylcysteine	Sigma-Aldrich	Cat #A7250
DCFH-DA (6-Carboxy-2',7'-Dichlorodihydrofluorescien Diacetate)	Invitrogen	
gp91ds-tat (NOX2-specific peptide inhibitor)	Bio-Synthesis Inc	N/A
FLAG peptide	University of Minnesota Genomics Center	N/A
ANTI-FLAG M2 Affinity Gel	Sigma-Aldrich	Cat #A2220
Human platelet actin protein (>99% pure)	Cytoskeleton, Inc.	Cat #APHL99
Recombinant FLAG-PrxII	This paper	N/A
Recombinant FLAG-Fascin-1	This paper	N/A
Recombinant γ_{cyto}-actin	Perrin et al., 2013	N/A
Critical Commercial Assays		
Wizard *Plus* SV Minipreps DNA Purification System	Promega	Cat #A1460
Amicon Ultra-15 mL Centrifugal Filters	EMD Millipore	Cat #UFC901024
PureLink Quick Gel Extraction Kit	ThermoFisher Scientific	Cat #K210012
QIAEX II Gel Extraction Kit	Qiagen	Cat #20021
PureLink Quick PCR Purification Kit	ThermoFisher Scientific	Cat #K310001
QuikChange II XL Site-Directed Mutagenesis Kit	Agilent Technologies	Cat #200521
PfuUltra II Fusion HS DNA Polymerase	Agilent Technologies	Cat #600670
Aurum Total RNA Mini Kit	Bio-Rad	Cat #732-6820
iScript Advanced cDNA Synthesis Kit for RT-qPCR	Bio-Rad	Cat #172-5038
SsoAdvanced Universal SYBR Green Supermix	Bio-Rad	Cat #172-5271
Pierce Crosslink Magnetic IP/Co-IP Kit	ThermoFisher Scientific	Cat #88805
Pierce BCA Protein Assay Kit	ThermoFisher Scientific	Cat #23225
T4 Polynucleotide Kinase	New England Biolabs	Cat #M0201
T4 DNA Ligase	New England Biolabs	Cat #M0202
Gateway LR Clonase II Enzyme Mix	Invitrogen	Cat #11791100
Experimental Models: Cell Lines		
Sf9 Insect Cells	ATCC	Cat #CRL-1711
Experimental Models: Organisms/Strains		
Mouse: C57BL/10 WT	The Jackson Laboratory	Stock #000666
Mouse: *mdx*	The Jackson Laboratory	Stock #001801

Mouse: *mdx*/Actg1-TG	Baltgalvis et al., 2011	N/A
Mouse: *mdx*/Coco	This paper	N/A
Mouse: p47$^{-/-}$	The Jackson Laboratory	Stock #004742
Mouse: *mdx*/p47$^{-/-}$	Pal et al., 2014	N/A
Mouse: *mdx*/mb$^{-/-}$	This paper	N/A
Mouse: PrxII$^{-/-}$	Lee et al., 2003	N/A
Mouse: *mdx*/PrxII$^{-/-}$	This paper	N/A
Mouse: PrxII-TG	This paper	N/A
Mouse: *mdx*/PrxII-TG	This paper	N/A
Mouse: *mdx*/C272A-TG	This paper	N/A
Mouse: *mdx*/Actb-TG	This paper	N/A
Oligonucleotides		
PrxII qPCR Forward primer: 5'-GGTTTGGGCCACGCATAAAA-3'	This paper	N/A
PrxII qPCR Reverse primer: 5'-GCCATGACTGCGTGAGCAAG-3'	This paper	N/A
HPRT qPCR Forward primer: 5'-CCCTGGTTAAGCAGTACAGCCCC-3'	Patrinostro et al., 2017	N/A
HPRT qPCR Reverse primer: 5'-GGCCTGTATCCAACACTTCGAGAGG-3'	Patrinostro et al., 2017	N/A
HSA Genotyping Forward primer: 5'-GTCAGGAGGGGCAAACCCGC-3'	N/A	N/A
HSA Genotyping Reverse primer: 5'-GTCGCTGCCCTTCTCGAGCC-3'	N/A	N/A
Recombinant DNA		
PRDX2 in pDONR221 vector	DNASU	HsCD00076134
PRDX2-pENTR/D-TOPO	This paper	N/A
N-FLAG-PRDX2-pENTR/D-TOPO	This paper	N/A
N-FLAG-PRDX2-pDEST8	This paper	N/A
HSA-VP1-PRDX2-SV40-SV40-pDEST8	This paper	N/A
HSA-VP1-ACTG1-SV40-SV40-pDEST8	Jaeger et al., 2009	N/A
HSA-VP1-C272A-SV40-SV40-pDEST8	This paper	N/A
HSA-VP1-ACTB-SV40-SV40-pDEST8	This paper	N/A
FSCN1-pENTR/D-TOPO	This paper	N/A
N-FLAG-FSCN1-pENTR/D-TOPO	This paper	N/A
N-FLAG-FSCN1-pDEST8	This paper	N/A
Software and Algorithms		
Image Studio Lite v5.2	LI-COR	https://www.licor.com/bio/products/software/image_studio_lite/

NanoDrop 1000	ThermoFisher Scientific	http://nanodrop.w01.wh-2.com/Download.aspx?Type=Software&Cat=NanoDrop%201000
ImageJ	NIH	https://imagej.nih.gov/ij/
CFX Manager	Bio-Rad	http://www.bio-rad.com/en-us/category/qpcr-analysis-software
ProteinPilot	Sciex	https://sciex.com/products/software/proteinpilot-software
Primer-BLAST	NIH	https://www.ncbi.nlm.nih.gov/tools/primer-blast/
TestPoint software	SuperLogics	http://www.superlogics.com/specpage.asp?Items=1500

Mice

All animals were housed and treated in accordance with the standards set by the University of Minnesota Institutional Animal Care and Use Committee. Mice were maintained on regular diet in a SPF facility on a 12-hour light/dark cycle with continuous access to food and water. All wild-type mice used in this study were on the C57BL/10SnJ background. All transgenic overexpression mice are skeletal muscle-specific using the human skeletal actin (HSA) promoter. All mice on the *mdx* background utilized the C57BL/10ScSn-*Dmd*^{mdx}/J strain of *mdx* mice from The Jackson Laboratory. Transgenic mice overexpressing γ_{cyto}-actin on the *mdx* background (*mdx*/Actg1-TG) was previously described (Baltgalvis et al., 2011). Transgenic mice overexpressing $\alpha_{cardiac}$-actin (Coco) were previously

described (Nowak et al., 2009a) and bred onto the *mdx* background in this study. Mice with a genetic deletion of the NOX2 scaffolding subunit $p47^{phox}$ ($p47^{-/-}$) were obtained from The Jackson Laboratory (B6(Cg)-*Ncf1*^{m1J}/J) and bred onto the *mdx* background as previously described (Pal et al., 2014). Mice with a genetic knockout of myoglobin ($mb^{-/-}$) have been previously described (Garry et al., 1998) and were bred onto the *mdx* background in this study. Mice lacking peroxiredoxin-2 ($PrxII^{-/-}$) were rederived from sperm donated by Dr. Dae-Yeul Yu (Korean Research Institute of Bioscience and Biotechnology) and bred onto the *mdx* background in this study. Transgenic mice overexpressing peroxiredoxin-2 (PrxII-TG), γ_{cyto}^{C272A} (C272A-TG), and β_{cyto}-actin (Actb-TG) were described in this paper (Cloning and generation of transgenic mice), and all three were bred onto the *mdx* background, resulting in *mdx*/PrxII-TG, *mdx*/C272A-TG, and *mdx*/Actb-TG mice. For all transgenic lines on the *mdx* background, non-transgenic *mdx* littermates were used as controls. Animals used for physiological experiments were all 3 months of age, while mice used for all other experiments were 3-6 months of age. All mice used in this study were male.

Ex vivo EDL force measurements

Contractile functions of EDL muscles were assessed according to methods described previously (Moran et al., 2005). Mice were anesthetized with sodium pentobarbital (75-100 mg/kg body mass). EDL muscles were dissected and mounted on a 300B-LR dual-mode muscle lever system (Aurora Scientific

Inc.) with 5-0 suture in a 1.2 mL bath assembly with oxygenated (95:5 % O_2:CO_2) Krebs-Ringer bicarbonate (Krebs) buffer maintained at 25 ˚C. The stimulator and muscle lever system was controlled by computer using a KPCI-3108 interface board (Keithley Instruments) and TestPoint software (SuperLogics). Muscles were adjusted to their anatomical optimal length (L_o) based on resting tension, with length being measured from the distal myotendonous junction to the proximal myotendonous junction using digital calipers. Prior to performing eccentric contractions, maximal isometric tetanic force (P_o) was measured every 2 min by stimulating the muscle to contract for 200 ms at 175 Hz until force plateaued, with this value being designated “pre P_o”, or simply “Pre”. In our standard ECC protocol, a series of 10 eccentric contractions were performed and the peak force of each contraction was recorded. For each ECC force measurement, the muscle was passively shortened to 95% L_o and then stimulated for 200 ms while the muscle was simultaneously lengthened to 105% L_o at 0.5 L_o/s. Each eccentric contraction was separated by 3 min of rest before performing the next eccentric contraction to prevent fatigue (Lowe et al., 1994). The force measured at each eccentric contraction was expressed as a percentage of the force produced during the first (“initial”) contraction. This standard ECC protocol was used in Figure 2-2C, Figure 2-2F, Figure 2-5C, Figure 2-7B, Figure 2-8B, Figure 2-9D (10%: *mdx* and 10%: *mdx*/PrxII$^{-/-}$), Figure 2-11A, and Figure 2-14C. Experiments where variations of the standard ECC protocol were used are explained below.

For Figure 2-1A, *mdx* muscles were either subjected to the standard ECC protocol described above, or the same protocol substituting isometric contractions for eccentric contractions performed on the contralateral EDL. After each 10-contraction protocol, P_o was measured immediately (Post 0') as well as at the 20, 40, 60, 90, and 120 min timepoints (Post 20', Post 40', etc.). Each P_o was then expressed as a percentage of the P_o measured before the 10 eccentric or isometric contractions (Pre). For the eccentric protocol, statistical significance was determined for the P_o measured at Post 20' through Post 120' compared to the P_o measured at Post 0' (see Statistical Analysis).

In Figure 2-1B, *mdx* EDLs were subjected to only 5 eccentric contractions. The first muscle used a standard 3 min of rest between each eccentric contraction, while the contralateral muscle was allowed 30 min of rest between contractions.

Figure 2-7B involves a group where N-acetylcysteine (NAC) treatment was performed on *mdx* EDLs. For this group, NAC (Sigma-Aldrich) was dissolved directly into Krebs Buffer at 20 mM immediately prior to bath assembly (Whitehead et al., 2008). The control *mdx* group used standard Krebs Buffer without NAC. For both groups, EDL muscles were incubated for 30 minutes so NAC could efficiently penetrate the muscle before being subjected to the standard ECC protocol.

For Figure 2-9D, the standard ECC protocol was used for 10%: *mdx* and 10%: *mdx*/PrxII$^{-/-}$ experiments (solid lines). For the other two experiments (dash

lines), the standard ECC protocol was used except that a 5% length change was performed instead of a 10% change. Here, EDL muscles were passively shortened to 97.5% L_o and then stimulated for 200 ms while the muscle was simultaneously lengthened to 102.5% L_o at 0.25 L_o/s, resulting in lower peak eccentric force being generated compared to the 10% length change.

Immunoblot Analysis

Gastrocnemius muscles from mice of the indicated genotypes were dissected, flash-frozen in liquid N_2, pulverized to a powder with a liquid N_2-cooled mortar and pestle, and resuspended in 1% SDS in PBS with protease inhibitors (100 nM aprotinin, 1 mM benzamidine, 10 µM E-64, 10 µM leupeptin, 1 mM pepstatin A, 1 mM phenylmethanesulfonylfluoride, 1 µM calpain inhibitor I, and 1 µM calpeptin). Samples were then incubated at RT with end-over-end rotation for 30 min, followed by centrifugation at 14,000 rpm for 10 min to clear lysates of insoluble material. Total protein concentration of the lysates was determined by A_{280} measurement (NanoDrop 1000, ThermoFisher Scientific). Lysates were then diluted to equal concentrations before Laemmli sample buffer was added and boiled for 5 minutes. Equal amounts of protein were then separated by SDS-PAGE, transferred to PVDF membranes, blocked with 5% milk in PBS, and incubated with the indicated primary antibodies overnight at 4°C. The next day, membranes were washed 4 x 5 min in 0.1% Tween in PBS before incubation with DyLight secondary antibodies (1:10,000 each; see Key Resources Table) for

1 hour at RT. Membranes were again washed 4 x 5 min before being imaged with an Odyssey Infrared Scanner (LI-COR Biosciences). Protein bands were then quantified using LI-COR Image Studio software.

Muscle histology and immunofluorescence

Quadriceps muscles from each mouse line were cryopreserved in melting isopentane for 30 seconds and 10 µm transverse cryosections were obtained (Leica CM3050 S). For histology, sections were stained with hematoxylin and eosin and imaged on a Leica DM5500 B microscope equipped with a Leica HC PLAN APO 20x objective. Centrally nucleated fibers (CNFs) were counted using the Cell Counter plugin on ImageJ software (NIH) and expressed as a percentage of the total number of myofibers (%CNFs). For immunofluorescence, sections were fixed in 4% paraformaldehyde in PBS at RT for 10 min and subsequently washed three times in PBS before being permeabilized in 0.1% Triton X-100 in PBS for 10 min at RT. Sections were then blocked in 5% BSA and 0.1% Triton X-100 in PBS for 1 hour at RT before incubating with primary antibodies overnight at 4°C. Slides were then washed three times in PBS before incubating with Alexa Fluor secondary antibodies (1:500 each; see Key Resources Table) for 1 hour at RT. Sections were finally wash three times in PBS and mounted in ProLong Gold Antifade with DAPI to visualize nuclei (ThermoFisher Scientific). Images were acquired on a Deltavision PersonalDV deconvolution microscope equipped with an Olympus UApo 20x objective.

iTRAQ Proteomics

Tibialis anterior (TA) muscles were dissected from 5 *mdx*/Actg1-TG mice and 3 non-transgenic *mdx* littermates and pulverized into powder with a liquid nitrogen-cooled mortar and pestle. We closely followed the protein extraction and preparation steps as well as offline peptide fractionation described previously (Oliva Chávez et al., 2015) with slight modifications. We added 10 µL of lysis buffer per milligram of tissue for protein extraction and sonicated. A 105 µL aliquot of each lysate was run in the Barocycler NEP2320 (Pressure Biosciences, South Easton, MA) after which a Bradford assay was performed to determine protein concentrations. We digested 100 µg of each sample with trypsin, performed solid phase extractions (SPE) clean-up, and reacted 40 µg of each of the eight protein samples with one of the iTRAQ® 8-plex reagents (Sciex, Framingham, MA). iTRAQ labels 113, 114, and 115 were used to label peptides from the 3 *mdx* samples, while iTRAQ labels 116, 117, 118, 119, and 121 were used to label peptides from the 5 *mdx*/Actg1-TG samples. We mixed equal aliquots of each protein sample (40 µg), processed by SPE clean-up, and performed peptide fractionation by liquid chromatography (LC). We performed the 2nd dimension capillary LC separation of peptides in-line with an Orbitrap Velos mass spectrometer as previously described (Lin-Moshier et al., 2013). Slight variations in the mass spectrometer acquisition method were: lock mass was not used, HCD activation time was 20 msec, dynamic exclusion duration

was 15 sec and the minimum signal threshold for data dependent trigger was 20,000 counts.

We converted the raw MS datafiles to MGF files with MS Convert from ProteoWizard Toolkit (Chambers et al., 2012). We used ProteinPilot™ v4.5 (Sciex, Framingham, MA) for the database search and quantification report with the following parameters: NCBI RefSeq mouse (Taxonomy ID: 10088) protein database combined with the contaminants database (http://www.thegpm.org/cRAP/index.html); 8-plex peptide label sample type; cysteine methyl methanethiosulfonate; trypsin; instrument Orbi MS (1–3ppm) Orbi MS/MS; biological modifications ID focus; thorough search effort; detected protein threshold 0.05 (10%); competitive error margin 2.00; and false discovery rate analysis invoked (with reversed database). False discovery rate (FDR) calculations were performed in ProteinPilot™ with the concatenated forward and reversed protein sequence databases according to the method previously reported (Tang et al., 2008). ProteinPilot™ calculates an average protein relative fold change between two conditions along with a 95% confidence interval for the fold change and a p-value for a test of the null hypothesis unity (1:1 ratio), which helps assess the statistical significance of a fold change.

qRT-PCR

Gastrocnemius of WT, *mdx*, and *mdx*/Actg1-TG mice were flash frozen in liquid N_2 and pulverized to a powder with a cooled mortar and pestle. Total RNA

was then extracted from each sample using the Aurum Total RNA Mini Kit (Bio-Rad) following the manual's instructions. RNA concentration and purity ($A_{260/280}$ ratio) were determined using a NanoDrop 1000 spectrophotometer (ThermoFisher Scientific). Reverse transcription was performed using the iScript Advanced cDNA Synthesis Kit for qRT-PCR (Bio-Rad) using the same initial RNA amount (1 µg) for all samples. qPCR reactions were prepared with the SsoAdvanced Universal SYBR Green Supermix (Bio-Rad) and quantified on a CFX96 Real Time System C1000 Touch Thermal Cycler (Bio-Rad). Primer sets for both PrxII and HPRT (loading control) were generated with Primer-BLAST software (NIH) to amplify across an exon junction, and are listed in the Key Resources Table. Significance of gene expression differences was determined by one-way ANOVA with Tukey post hoc test analysis. Resulting qRT-PCR reactions were further run on a 1% agarose gel for visualization.

Protein expression and purification

FLAG-tagged PrxII and Fascin-1 proteins were expressed and purified in Sf9 insect cells using the Bac-to-Bac protocol (Invitrogen). Briefly, recombinant baculoviral DNA was transfected into a small culture of Sf9 insect cells using CellFectin II (Invitrogen). Four days later, the media containing the recombinant baculovirus was harvested and the transfected cells were analyzed for protein expression by anti-FLAG western blot. Once expression was validated, large (250 mL) cultures were incubated for 3 days with amplified baculovirus before

being harvested for protein purification. For purification, cells were lysed using 1% Triton X-100 in PBS (8 mM NaH_2PO_4, 42 mM Na_2HPO_4, 150 mM NaCl, pH 7.5) containing protease inhibitors (100 nM aprotinin, 1 mM benzamidine, 10 µM E-64, 10 µM leupeptin, 1 mM pepstatin A, and 1 mM phenylmethanesulfonylfluoride) and protein was purified using ANTI-FLAG M2 affinity gel (Sigma-Aldrich). Proteins were dialyzed into PBS overnight at 4°C before being concentrated and used in *in vitro* F-actin and G-actin binding assays (Figure S1). Recombinant γ_{cyto}-actin was expressed in the Bac-to-Bac insect cell expression system and purified as previously described (Patrinostro et al., 2017; Perrin et al., 2013) before being used as a standard curve in determination of C272A-TG and Actb-TG transgene concentrations (Figure S6).

F-actin cosedimentation assay

A previously described F-actin high speed cosedimentation assay (Perrin et al., 2013) was used to measure binding properties of PrxII and Fascin-1 (positive control). Briefly, human platelet actin (Cytoskeleton) was resuspended in G-Buffer (5 mM Tris-HCl pH 8.0, 0.2 mM $CaCl_2$, 0.2 mM ATP, and 0.5 mM DTT), then induced to polymerize with the addition of 10x Polymerization Buffer (100 mM Tris pH 7.5, 500 mM KCl, 20 mM $MgCl_2$, and 10 mM ATP). Recombinant FLAG-PrxII or FLAG-Fascin-1 (1 µM each) was then incubated with various concentrations of F-actin (0-15 µM) for 30 min at RT. Samples then underwent high speed centrifugation at 100,000 x *g* for 30 min at 4°C. Resulting

supernatant and pellet fractions were subjected to SDS-PAGE, stained with Coomassie blue, and scanned using the Licor Odyssey system allowing quantification of supernatant and pellet fractions. The values from these experiments were plotted in GraphPad Prism software and nonlinear regression analysis was performed.

G-actin binding assay

Human platelet actin (Cytoskeleton) was resuspended in G-Buffer (5 mM Tris-HCl pH 8.0, 0.2 mM $CaCl_2$, 0.2 mM ATP, and 0.5 mM DTT) to maintain actin in its globular form (G-actin). 400 µL mixtures of 1 µM G-actin alone (negative control) and 1 µM G-actin + 1 µM FLAG-PrxII (experiment) were made. 100 µL of both mixtures were taken as the "Load" fraction. 100 µL of each protein mixture was then added to 25 µL of ANTI-FLAG M2 affinity beads and incubated for 1 hour at 4°C with end-over-end rotation. The beads were then centrifuged at 1,000 rpm for 3 minutes at 4°C and the supernatant was collected as the "Void" fraction. The beads were then washed three times with 400 µL G-buffer before adding 100 µL of 0.1 mg/mL FLAG peptide in G-Buffer and incubating at RT for 10 minutes. Samples were then centrifuged as before and the supernatants were collected as the "Elute" fraction. To ensure the G-actin was indeed in its globular form, 100 µM of both protein mixtures was incubated at RT for 30 minutes before being subjected to high speed centrifugation (100,000 x *g*) for 30 min at 4°C. The supernatant and pellet fractions were then collected and run with each Load,

Void, and Elute fraction on SDS-PAGE. Gels were then Coomassie stained and scanned on the Licor Odyssey imaging system.

PrxII Immunoprecipitation

PrxII was immunoprecipitated from *mdx*/Actg1-TG muscle using the Pierce Crosslink Magnetic IP/Co-IP Kit (ThermoFisher Scientific) following the manual's instructions. Briefly, gastrocnemius muscles from *mdx*/Actg1-TG mice were flash frozen and pulverized to a powder with a cooled mortar and pestle. *mdx*/Actg1-TG muscles were used because γ_{cyto}-actin is expressed at such low levels in WT mice that it cannot be detected with typical western blotting. Samples were then solubilized with the kit's IP Lysis Buffer (25 mM Tris pH 7.4, 150 mM NaCl, 1 mM EDTA, 1% NP-40, and 5% glycerol) supplemented with protease inhibitors (100 nM aprotinin, 1 mM benzamidine, 10 µM E-64, 10 µM leupeptin, 1 mM pepstatin A, 1 mM phenylmethanesulfonylfluoride, 1 µM calpain inhibitor I, and 1 µM calpeptin) by incubating for 30 min at 4°C with end-over-end rotation. Lysates were then cleared by centrifugation at 14,000 rpm for 10 minutes at 4°C and protein concentrations were determined using the Pierce BCA Protein Assay Kit (ThermoFisher Scientific). Samples were diluted to 0.5 mg/mL in 1mL of IP Lysis Buffer. During the protein sample preparation, 10 µg PrxII antibody (Sigma) was coupled to Protein A/G magnetic beads and crosslinked using DSS (disuccinimidyl suberate). Diluted protein was then incubated with the crosslinked magnetic beads for 1 hour at RT. Beads were

washed thoroughly before the sample was eluted with low pH Elution Buffer. Load, Void, Wash, and Elute fractions collected during the Immunoprecipitation were subjected to SDS-PAGE, transferred to PVDF membranes, blocked with 5% milk in PBS, and probed with PrxII (Sigma) and γ_{cyto}-actin (2-4) primary antibodies overnight at 4°C. Membranes were incubated with DyLight secondary antibodies before being scanned on the Licor Odyssey imaging system.

Cloning and Generation of transgenic mice

Human peroxiredoxin-2 plasmid cDNA was purchased from DNASU Plasmid Repository (Cat #HsCD00076134), PCR amplified, inserted into the Gateway entry vector pENTR/D-TOPO (Invitrogen), and sequence verified. All PCRs were performed using PfuUltra Fusion HS DNA Polymerase (Agilent Technologies). To make recombinant FLAG-PrxII protein, pENTR/D-TOPO-PRDX2 was N-terminally FLAG-tagged (pENTR/D-TOPO-N-FLAG-PRDX2) via PCR using primers that amplified the entire plasmid with FLAG sequence overhangs. The linear PCR product was circularized via the addition of T4 polynucleotide kinase and T4 DNA ligase (New England Biolabs) and sequence verified. Once verified, the entry vector was recombined into the Gateway insect cell destination vector pDEST8 (pDEST8-N-FLAG-PRDX2) using LR Clonase II (Invitrogen) and subsequently expressed in Sf9 insect cells using the Bac-to-Bac system (Invitrogen; see Protein expression and purification). To generate the PrxII-TG transgene, pENTR/D-TOPO-PRDX2 was recombined into a pDEST8

destination vector already containing the HSA promoter followed by the VP1 intron and tandem SV40 polyadenylation sequences (pDEST8-HSA-VP1-SV40-SV40). The PrxII cDNA was inserted in-frame between the VP1 intron and the first SV40 polyadenylation sequence (pDEST8-HSA-VP1-PRDX2-SV40-SV40). The construct was transformed into DH5α bacteria cells and extracted using the Wizard *Plus* SV Minipreps DNA Purification System (Promega). The DNA fragment from the HSA promoter through the polyadenylation sequence was restriction digested to linearize the transgene, gel purified via the QIAEX II Gel Extraction Kit (Qiagen), and sent to the Murine Genetics Core at The Scripps Research Institute for pronuclear microinjection into fertilized C57BL/6 zygotes, which were then implanted into pseudo-pregnant female mice.

We obtained Fascin-1 cDNA (FSCN1) as a kind gift from Dr. Steven Almo of the Albert Einstein College of Medicine. FSCN1 was PCR amplified, inserted into the Gateway entry vector pENTR/D-TOPO (Invitrogen), and sequence verified. To make recombinant FLAG-Fascin-1 protein, pENTR/D-TOPO-FSCN1 was N-terminally FLAG-tagged (pENTR/D-TOPO-N-FLAG-FSCN1) via PCR using primers that amplified the entire plasmid with FLAG sequence overhangs. The linear PCR product was circularized via the addition of T4 polynucleotide kinase and T4 DNA ligase (New England Biolabs) and sequence verified. Once verified, the entry vector was recombined into the Gateway insect cell destination vector pDEST8 (pDEST8-N-FLAG-FSCN1) using LR Clonase II (Invitrogen) and

subsequently expressed in Sf9 insect cells using the Bac-to-Bac system (Invitrogen; see Protein expression and purification).

To generate C272A-TG and Actb-TG transgenes, both the pDEST8-HSA-VP1-C272A-SV40-SV40 (C272A-TG) and pDEST8-HSA-VP1-ACTB-SV40-SV40 (Actb-TG) constructs were cloned based on the original pDEST8-HSA-VP1-ACTG1-SV40-SV40 (Actg1-TG) construct previously described (Jaeger et al., 2009). The C272A-TG construct was generated via site-directed mutagenesis using the QuikChange II XL kit (Agilent Technologies, Cat# 200521) according to manufacture protocols and sequence verified. Primers were designed to allow a two-nucleotide change within the codon normally encoding Cysteine to then encode for Alanine at position 272 (TGT to GCT). For Actb-TG, only the ACTG1 nucleotides that coded for the 4 γ_{cyto}-actin-specific amino acids (Glu2, Glu3, Glu4, and Ile10) were altered to instead code for the 4 β_{cyto}-actin-specific amino acids (Asp2, Asp3, Asp4, and Val10) by editing the wobble base in each codon within the construct. This ensures any differences described between transgenic mice are only due to the altered amino acids, and not plasmid differences. The Actb-TG construct was generated via PCR using primers designed such that they amplified the Actg1-TG plasmid with ACTB-specific overhangs. The linear PCR product was circularized via the addition of T4 polynucleotide kinase and T4 DNA ligase (New England Biolabs) and sequence verified. Both constructs were transformed into DH5α bacteria cells and extracted using the Wizard *Plus* SV Minipreps DNA Purification System (Promega). The DNA fragment from the HSA

promoter through the polyadenylation sequence was restriction digested to linearize the transgene, gel purified via the QIAEX II Gel Extraction Kit (Qiagen), and sent to the Murine Genetics Core at The Scripps Research Institute for pronuclear microinjection into fertilized C57BL/6 zygotes, which were then implanted into pseudo-pregnant female mice.

Resultant PrxII-TG, C272A-TG, and Actb-TG transgenic founder mice were identified by PCR using HSA-specific primers (Forward: 5'-GTC AGG AGG GGC AAA CCC GC-3', Reverse: 5'-GTC GCT GCC CTT CTC GAG CC-3', Product Size: 187 bp) and crossed with C57BL/10 mice to check for transgene transmission. Transgenic PrxII (PrxII-TG), γ_{cyto}-actin (C272A-TG), and β_{cyto}-actin (Actb-TG) protein expression was assessed in several different muscles from each transgenic line crossed onto the *mdx* (C57BL/10ScSn-*Dmd*^{mdx}/J) background using quantitative western blotting. All *mdx*-transgenic mice used in this study were compared with non-transgenic littermate *mdx* mice as controls.

Stretch-induced ROS measurements

Flexor digitorum brevus (FDB) muscles were surgically isolated and incubated in DMEM (ThermoFisher Scientific) containing 0.1% penicillin-streptomycin (ThermoFisher Scientific) and 0.4% Collagenase A (Sigma-Aldrich) at 37˚C for 2 hours. Single FDB fibers were isolated by gentle trituration in DMEM containing 0.1% penicillin-streptomycin and 10% fetal bovine serum (ThermoFisher Scientific) and incubated at 37˚C, 5% CO_2 until used, typically

16–20 hours later. Isolated FDB fibers were washed three times with HEPES solution (120 mM NaCl, 4.7 mM KCl, 1.8 mM $CaCl_2$, 600 µM $MgSO_4$, 1.6 mM $NaHCO_3$, 130 µM NaH_2PO_4, 7.8 mM Glucose, and 20 mM HEPES) and loaded with 15 µM DCFH-DA (6-Carboxy-2',7'-Dichlorodihyrofluorescin Diacetate, Invitrogen) for 25 minutes at RT in the dark. The fibers were then washed three times with HEPES solution containing either DMSO (0.1%) or gp91ds-tat (10µM) and the DCFH-DA dye was allowed to de-esterify for 15 min at RT in the dark. The ends of each fiber were attached to a micro-glass pipet coated with a biological adhesive (ECM Gel from Engelbreth-Holm-Swarm murine sarcoma, Sigma-Aldrich) and connected to micro-manipulators (Sutter Instruments). DCF Fluorescence (Ex: 480 nm, Em: 535/40 nm) and sarcomere length were acquired using an IonOptix system (Westwood, MA) atop a Motic AE31 microscope equipped with a 40x objective (Olympus UAP040X3/340). Each fiber was cyclically stretched to 110% of resting sarcomeric length (2 µm - 2.2 µm) at 10 µm/s for 15 min. The rate of DCF fluorescence was reported during the last 2.5 min of stretch.

Quantification and Statistical Analysis

All statistics were calculated using GraphPad Prism software. All data are presented as mean ± SEM in force loss graphs, dot plots, and bar graphs. In force loss graphs, two-way ANOVA with Bonferroni post hoc test analyses were performed. For dot plots and bar graphs, one-way ANOVA with Tukey post hoc

test analyses were performed. For applicable experiments, the exact value of n (defined by number of animals) and the definition of significance can be found in the figure legend.

Figures

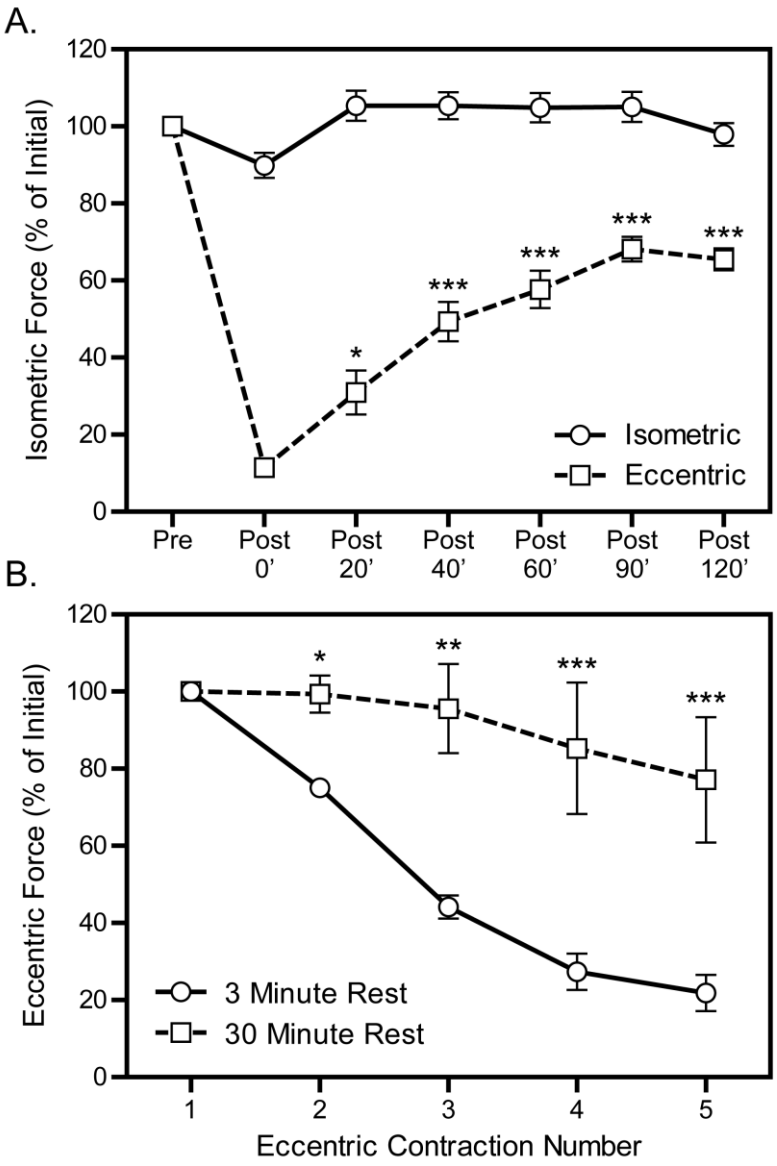

Figure 2-1. Rapid recovery of eccentric contraction-induced force loss in *mdx* muscle. (A) Recovery of isometric force production in isolated extensor digitorum longus (EDL) muscles from *mdx* mice subjected to 10 maximal isometric or eccentric contractions. Values are expressed as a percentage of the isometric force measured before the 10 contractions (Pre) for each timepoint

listed. n ≥ 4 for both conditions. *P < 0.05, ***P < 0.001 compared with Post 0'. (B) Increasing the time interval between eccentric contractions from 3 to 30 minutes significantly diminishes the measured force loss in EDL muscles from *mdx* mice. n ≥ 4 for both conditions. *P < 0.05, **P < 0.01, ***P < 0.001.

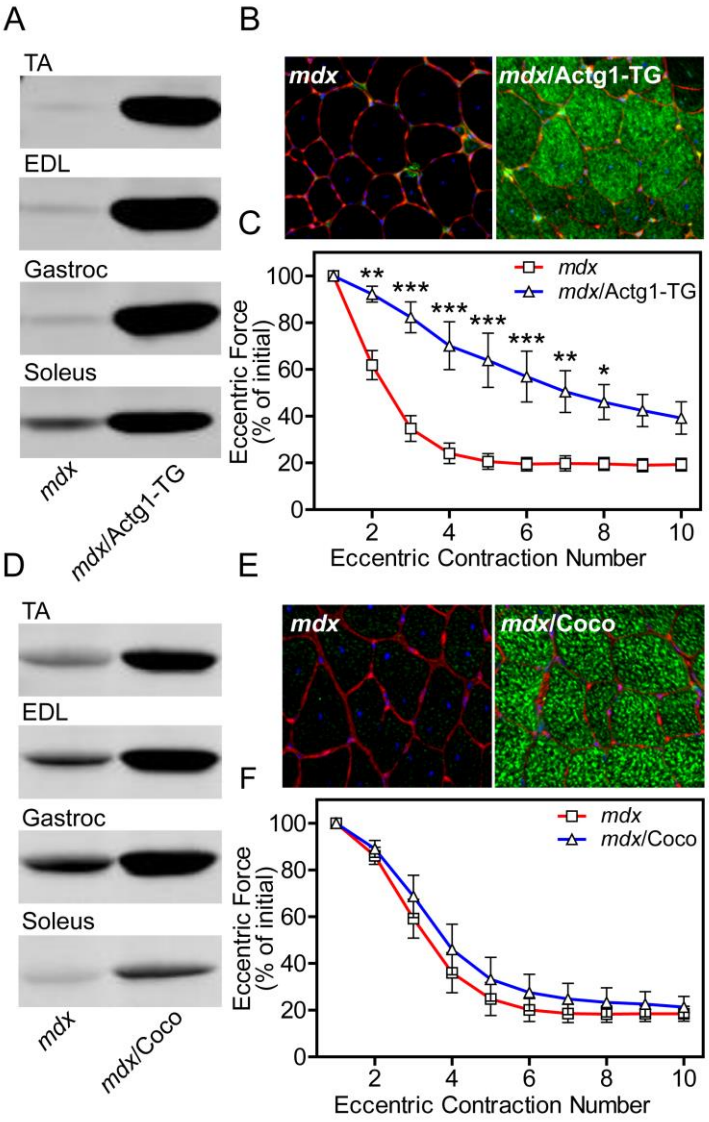

Figure 2-2. Partial protection of *mdx* muscle from eccentric contraction-induced force loss by muscle-specific overexpression of γ_{cyto}-, but not $\alpha_{cardiac}$-actin. (A) Immunoblot analysis of γ_{cyto}-actin in tibialis anterior (TA), extensor digitorum longus (EDL), gastrocnemius (Gastroc), and soleus muscles from *mdx*/Actg1-TG mice versus non-transgenic *mdx* littermates. (B) Immunofluorescence analysis of γ_{cyto}-actin (green), laminin (red), and DAPI

(blue) in 10 µm cryosections of quadriceps muscle from *mdx*/Actg1-TG mice versus non-transgenic *mdx* littermates. (C) EDL muscles isolated from *mdx*/Actg1-TG mice and non-transgenic *mdx* littermates were subjected to 10 eccentric contractions and the force measured at each contraction expressed as a percentage of the force produced during the first contraction. n ≥ 4 for both genotypes. *P < 0.05, **P < 0.01, ***P < 0.001. (D) Immunoblot analysis of α_{ca}-actin in tibialis anterior (TA), extensor digitorum longus (EDL), gastrocnemius (Gastroc), and soleus muscles from *mdx*/Coco mice versus non-transgenic *mdx* littermates. (E) Immunofluorescence analysis of α_{ca}-actin (green), laminin (red), and DAPI (blue) in 10 µm cryosections of quadriceps muscle from *mdx*/Coco mice versus non-transgenic *mdx* littermates. (F) EDL muscles isolated from *mdx*/Coco mice and non-transgenic *mdx* littermates were subjected to 10 eccentric contractions and the force measured at each contraction expressed as a percentage of the force produced during the first contraction. n ≥ 4 for both genotypes.

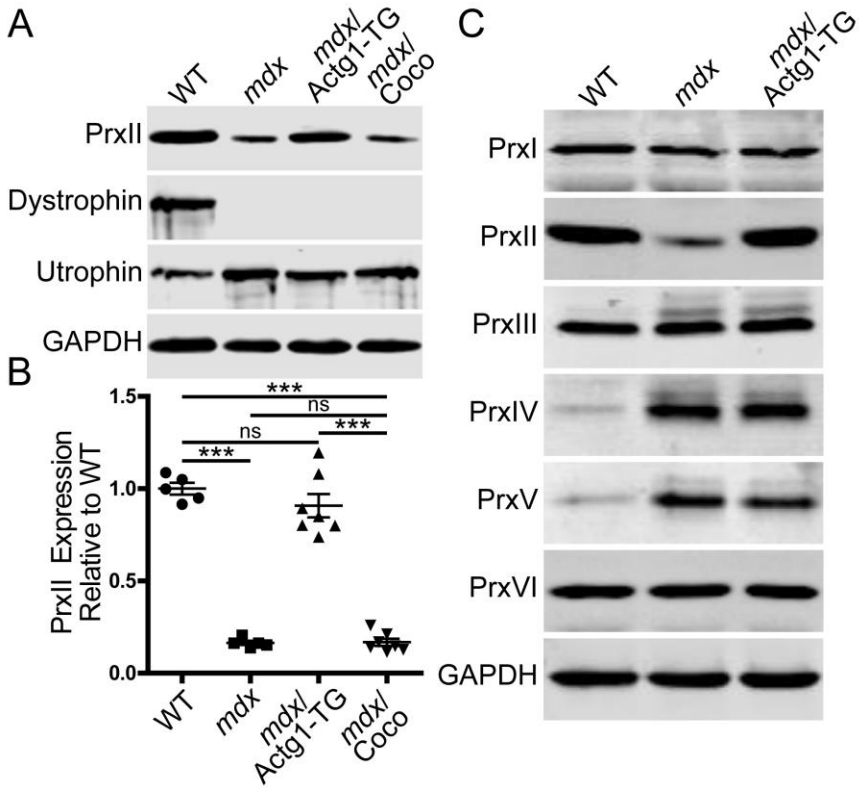

Figure 2-3. Peroxiredoxin-2 is significantly decreased in *mdx* skeletal muscle and restored by γ_{cyto}-actin overexpression. (A) Immunoblot analysis of PrxII, dystrophin, utrophin, and GAPDH in WT, *mdx*, *mdx*/Actg1-TG, and *mdx*/Coco gastrocnemius muscles. (B) Immunoblot quantitation demonstrated that PrxII levels in *mdx* skeletal muscle were 16.5 ± 0.03% of WT and restored in *mdx*/Actg1-TG muscle to levels not different from WT, but not in *mdx*/Coco muscle. n ≥ 5 for each genotype. ***P < 0.001. (C) Immunoblot analysis of peroxiredoxins 1-6 in gastrocnemius muscles from WT, *mdx*, and *mdx*/Actg1-TG mice. PrxII was the only peroxiredoxin isoform that was both altered in *mdx* compared to WT, and also restored to its WT level by muscle-specific γ_{cyto}-actin overexpression.

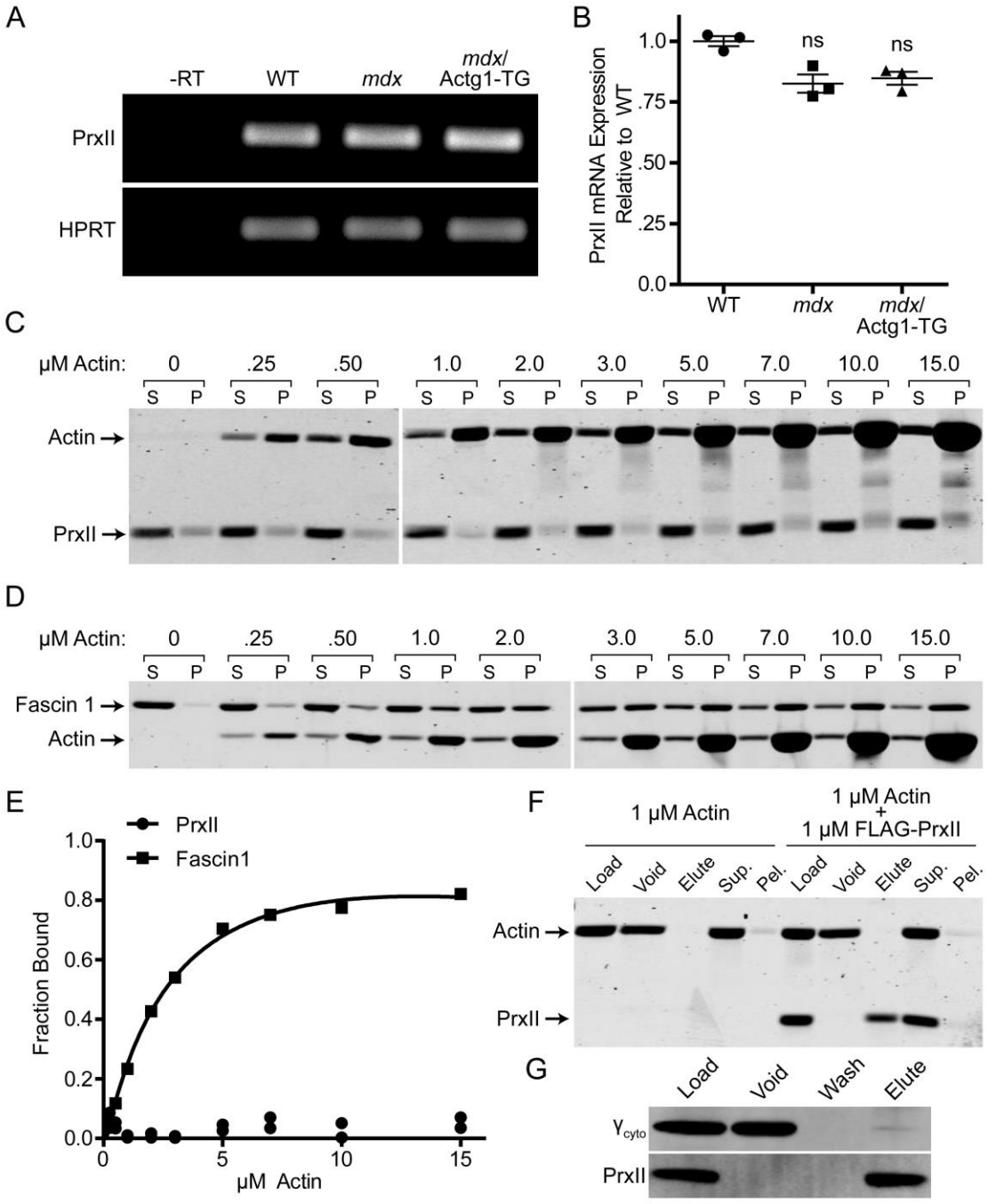
A
-RT
WT
mdx
mdx/ Actg1-TG
PrxII
HPRT
B
PrxII mRNA Expression Relative to WT
1.0
.75
.50
.25
0.0
ns
ns
WT
mdx
mdx/ Actg1-TG
C
µM Actin:
0
.25
.50
1.0
2.0
3.0
5.0
7.0
10.0
15.0
S P
Actin
PrxII
D
µM Actin:
0
.25
.50
1.0
2.0
3.0
5.0
7.0
10.0
15.0
S P
Fascin 1
Actin
E
PrxII
Fascin1
Fraction Bound
1.0
0.8
0.6
0.4
0.2
0.0
0
5
10
15
µM Actin
F
1 µM Actin
1 µM Actin + 1 µM FLAG-PrxII
Load
Void
Elute
Sup.
Pel.
Actin
PrxII
G
Load
Void
Wash
Elute
γcyto
PrxII

Figure 2-4. Decreased peroxiredoxin-2 in *mdx* muscle is post-transcriptional and recovery of protein levels in *mdx*/Actg1-TG is independent of direct γ_{cyto}-actin binding. (A and B) qRT-PCR analysis of PrxII transcript in WT, *mdx*, and *mdx*/Actg1-TG gastrocnemius muscles. n = 3 per genotype. ns = not significant. (C) F-actin cosedimentation assay with increasing platelet actin concentrations (0 – 15 µM) and constant concentrations of recombinant PrxII (1 µM). (D) F-actin cosedimentation assay with increasing platelet actin concentrations (0 – 15 µM) and constant concentrations of recombinant Fascin-1 (1 µM). (E) Binding curves of PrxII and Fascin-1 with platelet actin fitted with regression analysis. (F) G-actin binding assay with either 1 µM platelet actin only, or 1 µM platelet actin + 1 µM FLAG-PrxII. (G) Immunoprecipitation of PrxII from *mdx*/Actg1-TG gastrocnemius muscle immunoblotted for both γ_{cyto}-actin and PrxII.

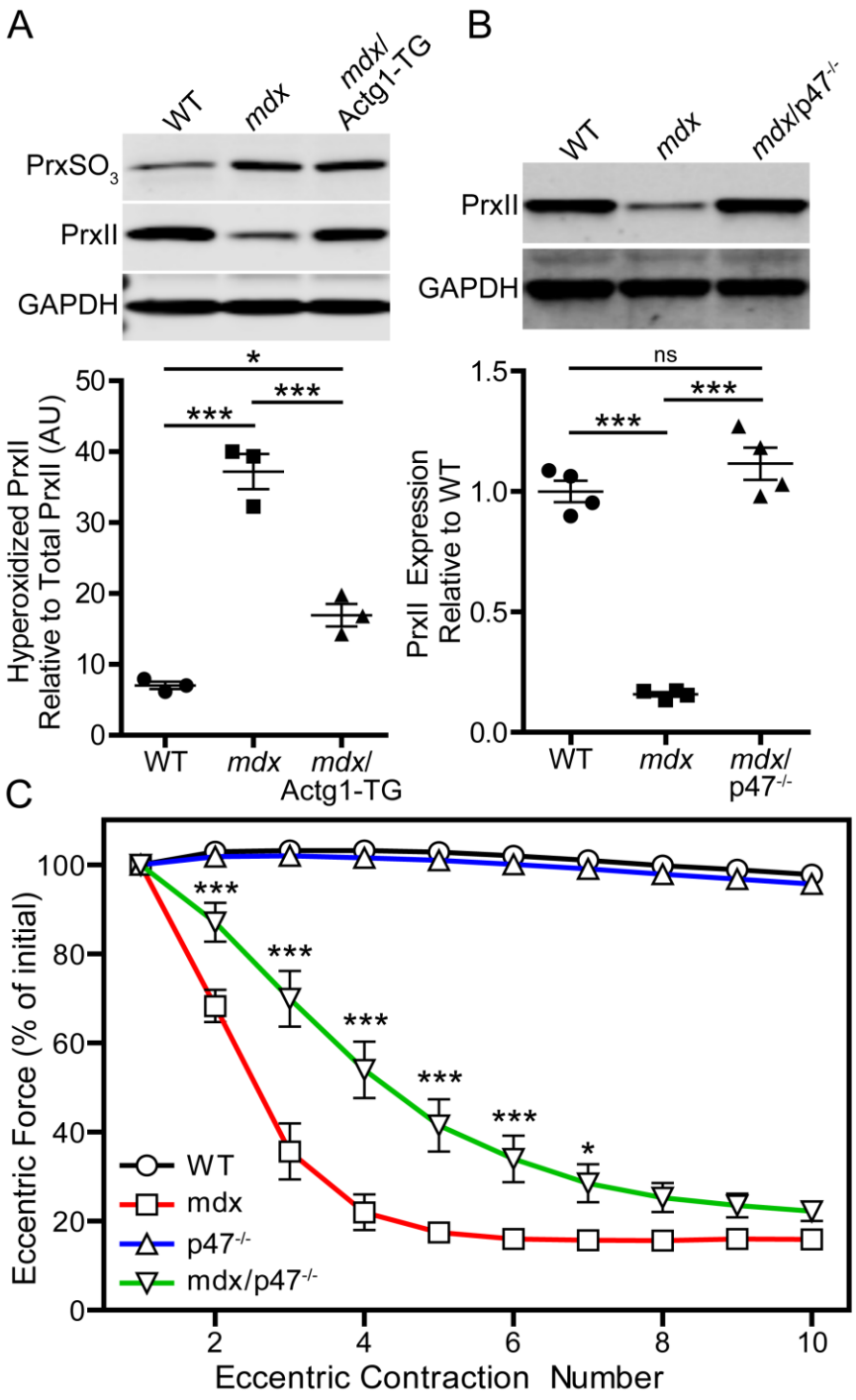
A
WT
mdx
mdx/ Actg1-TG
PrxSO3
PrxII
GAPDH
Hyperoxidized PrxII Relative to Total PrxII (AU)
WT
mdx
mdx/ Actg1-TG
B
WT
mdx
mdx/p47-/-
PrxII
GAPDH
PrxII Expression Relative to WT
ns
WT
mdx
mdx/ p47-/-
C
Eccentric Force (% of initial)
WT
mdx
p47-/-
mdx/p47-/-
Eccentric Contraction Number

Figure 2-5. Genetic ablation of NOX2 activity rescues peroxiredoxin-2 levels and partially protects *mdx* muscle from eccentric contraction-induced force loss. (A) Immunoblot analysis demonstrated significantly elevated hyperoxidized peroxiredoxin ($PrxSO_3$) in *mdx* compared to WT and *mdx*/Actg1-TG gastrocnemius muscles. n = 3 for each genotype. *P < 0.05, ***P < 0.001. (B) Immunoblot analysis of PrxII in WT, *mdx*, and *mdx*/p47$^{-/-}$ gastrocnemius muscles demonstrated a restoration of PrxII to WT levels in *mdx*/p47$^{-/-}$ muscle. n = 4 for each genotype. ns = no significance, ***P < 0.001. (C) EDL muscles isolated from WT, *mdx*, p47$^{-/-}$, and *mdx*/p47$^{-/-}$ mice were subjected to 10 eccentric contractions and the forces measured expressed as a percentage of the force generated during the first eccentric contraction. n ≥ 3 for each genotype. *P < 0.05, ***P < 0.001.

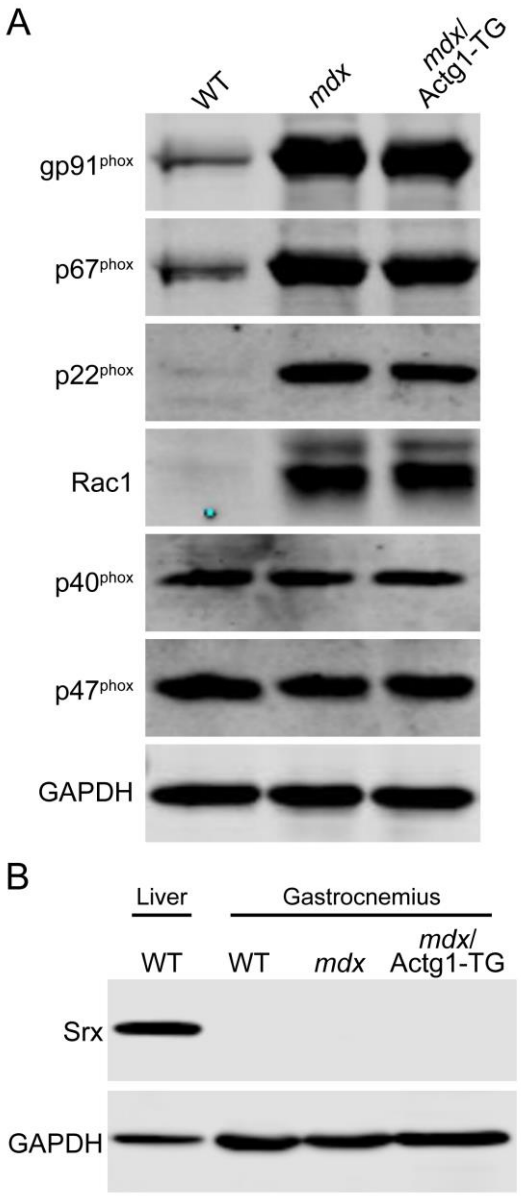

Figure 2-6. Validation of NOX2 increase in *mdx* muscle and lack of sulfiredoxin in skeletal muscle. (A) Immunoblot analysis of all six NOX2 subunits in WT, *mdx*, and *mdx*/Actg1-TG gastrocnemius muscles. (B) Immunoblot analysis of sulfiredoxin in WT liver (positive control), as well as WT, *mdx*, and *mdx*/Actg1-TG gastrocnemius.

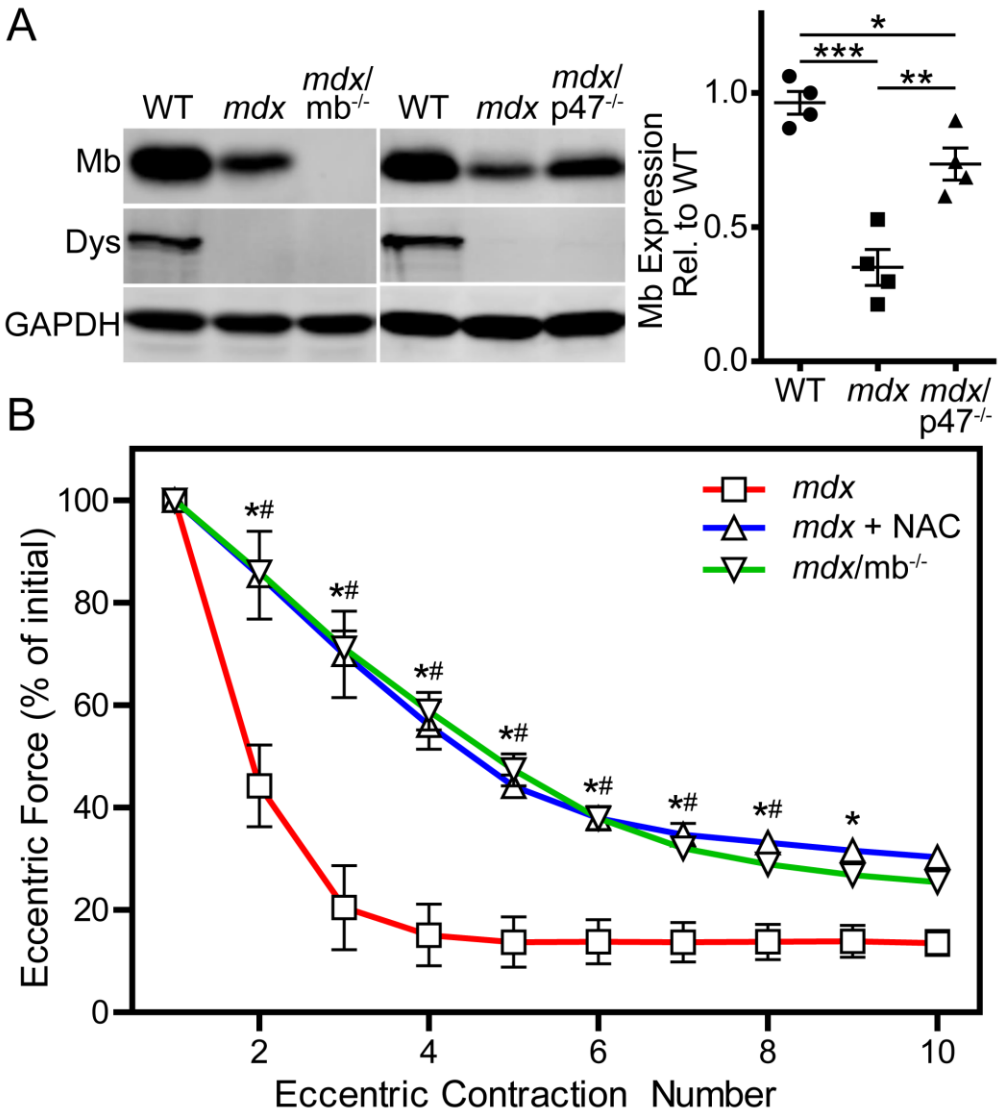

Figure 2-7. Genetic ablation of myoglobin partially protects *mdx* muscle from eccentric contraction-induced force loss. (A) Immunoblot analysis demonstrated the absence of myoglobin in *mdx*/mb$^{-/-}$ muscle, that myoglobin levels are decreased in *mdx,* and that myoglobin levels are partially restored in *mdx*/p47$^{-/-}$ gastrocnemius muscle. n ≥ 4 for each genotype. *P < 0.05, **P < 0.01, ***P < 0.001. (B) EDL muscles isolated from *mdx* and *mdx*/mb$^{-/-}$ mice, or *mdx*

muscles treated with 20 mM N-acetylcysteine (NAC) were subjected to 10 eccentric contractions and the forces measured expressed as a percentage of the force generated during the first eccentric contraction. n ≥ 4 for each genotype. **mdx* + NAC significantly different from *mdx* ($P \leq 0.05$), $^{\#}$*mdx*/mb$^{-/-}$ significantly different from *mdx* ($P \leq 0.05$).

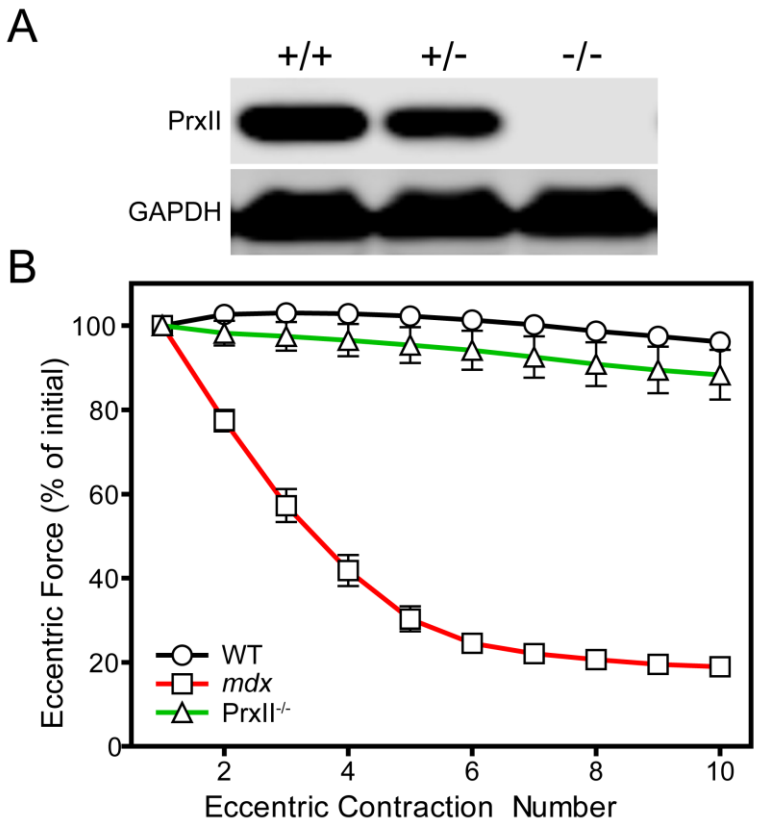

Figure 2-8. Validation of PrxII-specific antibody and lack of effect of PrxII deletion on ECC-induced force loss in WT muscle. (A) Immunoblot analysis of PrxII (Sigma-Aldrich, R8656) in PrxII$^{+/+}$, PrxII$^{+/-}$, and PrxII$^{-/-}$ gastrocnemius. (B) EDL muscles isolated from WT, *mdx*, and PrxII$^{-/-}$ mice were subjected to 10 eccentric contractions and the force measured at each contraction expressed as a percentage of the force produced during the first contraction. n ≥ 3 for all genotypes.

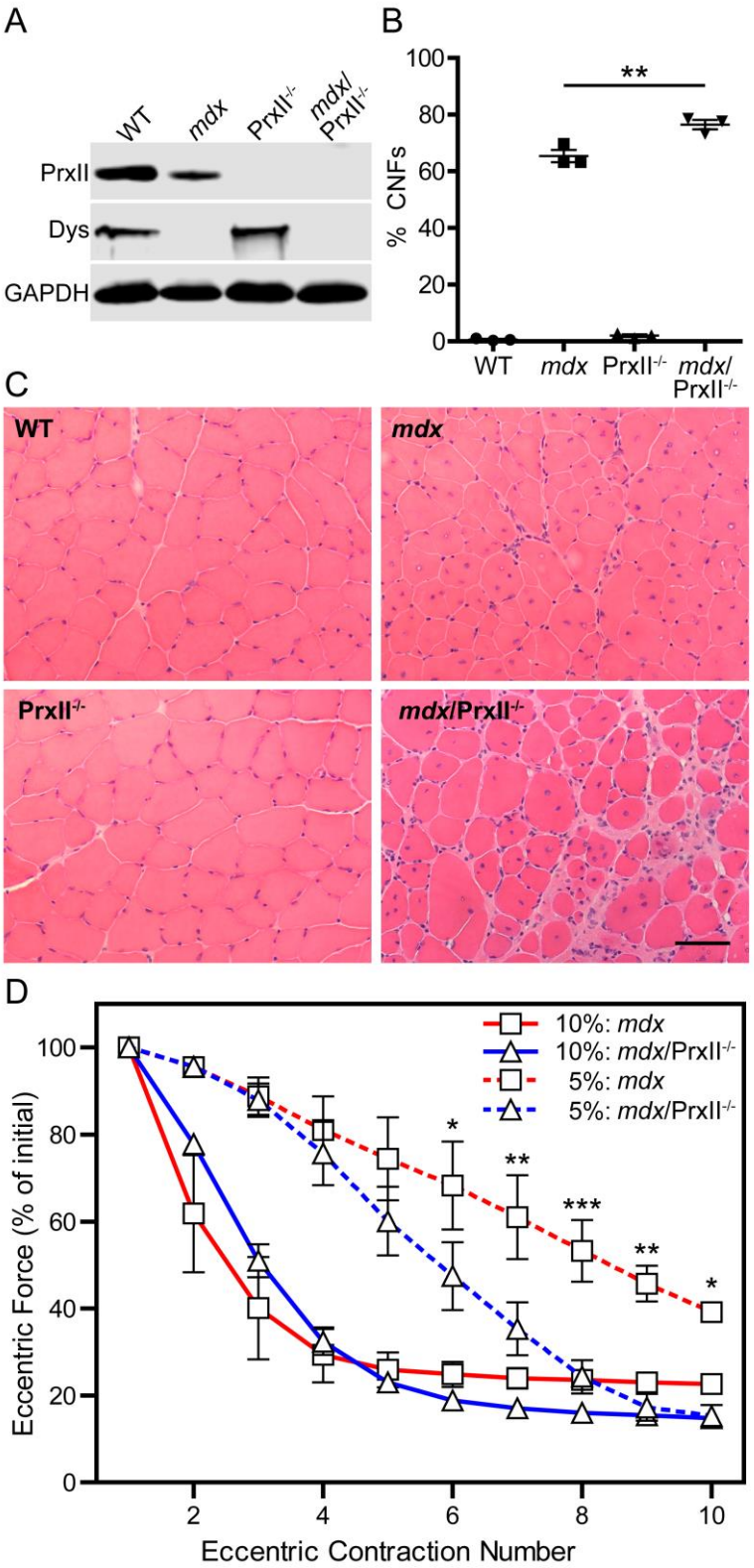
A
WT
mdx
PrxII-/-
mdx/ PrxII-/-
PrxII
Dys
GAPDH
B
% CNFs
100
80
60
40
20
0
**
WT
mdx
PrxII-/-
mdx/ PrxII-/-
C
WT
mdx
PrxII-/-
mdx/PrxII-/-
D
10%: mdx
10%: mdx/PrxII-/-
5%: mdx
5%: mdx/PrxII-/-
Eccentric Force (% of initial)
100
80
60
40
20
0
2
4
6
8
10
Eccentric Contraction Number
*
**
***
**
*

Figure 2-9. Genetic ablation of peroxiredoxin-2 further sensitizes *mdx* muscle to eccentric contraction-induced force loss. (A) Immunoblot analysis of PrxII in WT, *mdx*, PrxII$^{-/-}$, and *mdx*/PrxII$^{-/-}$ gastrocnemius demonstrated the absence of PrxII in PrxII$^{-/-}$ and *mdx*/PrxII$^{-/-}$ muscle. (B) A small but significant increase in the percentage of centrally nucleated fibers (%CNFs) was seen in *mdx*/PrxII$^{-/-}$ versus *mdx* muscle quantified from 10 µm cryosections of quadriceps stained with H&E. n = 3 for each genotype. **P < 0.01. (C) Representative images of 10 µm cryosections of quadriceps from WT, *mdx*, PrxII$^{-/-}$, and *mdx*/PrxII$^{-/-}$ stained with H&E. Scale bar: 50 µm. (D) EDL muscles isolated from *mdx* and *mdx*/PrxII$^{-/-}$ mice were subjected to 10 eccentric contractions with either a 5% or 10% length change, and the forces measured expressed as a percentage of the force generated during the first eccentric contraction. There was no significant difference between *mdx* and *mdx*/PrxII$^{-/-}$ with a 10% length change, but a 5% length change revealed a significant difference between *mdx* and *mdx*/PrxII$^{-/-}$ for contractions 6-10. n = 4 for each genotype/condition. *P < 0.05, **P < 0.01, ***P < 0.001.

A

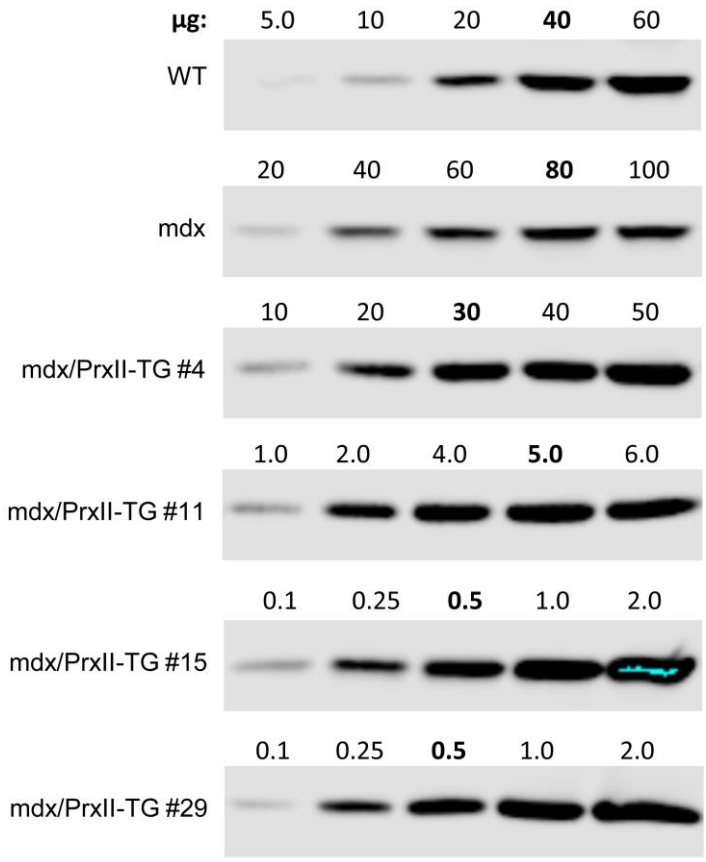

B

PrxII-TG Line	Overexpression Rel. to WT
#4	1.33 ±0.22
#11	11.93 ±1.49
#15	58.32 ±10.31
#29	111.70 ±9.84

Figure 2-10. Relative quantitation of PrxII overexpression levels in *mdx* skeletal muscle. (A) Linear ranges of PrxII immunoreactivity were found for WT, *mdx*, and each *mdx*/PrxII-TG line (#4, #11, #15, and #29). The amount of lysate (in µg) in each line that best matched the signal seen in 40 µg of WT lysate is

labeled in bold. (B) Using the bold values in (A) for each *mdx*/PrxII-TG line compared to 40 µg of WT, PrxII overexpression levels relative to WT were obtained. n ≥ 3 for each *mdx*/PrxII-TG line.

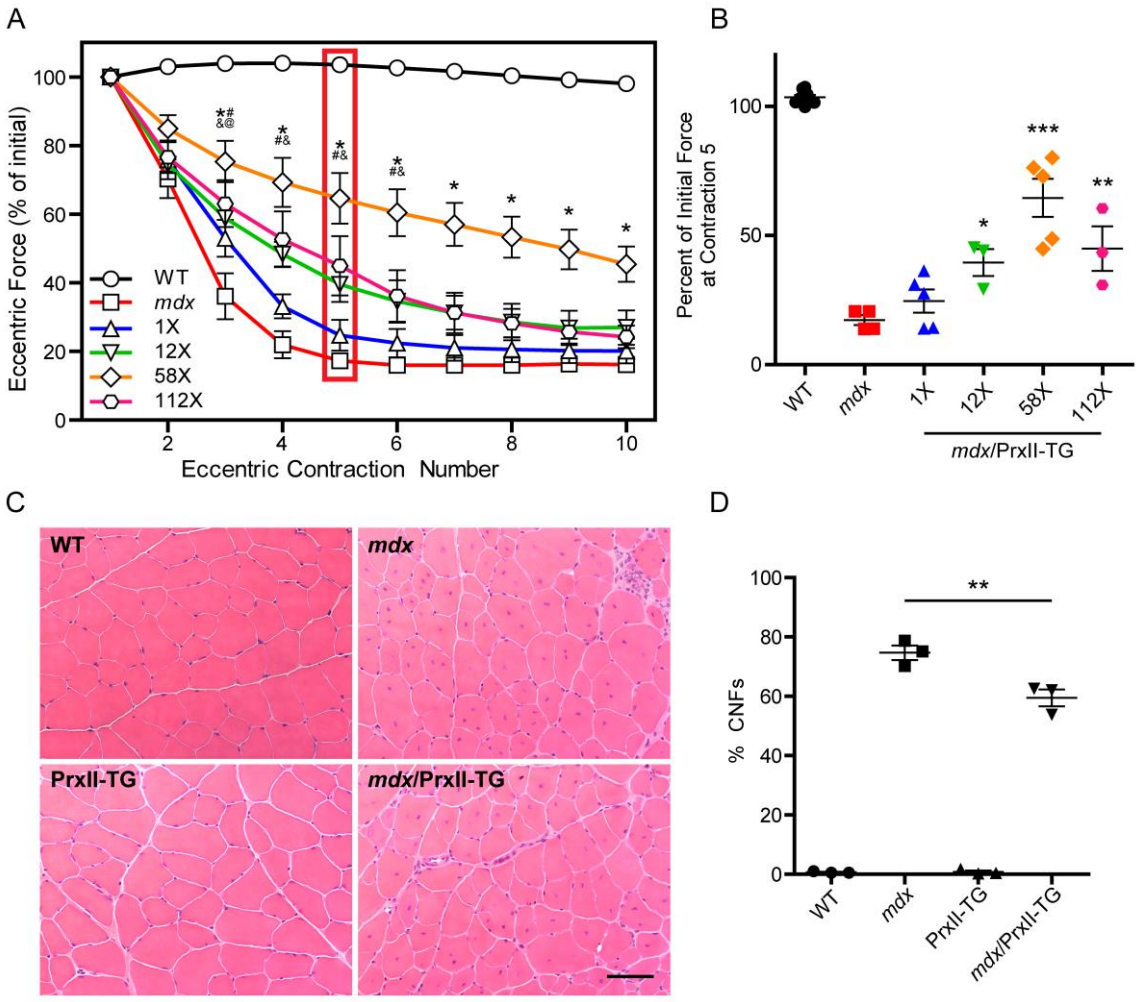

Figure 2-11. Muscle-specific peroxiredoxin-2 overexpression partially protects *mdx* muscle from eccentric contraction-induced force loss. (A) EDL muscles isolated from WT, *mdx*, and *mdx*/PrxII-TG lines expressing PrxII at 1-, 12-, 58-, and 112-fold relative to WT were subjected to 10 eccentric contractions and the forces measured expressed as a percentage of the force generated during the first eccentric contraction. n ≥ 3 for each genotype. $^{@}$1X significantly different from *mdx* ($P < 0.05$), $^{\#}$12X significantly different from *mdx* (P

< 0.05), *58X significantly different from *mdx* (P < 0.001), &112X significantly different from *mdx* (P < 0.05). (B) The force produced at contraction 5 for each line was presented as a percentage of initial force. n ≥ 3 for each genotype. *P < 0.05, **P < 0.01, ***P < 0.001. (C) Representative images of 10 μm cryosections of quadriceps from WT, *mdx*, PrxII-TG, and *mdx*/PrxII-TG (58X) stained with H&E. Scale bar: 50 μm. (D) 58-fold PrxII overexpression caused a small but significant decrease in the percentage of centrally nucleated fibers (%CNFs) in *mdx* quadriceps muscle. n = 3 for each genotype. **P < 0.01.

alpha-skeletal actin

Ac-DEDETTALVCDNGSGLVKAGFAGDDAPRAVFPSIVGRPRHQGVMVGMGQKDSYVGDEAQSKRGILTL
KYPIEHGIITNWDDMEKIWHHTFYNELRVAPEEHPTLLTEAPLNPKANREKMTQIMFETFNVPAMYVAIQ
AVLSLYASGRTTGIVLDSGDGVTHNVPIYEGYALPHAIMRLDLAGRDLTDYLMKILTERGYSFVTTAERE
IVRDIKEKLCYVALDFENEMATAASSSSLEKSYELPDGQVITIGNERFRCPETLFQPSFIGMESAGIHET
TYNSIMKCDIDIRKDLYANNVMSGGTTMYPGIADRMQKEITALAPSTMKIKIIAPPERKYSVWIGGSILA
SLSTFQQMWITKQEYDEAGPSIVHRKCF

alpha-cardiac actin

Ac-DDEETTALVCDNGSGLVKAGFAGDDAPRAVFPSIVGRPRHQGVMVGMGQKDSYVGDEAQSKRGILTL
KYPIEHGIITNWDDMEKIWHHTFYNELRVAPEEHPTLLTEAPLNPKANREKMTQIMFETFNVPAMYVAIQ
AVLSLYASGRTTGIVLDSGDGVTHNVPIYEGYALPHAIMRLDLAGRDLTDYLMKILTERGYSFVTTAERE
IVRDIKEKLCYVALDFENEMATAASSSSLEKSYELPDGQVITIGNERFRCPETLFQPSFIGMESAGIHET
TYNSIMKCDIDIRKDLYANNVLSGGTTMYPGIADRMQKEITALAPSTMKIKIIAPPERKYSVWIGGSILA
SLSTFQQMWISKQEYDEAGPSIVHRKCF

gamma-cytoplasmic actin

Ac-EEEIAALVIDNGSGMCKAGFAGDDAPRAVFPSIVGRPRHQGVMVGMGQKDSYVGDEAQSKRGILTLK
YPIEHGIVTNWDDMEKIWHHTFYNELRVAPEEHPVLLTEAPLNPKANREKMTQIMFETFNTPAMYVAIQA
VLSLYASGRTTGIVMDSGDGVTHTVPIYEGYALPHAILRLDLAGRDLTDYLMKILTERGYSFTTTAEREI
VRDIKEKLCYVALDFEQEMATAASSSSLEKSYELPDGQVITIGNERFRCPEALFQPSFLGMESCGIHETT
FNSIMKCDVDIRKDLYANTVLSGGTTMYPGIADRMQKEITALAPSTMKIKIIAPPERKYSVWIGGSILAS
LSTFQQMWISKQEYDESGPSIVHRKCF

beta-cytoplasmic actin

Ac-DDDIAALVVDNGSGMCKAGFAGDDAPRAVFPSIVGRPRHQGVMVGMGQKDSYVGDEAQSKRGILTLK
YPIEHGIVTNWDDMEKIWHHTFYNELRVAPEEHPVLLTEAPLNPKANREKMTQIMFETFNTPAMYVAIQA
VLSLYASGRTTGIVMDSGDGVTHTVPIYEGYALPHAILRLDLAGRDLTDYLMKILTERGYSFTTTAEREI
VRDIKEKLCYVALDFEQEMATAASSSSLEKSYELPDGQVITIGNERFRCPEALFQPSFLGMESCGIHETT
FNSIMKCDVDIRKDLYANTVLSGGTTMYPGIADRMQKEITALAPSTMKIKIIAPPERKYSVWIGGSILAS
LSTFQQMWISKQEYDESGPSIVHRKCF

= Conserved

= Muscle actin only

= Cytoplasmic actin only

= Oxidation known

= Oxidation known in cytoplasmic actin only

Figure 2-12. Cysteine residues of striated muscle ($\alpha_{skeletal}$ and $\alpha_{cardiac}$) and cytoplasmic (γ_{cyto} and β_{cyto}) actins. Amino acid sequences of $\alpha_{skeletal}$-, $\alpha_{cardiac}$-, γ_{cyto}-, and β_{cyto}-actin are listed. Cysteines conserved in all four actins are highlighted in yellow, while cysteines present in muscle actins only are highlighted in red and cysteines present in only cytoplasmic actins are highlighted in green. Cysteines that are known from the literature to undergo oxidation *in vivo* are underlined in blue, while oxidative cysteines unique to cytoplasmic actins are circled in blue.

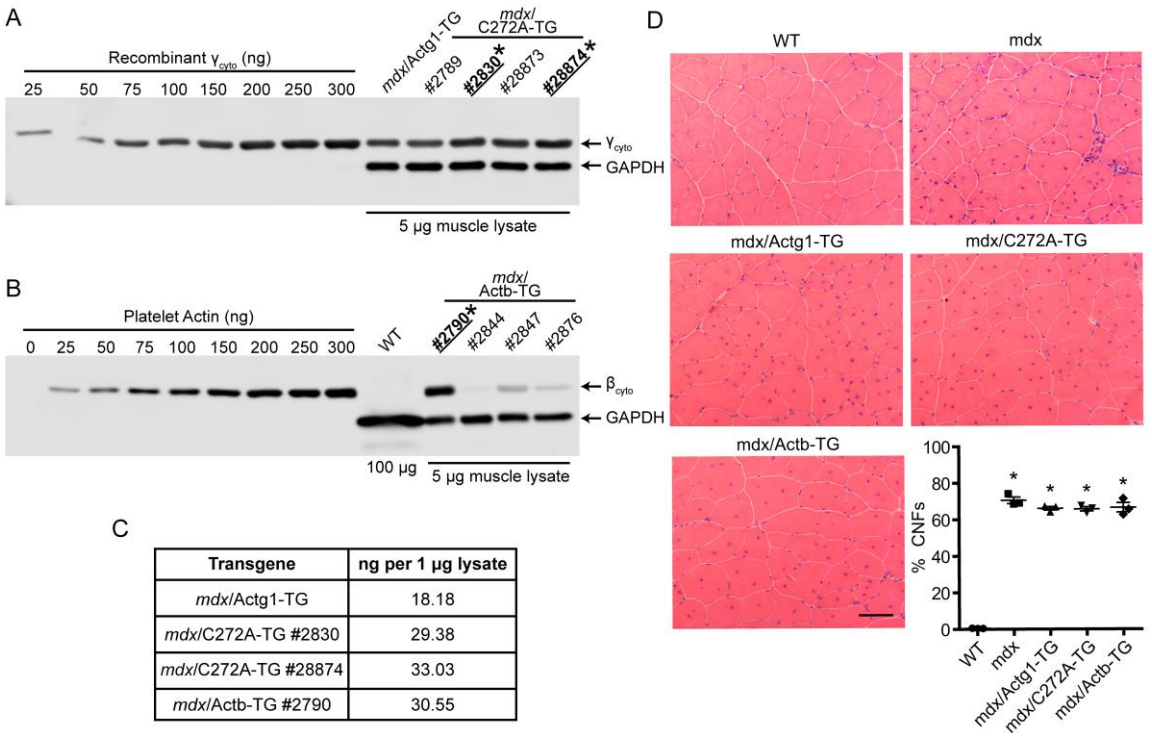

Transgene	ng per 1 µg lysate
mdx/Actg1-TG	18.18
mdx/C272A-TG #2830	29.38
mdx/C272A-TG #28874	33.03
mdx/Actb-TG #2790	30.55

Figure 2-13. Determination of γ_{cyto}^{C272A} and β_{cyto} protein concentrations and histopathology in *mdx*/C272A-TG and *mdx*/Actb-TG muscle. (A) Determination of γ_{cyto}-actin protein expression in 4 *mdx*/C272A-TG lines of mice compared to *mdx*/Actg1-TG using a standard curve of recombinant γ_{cyto}-actin. The standard curve and muscle lysates were immunoblotted for γ_{cyto}-actin. (B) Determination of β_{cyto}-actin protein expression in 4 *mdx*/Actb-TG lines of mice using a standard curve of platelet actin. The standard curve and muscle lysates were immunoblotted for β_{cyto}-actin. (C) Concentrations of γ_{cyto}-actin in the two surviving *mdx*/C272A-TG lines (#2830 and #28874) and β_{cyto}-actin in the one surviving *mdx*/Actb-TG line (#2790) were calculated along with γ_{cyto}-actin in

mdx/Actg1-TG mice. (D) Representative H&E staining and percentage of centrally nucleated fibers (%CNFs) in 10 µm cryosections of quadriceps from WT, *mdx*, *mdx*/Actg1-TG, *mdx*/C272A-TG, and *mdx*/Actb-TG. n = 3. *P < 0.001 compared to WT.

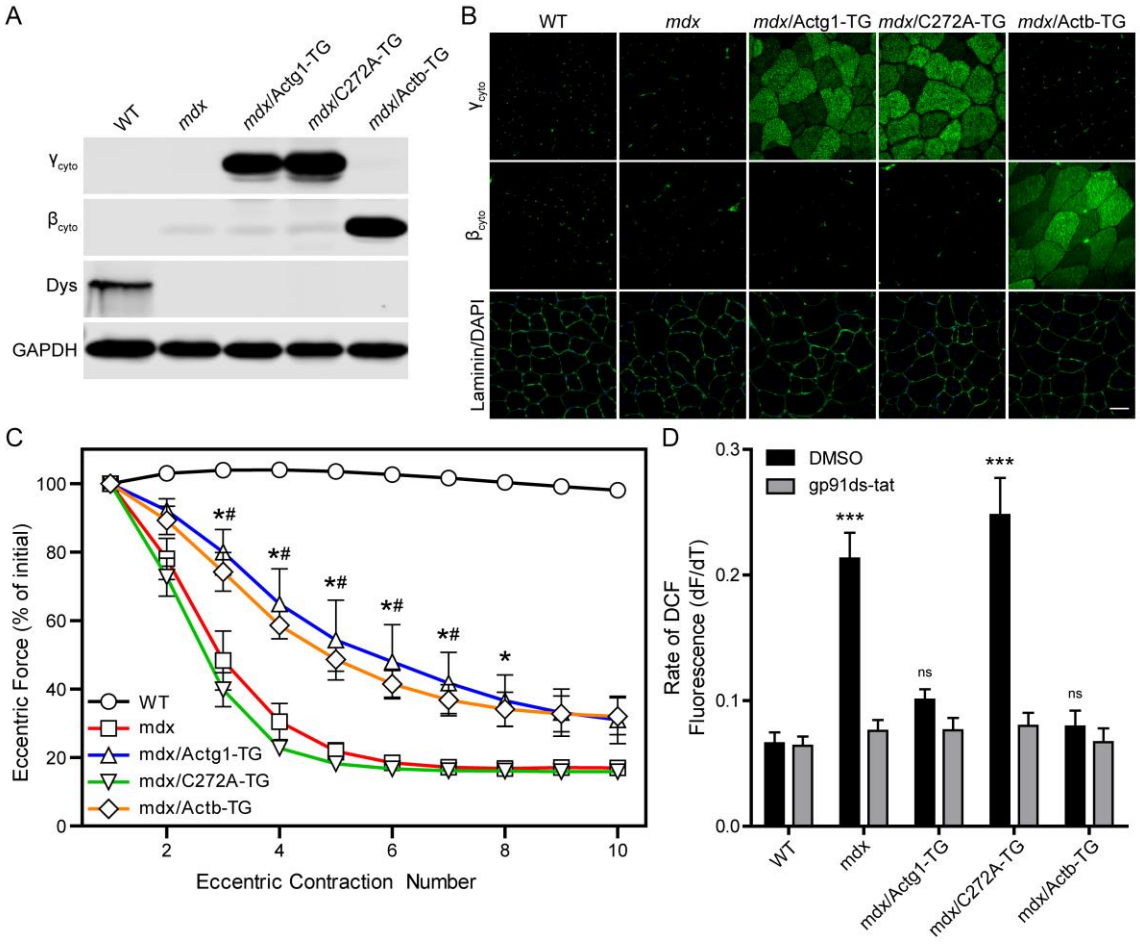

Figure 2-14. Cysteine 272 of γ_{cyto}-actin is necessary for protection of *mdx* muscle from eccentric contraction-induced force loss. (A) Immunoblot comparison of γ_{cyto} (Actg1-TG), γ_{cyto}^{C272A} (C272A-TG), and β_{cyto} (Actb-TG) overexpression in *mdx* gastrocnemius muscle. (B) Immunofluorescence analysis demonstrates similar distributions of γ_{cyto}, γ_{cyto}^{C272A}, and β_{cyto} in 10 µm quadriceps cryosections. Scale bar = 50 µm. (C) EDL muscles isolated from WT, *mdx*, *mdx*/Actg1-TG, *mdx*/C272A-TG, and *mdx*/Actb-TG mice were subjected to 10 eccentric contractions and the forces measured expressed as a percentage of

the force generated during the first eccentric contraction. n ≥ 5 for each genotype. **mdx*/Actg1-TG significantly different from *mdx* (P ≤ 0.05), [#]*mdx*/Actb-TG significantly different from *mdx* (P ≤ 0.05). (D) Rate of DCF fluorescence in single flexor digitorum brevis (FDB) muscles from WT, *mdx*, *mdx*/Actg1-TG, *mdx*/C272A-TG, and *mdx*/Actb-TG mice exposed to cyclic stretch in the presence of DMSO (vehicle) or the NOX2 inhibitor gp91ds-tat. n ≥ 7 for each genotype. ***P < 0.001.

Table 2-1. Physiological parameters of isolated EDL muscles used in *ex vivo* force measurements.

Parameter	WT	*mdx*	*mdx*/ Actg1-TG	*mdx*/ Coco	*mdx*/ C272A-TG	*mdx*/ Actb-TG	*mdx*/p47$^{-/-}$	*mdx*/mb$^{-/-}$	*mdx*/PrxII$^{-/-}$	*mdx*/ PrxII-TG$^{@}$	*P* value$^{\$}$
N	6	6	5	5	6	5	7	8	6	5	---
EDL mass (g)	13.0 ± 0.4	19.9 ± 0.8*	13.4 ± 1.1$^{\#}$	18.0 ± 0.9*	17.6 ± 0.5*	14.9 ± 0.5$^{\#}$	15.9 ± 0.2$^{\#}$	21.1 ± 1.2*	19.8 ± 0.7*	15.6 ± 0.7$^{\#}$	< 0.001
L_o (mm)	12.6 ± 0.1	13.4 ± 0.2	11.9 ± 0.3$^{\#}$	12.8 ± 0.4	13.9 ± 0.1*	12.3 ± 0.1$^{\#}$	12.5 ± 0.2	12.5 ± 0.1	14.1 ± 0.3*	12.7 ± 0.1	< 0.001
CSA (μm^2)	2.2 ± 0.1	3.1 ± 0.2*	2.4 ± 0.2	3.0 ± 0.2	2.7 ± 0.1	2.6 ± 0.1	2.7 ± 0.1	3.6 ± 0.2*	3.0 ± 0.1*	2.6 ± 0.1	< 0.001
Passive stiffness (N/m)	11.9 ± 0.4	17.9 ± 0.7*	14.4 ± 0.4	15.0 ± 0.4	14.7 ± 0.5	15.2 ± 0.7	14.7 ± 0.8	15.4 ± 0.9	16.7 ± 0.7*	16.7 ± 1.5*	< 0.001
Peak twitch (mN)	165 ± 15.9	101.1 ± 5.2*	116.3 ± 8.5*	109.8 ± 8.6*	108.5 ± 6.4*	118.5 ± 5.1	118.2 ± 6.3*	117.9 ± 13.1*	111.7 ± 7.3*	105.9 ± 3.3*	< 0.01
P_o (mN)	396.8 ± 7.2	383.4 ± 16.7	345.5 ± 16.6	393.4 ± 28.6	372.4 ± 12.9	386.7 ± 13.5	313.6 ± 16.6	422.4 ± 33.5	391.6 ± 12.9	342.7 ± 14.7	< 0.05
Specific P_o (N/cm^2)	17.9 ± 0.2	11.0 ± 0.3*	11.5 ± 0.5*	13.2 ± 1.1*	13.7 ± 0.4*	14.9 ± 0.3$^{\#}$	11.5 ± 0.7*	11.6 ± 0.5*	13.2 ± 1.0*	14.7 ± 0.5$^{\#}$	< 0.001
ΔP_o (%)	7.0 ± 1.8	87.4 ± 1.5*	77.0 ± 2.1*	81.1 ± 2.9*	88.5 ± 1.3*	82.3 ± 2.5*	81.2 ± 2.8*	74.3 ± 2.4$^{*\#}$	89.3 ± 0.5*	60.5 ± 4.8$^{*\#}$	< 0.001
Eccentric force loss (%)	2.0 ± 1.5*	83.3 ± 1.4*	69.0 ± 6.9*	80.6 ± 4.0*	83.4 ± 0.6*	68.0 ± 5.4$^{*\#}$	77.8 ± 2.2*	74.2 ± 1.5*	85.2 ± 1.4*	54.6 ± 5.1$^{*\#}$	< 0.001

*Significantly different from WT (Tukey post-hoc test).
$^{\#}$Significantly different from *mdx* (Tukey post-hoc test).
$^{\$}$One-Way ANOVA *P* value.
$^{@}$58X PrxII-TG line.

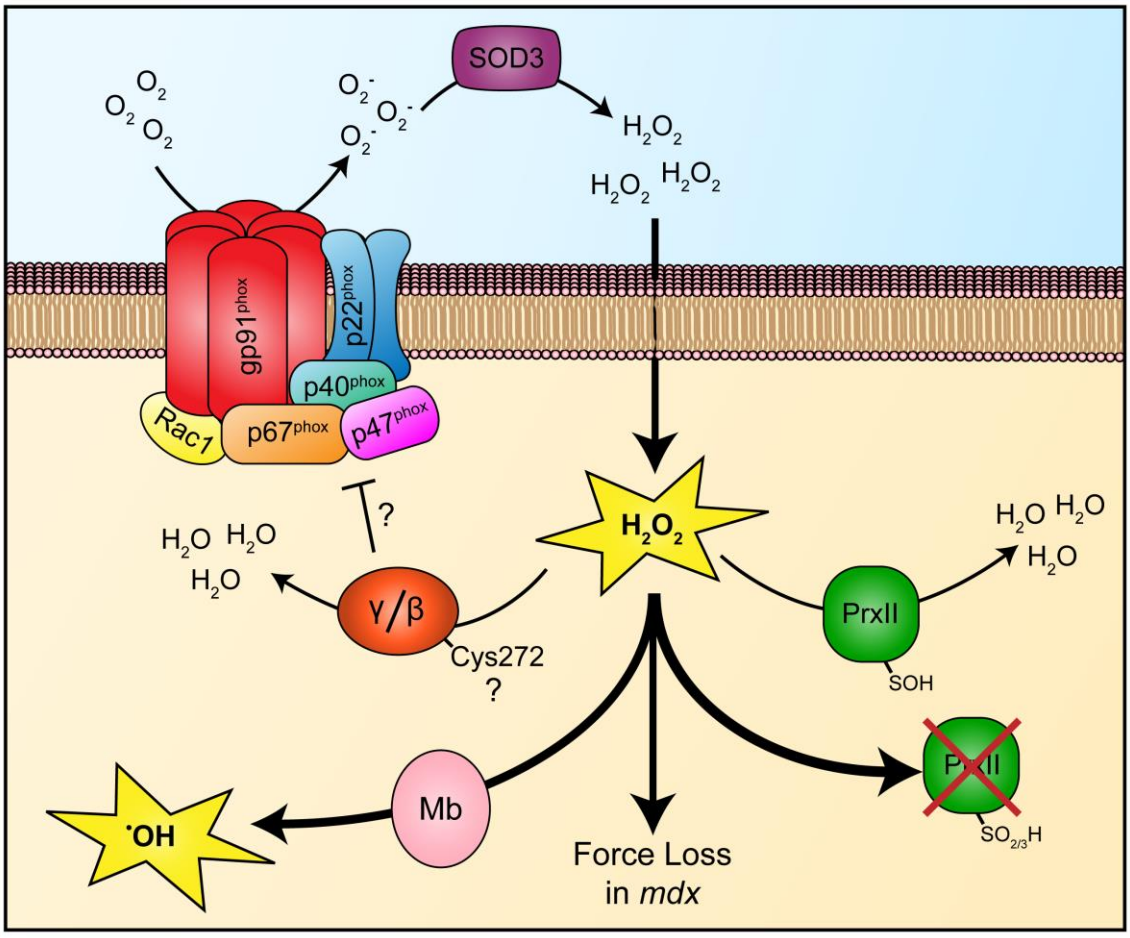

Figure 2-15. Model: Regulation of aberrant NOX2-dependent ROS production in *mdx* skeletal muscle. NOX2 hyperactivity in *mdx* skeletal muscle leads to aberrant ROS production. While PrxII may regulate normal levels of NOX2-dependent ROS, excessive ROS production leads to hyperoxidation and inactivation of PrxII. Transgenic overexpression of γ_{cyto}- or β_{cyto}-actin inhibits ROS signaling, either via direct inhibition of NOX2-dependent ROS production or by reducing ROS downstream of production. This inhibition of ROS depends on

cysteine 272, which is present in both γ_{cyto}- and β_{cyto}-actin but absent in striated muscle actins ($\alpha_{skeletal}$ and $\alpha_{cardiac}$). Myoglobin enhances NOX2-dependent ROS signaling via hydroxyl radical production through the Fenton reaction. Failure to regulate elevated ROS signaling results in increased sensitivity to eccentric contraction-induced force loss in dystrophin-deficient *mdx* skeletal muscle.

Chapter 3: Summary of Findings and Future Directions

Summary of Findings

While ECC force loss is the most robust and reproducible phenotype in dystrophin-deficient muscle, and its measurement is used in the assessment of pre-clinical therapeutic approaches for DMD, the molecular mechanisms leading to force loss remain poorly understood. Though often referred to as contraction-induced “damage” or “injury”, the contribution of such drastic, slowly-reversible structural damage to ECC force loss has not been fully assessed, and other more rapidly-reversible signaling pathways also contribute to ECC force loss. In this thesis, we demonstrate that ECC force loss in isolated *mdx* skeletal muscle recovers 65% of lost force in just 120 minutes, suggesting a more prominent contribution of rapidly-reversible molecular events versus slowly-reversible components that take on the order of days to recover. We also show that minimal force is lost in *mdx* muscle if the time interval between ECCs is increased from 3 to 30 minutes. These data indicate the ability of *mdx* muscle to recover force lost following ECC with rest, and suggest that ECC force loss is mostly the result of rapidly-reversible components.

To better understand the mechanisms involved in ECC force loss, we utilized iTRAQ proteomics to identify proteins that were differentially expressed in *mdx* mice overexpressing nonmuscle γ_{cyto}-actin (*mdx*/Actg1-TG), which our lab has previously shown to significantly protect *mdx* muscle against force loss (Baltgalvis et al., 2011). We discovered the antioxidant enzyme PrxII as

decreased in *mdx* muscle and recovered to WT levels upon overexpression of γ_{cyto}-actin, but not $\alpha_{cardiac}$-actin. This was intriguing given that overexpression of $\alpha_{cardiac}$-actin also did not protect *mdx* muscle against ECC force loss. We attributed the decrease of PrxII levels seen in *mdx* muscle to NOX2-dependent hyperoxidation and subsequent proteasomal degradation. Interestingly, genetic ablation of PrxII further sensitized *mdx* muscle to ECC force loss, while overexpression of PrxII protected *mdx* muscle from force loss in a clear dose-dependent manner. These data suggest PrxII may normally function to regulate NOX2-depedent ROS signaling, but increased NOX2 activity in *mdx* muscle leads to its degradation, allowing for ROS to accumulate in the myofiber and inhibit contractile force.

Another finding was the contribution of myoglobin to ECC force loss in *mdx* muscle. Myoglobin levels were found to be decreased in *mdx* muscle compared to WT, which was partially rescued upon genetic inhibition of NOX2 activity, suggesting ROS plays a role in its decrease. The ferrous iron within myoglobin is known to interact with ROS to produce to the highly volatile hydroxyl radical, a more potent form of ROS. To this end, we genetically ablated myoglobin in *mdx* muscle and demonstrated protection against ECC force loss.

Finally, we identified the presence of an extra cysteine residue found in the protein sequences of the cytoplasmic actins (γ_{cyto}- and β_{cyto}-actin) that is encoded by an alanine in the muscle actins ($\alpha_{skeletal}$- and $\alpha_{cardiac}$-actin) at position 272. Since overexpression of γ_{cyto}-actin, but not $\alpha_{cardiac}$-actin, led to the protection

of *mdx* muscle against ECC force loss, we wondered if this extra Cys272 played a role in this protection. We show that overexpression of γ_{cyto}-actin mutated at Cys272 (C272A-TG) failed to protect *mdx* muscle against ECC force loss. Furthermore, overexpression of β_{cyto}-actin, which contains Cys272, protected against ECC force loss to the same extent as our original γ_{cyto}-actin overexpression line. These data demonstrate that Cys272 of cytoplasmic actins is necessary to protect *mdx* muscle from ECC force loss. Finally, we show that both cytoplasmic actins inhibit NOX2-dependent ROS signaling in *mdx* myofibers in a manner that is dependent on Cys272. Together, the experiments described in this thesis lead us to hypothesize a highly-reversible, ROS-mediated component to ECC force loss in *mdx* skeletal muscle, adding to the existing mechanistic understanding of force loss.

Discussion

Together, the data presented in this thesis best fit a model in which PrxII functions as an off switch to regulate stretch-activated NOX2 signaling in normal skeletal muscle, but is lost from *mdx* muscle through hyperoxidation and proteolytic degradation effected by NOX2-mediated ROS production (Figure 2-15). PrxII is known to regulate NOX-dependent ROS production in other cell types (Finkel, 2011), and suppresses redox-mediated growth factor signaling in vascular endothelial cells (Choi et al., 2005; Kang et al., 2011). PrxII has also been recently found to exhibit a role in redox relay, where oxidation equivalents are passed from PrxII to protein targets of oxidation instead of being reduced by the canonical thioredoxin-reductase system (Rhee, 2016; Sobotta et al., 2015). However, the involvement of PrxII-dependent oxidative relay in skeletal muscle remains unknown. Regardless, PrxII was shown to play an important role in ECC force loss in *mdx* muscle, as genetic ablation increased sensitivity to force loss, while overexpression displayed a protective effect. Interestingly, the protection against ECC force loss by PrxII overexpression was dose-dependent, with the largest degree of protection resulting from 58X overexpression. Instead of increasing protection, the 112X PrxII overexpression line displayed reduced protection compared to the 58X line. This may be due to proteotoxicity of the highly-expressed transgenic line, or due to reductive stress. Contractility normally depends on tightly-regulated ROS signaling (Powers et al., 2011), but if highly-

expressed PrxII reduces all of the ROS signal, it may have a negative impact on contraction.

We have shown that Cys272 of γ_{cyto}- and β_{cyto}-actin is necessary for protection of *mdx* muscle from ECC force loss, and that this protection involves inhibition of NOX2-dependent ROS signaling. However, the precise mechanism of protection and the involvement of Cys272 remains to be understood. Cys272 may be important for a direct inhibition of NOX2 activity by cytoplasmic actins. It has been shown that the NOX2 scaffolding subunits $p40^{phox}$ and $p47^{phox}$ directly interact with actin (Tamura et al., 2000, 2006; Touyz et al., 2005). This interaction was thought to inhibit NOX2 formation by blocking the scaffolding subunits and disrupting full complex formation (Touyz et al., 2005). Another possibility is that Cys272 is used by cytoplasmic actins to shunt away ROS from other targets of oxidation. Actin has been implicated in having antioxidant properties (Farah et al., 2011), and oxidation of certain cysteines within actin are known to inhibit polymerization (Fedorova et al., 2010; Lassing et al., 2007). Interestingly, Cys272 has been found to be the most reactive cysteine in actin (Lassing et al., 2007). Therefore, overexpressed cytoplasmic actins may rely on Cys272 to “soak up” aberrant NOX2-dependent ROS to decrease oxidation of protein targets involved in muscle contraction. A combination of these two potential mechanisms may also exist.

We show that 65% of force lost during ECC is recovered within just 120 minutes, and that increasing the time interval between contractions from 3 to 30

minutes leads to minimal force loss in *mdx* muscle. These data demonstrate that the majority of ECC force loss is due to molecular events that are rapidly-reversible, while only a minority of force loss is due to slowly-reversible components. Several signaling events other than ROS have been attributed to ECC force loss that would fit a rapidly-reversible paradigm, such as sarcolemma membrane excitability and neuronal nitric oxide synthase, calcium, and Akt/PKB signaling pathways (Allen et al., 2010; Blaauw et al., 2008; Call et al., 2013; Pratt et al., 2013; Rebolledo et al., 2016). However, ROS signaling has been shown to be involved with the regulation of several of these different pathways (De Figueiredo et al., 2015; Song et al., 2011), and therefore is not mutually exclusive of such mechanisms during ECC force loss.

The slowly-reversible events that occur during ECC force loss in *mdx* muscle could be membrane damage (Petrof et al., 1993), myofiber necrosis (Sudo and Kano, 2009), loss of the neuromuscular junction (Pratt et al., 2013), or a combination of these abnormalities. However, oxidative stress could also explain part of the slowly-reversible component of ECC force loss in dystrophic muscle. High concentrations of ROS are known to hyperoxidize certain proteins such that reversibly-sulfenylated cysteine residues become irreversibly sulfinylated or sulfonylated (Finkel, 2011). Such hyperoxidation of proteins involved with contractility in *mdx* muscle could lead to their irreversible inactivation, and possible proteasomal degradation, contributing to the slowly-reversible component of ECC force loss. Altogether, our data suggest that ECC

force loss functions as an adaptive “circuit breaker” that protects dystrophin-deficient muscle from potentially cell-lethal structural damaged during repeated high force contractions.

Future Directions

The studies presented in this thesis have provided new insight into the mechanisms involved in ECC force loss that occurs during and immediately following eccentric contractions, but they have also raised new questions about the involvement of ROS in force loss. As noted in the Discussion, the mechanism of protection against ECC force loss by cytoplasmic actins involving Cys272 remains unknown. One possibility is a direct inhibition of NOX2-dependent ROS signaling through the interaction of cytoplasmic actins and $p40^{phox}$/$p47^{phox}$ NOX2 subunits. To test this possibility, we would perform co-immunoprecipitation experiments in *mdx* muscle overexpressing either γ_{cyto}-actin, β_{cyto}-actin, or γ_{cyto}^{C272A}-actin to assess direct interactions of cytoplasmic actins with $p40^{phox}$ and $p47^{phox}$. If Cys272 is indeed involved with direct inhibition of NOX2, we should not see an interaction in *mdx* overexpressing γ_{cyto}^{C272A}-actin. Another explanation of the protection against force loss in *mdx* muscle by cytoplasmic actins is a shunting mechanism (described in the Discussion). To test this, we would label oxidized cysteines in whole skeletal muscle and enrich for these proteins using alkylation-based chromatography. We can then immunoblot these samples for γ_{cyto}- and β_{cyto}-actin to understand the level of oxidation. If Cys272 is truly involved as a ROS shunt, we should see lower levels of γ_{cyto}-actin cysteine oxidation in *mdx* muscle overexpressing γ_{cyto}^{C272A}-actin versus unmutated γ_{cyto}-actin.

We showed that overexpression of PrxII protects *mdx* muscle against ECC force loss in a dose-dependent manner. We assume this protection is a result of the canonical antioxidant role of PrxII; however, PrxII has recently been shown to relay oxidation as opposed to strictly functioning as an antioxidant (Sobotta et al., 2015). PrxII may be operating, in part, to fine-tune ROS signaling pathways within the myofiber. If this is the case, it would be beneficial to uncover possible binding partners of PrxII in skeletal muscle. To this end, we would use co-immunoprecipitation of PrxII, which we have already validated with a commercial antibody (Figure 2-4G), and mass spectrometry to discover potential binding partners of PrxII that may help explain its function during ECC force loss.

PrxII was found to be decreased in *mdx* skeletal muscle due to hyperoxidation by NOX2-dependent ROS (Figure 2-5), which irreversibly inactivates PrxII and leads to its degradation by the 20S proteasome (Cho et al., 2014). Hyperoxidized PrxII may only be reactivated by sulfiredoxin-catalyzed reduction (Rhee et al., 2007). Although sulfiredoxin is expressed in many tissues throughout the mammalian body (Chang et al., 2004), we did not detect sulfiredoxin expression in skeletal muscle (Figure 2-6B). If sulfiredoxin was normally expressed in skeletal muscle, it would be possible that NOX2-dependent hyperoxidation of PrxII would be inhibited or limited, and functional PrxII could protect against ROS-induced ECC force loss. To this end, we would create a mouse line that transgenically overexpresses sulfiredoxin specifically in skeletal muscle using the HSA promoter and breed these mice onto the *mdx*

background. Our hypothesis is *mdx* mice overexpressing sulfiredoxin (*mdx*/SRXN-TG) would be partially protected from ECC force loss compared to transgene-negative *mdx* littermates, while also displaying recovered PrxII levels compared to WT animals.

Myoglobin was shown to contribute to ECC force loss in *mdx* skeletal muscle by interacting with NOX2-dependent ROS through Fenton chemistry to produce hydroxyl radicals. Hydroxyl radicals are the most volatile form of ROS, and were seen to be a component of ROS-induced contractile inhibition during ECC in *mdx* muscle. Since we demonstrated that genetic ablation of myoglobin protected against ECC force loss in dystrophic muscle, it would be interesting if overexpression may lead to an increase in hydroxyl radical production and therefore higher sensitivity to ECC force loss. Here, we would transgenically overexpress myoglobin specifically in skeletal muscle using the HSA promoter and breed these mice onto the *mdx* background. Our hypothesis is *mdx* mice overexpressing myoglobin (*mdx*/Mb-TG) would lose force more quickly following ECCs compared to transgene-negative *mdx* littermates.

Lastly, there is another important question that remains based on the work described in this thesis: What are the targets of NOX2-dependent ROS signaling involved in ECC force loss in dystrophic skeletal muscle? Existing work has described the role of aberrant NOX2 activity during ECC force loss, and our work has examined molecular events immediately downstream of NOX2 signaling, but the subsequent targets of ROS that lead to force loss in *mdx* muscle remain

unknown. To discover proteins in *mdx* muscle that are targets of cysteine oxidation, we would employ isotope-coded affinity tag (ICAT) proteomics (McDonagh et al., 2014; Sethuraman et al., 2004). Here, we could subject one EDL of an *mdx* mouse to isometric contractions, and subject the other EDL of the same mouse to eccentric contractions *ex vivo*. Then we would globally label oxidized cysteines in each sample, one with a light isotope tag and the other with a heavy isotope tag. These samples can then be sent for analysis by mass spectrometry to reveal: 1) the identification of the protein that is oxidized, 2) the identification of the particular cysteine residue(s) within that protein which is oxidized, and 3) the relative quantification of cysteine oxidation between the two groups (isometric vs. eccentric). The importance of certain cysteines within candidate proteins could then be validated *in vivo* using gene editing tools such as CRISPR/Cas9. The information revealed from this ICAT proteomic screen will undoubtedly lead to a better mechanistic understanding of ECC force loss in dystrophin-deficient muscle.

References

Aartsma-Rus, A., and Krieg, A.M. (2017). FDA Approves Eteplirsen for Duchenne Muscular Dystrophy: The Next Chapter in the Eteplirsen Saga. Nucleic Acid Ther. *27*, 1–3.

Aartsma-Rus, A., Fokkema, I., Verschuuren, J., Ginjaar, I., van Deutekom, J., van Ommen, G.-J., and den Dunnen, J.T. (2009). Theoretic applicability of antisense-mediated exon skipping for Duchenne muscular dystrophy mutations. Hum. Mutat. *30*, 293–299.

Allen, D.G., Gervasio, O.L., Yeung, E.W., and Whitehead, N.P. (2010). Calcium and the damage pathways in muscular dystrophy. Can. J. Physiol. Pharmacol. *88*, 83–91.

Allen, D.G., Whitehead, N.P., and Froehner, S.C. (2016). Absence of Dystrophin Disrupts Skeletal Muscle Signaling: Roles of Ca^{2+}, Reactive Oxygen Species, and Nitric Oxide in the Development of Muscular Dystrophy. Physiol. Rev. *96*, 253–305.

Alter, J., Lou, F., Rabinowitz, A., Yin, H., Rosenfeld, J., Wilton, S.D., Partridge, T.A., and Lu, Q.L. (2006). Systemic delivery of morpholino oligonucleotide restores dystrophin expression bodywide and improves dystrophic pathology. Nat. Med. *12*, 175–177.

Amann, K.J., Renley, B.A., and Ervasti, J.M. (1998). A cluster of basic repeats in the dystrophin rod domain binds F-actin through an electrostatic interaction. J. Biol. Chem. *273*, 28419–28423.

Angelini, C. (2007). The role of corticosteroids in muscular dystrophy: A critical appraisal. Muscle and Nerve *36*, 424–435.

Baltgalvis, K.A., Jaeger, M.A., Fitzsimons, D.P., Thayer, S.A., Lowe, D.A., and Ervasti, J.M. (2011). Transgenic overexpression of γ-cytoplasmic actin protects against eccentric contraction-induced force loss in mdx mice. Skelet. Muscle *1*, 32.

Barton-Davis, E.R., Cordier, L., Shoturma, D.I., Leland, S.E., and Sweeney, H.L. (1999). Aminoglycoside antibiotics restore dystrophin function to skeletal muscles of mdx mice. J. Clin. Invest. *104*, 375–381.

Belanto, J.J., Mader, T.L., Eckhoff, M.D., Strandjord, D.M., Banks, G.B., Gardner, M.K., Lowe, D.A., and Ervasti, J.M. (2014). Microtubule binding distinguishes

dystrophin from utrophin. Proc. Natl. Acad. Sci. U. S. A. *111*, 5723–5728.

Bengtsson, N.E., Hall, J.K., Odom, G.L., Phelps, M.P., Andrus, C.R., Hawkins, R.D., Hauschka, S.D., Chamberlain, J.R., and Chamberlain, J.S. (2017). Muscle-specific CRISPR/Cas9 dystrophin gene editing ameliorates pathophysiology in a mouse model for Duchenne muscular dystrophy. Nat. Commun. *8*, 14454.

Bentzinger, C.F., Wang, Y.X., and Rudnicki, M. a (2012). Building muscle: molecular regulation of myogenesis. Cold Spring Harb. Perspect. Biol. *4*.

Bigland-Ritchie, B.B., and Woods, J.J. (1976). Integrated Electromyogram and Oxygen Uptake. J. Physiol. *260*, 267–277.

Blaauw, B., Mammucari, C., Toniolo, L., Agatea, L., Abraham, R., Sandri, M., Reggiani, C., and Schiaffino, S. (2008). Akt activation prevents the force drop induced by eccentric contractions in dystrophin-deficient skeletal muscle. Hum. Mol. Genet. *17*, 3686–3696.

Blaauw, B., Agatea, L., Toniolo, L., Canato, M., Quarta, M., Dyar, K.A., Danieli-Betto, D., Betto, R., Schiaffino, S., and Reggiani, C. (2010). Eccentric contractions lead to myofibrillar dysfunction in muscular dystrophy. J. Appl. Physiol. *108*, 105–111.

Bladen, C.L., Salgado, D., Monges, S., Foncuberta, M.E., Kekou, K., Kosma, K., Dawkins, H., Lamont, L., Roy, A.J., Chamova, T., et al. (2015). The TREAT-NMD DMD Global Database: Analysis of More than 7,000 Duchenne Muscular Dystrophy Mutations. Hum. Mutat. *36*, 395–402.

Blake, D.J., Weir, A., Newey, S.E., and Davies, K.E. (2002). Function and Genetics of Dystrophin and Dystrophin-Related Proteins in Muscle. Physiol. Rev. *82*, 291–329.

Bork, P., and Sudol, M. (1994). The WW domain: a signalling site in dystrophin? Trends Biochem. Sci. *19*, 531–533.

Briguet, A., Courdier-Fruh, I., Foster, M., Meier, T., and Magyar, J.P. (2004). Histological parameters for the quantitative assessment of muscular dystrophy in the mdx-mouse. Neuromuscul. Disord. *14*, 675–682.

Brooks, S. V. (1998). Rapid recovery following contraction-induced injury to in situ skeletal muscles in mdx mice. J. Muscle Res. Cell Motil. *19*, 179–187.

Bulfield, G., Siller, W.G., Wight, P.A., and Moore, K.J. (1984). X chromosome-linked muscular dystrophy (mdx) in the mouse. Proc. Natl. Acad. Sci. U. S. A. *81*,

1189–1192.

Bunnell, T.M., Jaeger, M.A., Fitzsimons, D.P., Prins, K.W., and Ervasti, J.M. (2008). Destabilization of the Dystrophin-Glycoprotein Complex without Functional Deficits in α-Dystrobrevin Null Muscle. PLoS One *3*, e2604.

Bunnell, T.M., Burbach, B.J., Shimizu, Y., and Ervasti, J.M. (2011). β-Actin specifically controls cell growth, migration, and the G-actin pool. Mol. Biol. Cell *22*, 4047–4058.

Burghes, A.H.M., Logan, C., Hu, X., Belfall, B., Worton, R.G., and Ray, P.N. (1987). A cDNA clone from the Duchenne/Becker muscular dystrophy gene. Nature *328*, 434–437.

Bushby, K., Finkel, R., Wong, B., Barohn, R., Campbell, C., Comi, G.P., Connolly, A.M., Day, J.W., Flanigan, K.M., Goemans, N., et al. (2014). Ataluren treatment of patients with nonsense mutation dystrophinopathy. Muscle Nerve *50*, 477–487.

Byers, T.J., Lidov, H.G.W., and Kunkel, L.M. (1993). An alternative dystrophin transcript specific to peripheral nerve. Nat. Genet. *4*, 77–81.

Call, J.A., Warren, G.L., Verma, M., and Lowe, D.A. (2013). Acute failure of action potential conduction in *mdx* muscle reveals new mechanism of contraction-induced force loss. J. Physiol. *591*, 3765–3776.

Campbell, K.P., and Kahl, S.D. (1989). Association of dystrophin and an integral membrane glycoprotein. Nature *338*, 259–262.

Carlier, M.-F., and Pantaloni, D. (1997). Control of actin dynamics in cell motility. J. Mol. Biol. *269*, 459–467.

Chamberlain, J.S. (1992). X-linked dystrophies: from gene localization to gene therapy. Curr. Opin. Neurol. Neurosurg. *5*, 610–614.

Chamberlain, J.R., and Chamberlain, J.S. (2017). Progress toward Gene Therapy for Duchenne Muscular Dystrophy. Mol. Ther. *25*, 1125–1131.

Chamberlain, J.S., and Benian, G.M. (2000). Muscular dystrophy: the worm turns to genetic disease. Curr. Biol. *10*, R795-7.

Chambers, M.C., MacLean, B., Burke, R., Amodei, D., Ruderman, D.L., Neumann, S., Gatto, L., Fischer, B., Pratt, B., Egertson, J., et al. (2012). A cross-platform toolkit for mass spectrometry and proteomics. Nat. Biotechnol. *30*, 918–

920.

Chang, T.S., Jeong, W., Woo, H.A., Lee, S.M., Park, S., and Rhee, S.G. (2004). Characterization of mammalian sulfiredoxin and its reactivation of hyperoxidized peroxiredoxin through reduction of cysteine sulfinic acid in the active site to cysteine. J. Biol. Chem. *279*, 50994–51001.

Chen, J., He, R., Minshall, R.D., Dinauer, M.C., and Ye, R.D. (2007). Characterization of a mutation in the Phox homology domain of the NADPH oxidase component p40phox identifies a mechanism for negative regulation of superoxide production. J. Biol. Chem. *282*, 30273–30284.

Cho, C.S., Yoon, H.J., Kim, J.Y., Woo, H.A., and Rhee, S.G. (2014). Circadian rhythm of hyperoxidized peroxiredoxin II is determined by hemoglobin autoxidation and the 20S proteasome in red blood cells. Proc. Natl. Acad. Sci. U. S. A. *111*, 1–6.

Choi, M.H., Lee, I.K., Kim, G.W., Kim, B.U., Han, Y.H., Yu, D.Y., Park, H.S., Kim, K.Y., Lee, J.S., Choi, C., et al. (2005). Regulation of PDGF signalling and vascular remodelling by peroxiredoxin II. Nature *435*, 347–353.

Clarke, M., and Spudich, J.A. (1977). Nonmuscle Contractile Proteins: The Role of Actin and Myosin in Cell Motility and Shape Determination. Annu. Rev. Biochem. *46*, 797–822.

Cohn, R.D., and Campbell, K.P. (2000). Molecular basis of muscular dystrophies. Muscle Nerve *23*, 1456–1471.

Colliander, E.B., and Tesch, P.A. (1990). Effects of eccentric and concentric muscle actions in resistance training. Acta Physiol. Scand. *140*, 31–39.

Connolly, A.M., Keeling, R.M., Mehta, S., Pestronk, A., and Sanes, J.R. (2001). Three mouse models of muscular dystrophy: the natural history of strength and fatigue in dystrophin-, dystrophin/utrophin-, and laminin alpha2-deficient mice. Neuromuscul. Disord. *11*, 703–712.

Cooper, B.J., Winand, N.J., Stedman, H., Valentine, B.A., Hoffman, E.P., Kunkel, L.M., Scott, M.-O.O., Fischbeck, K.H., Kornegay, J.N., Avery, R.J., et al. (1988). The homologue of the Duchenne locus is defective in X-linked muscular dystrophy of dogs. Nature *334*, 154–156.

Craig, S.W., and Pardo, J. V (1983). Gamma actin, spectrin, and intermediate filament proteins colocalize with vinculin at costameres, myofibril-to-sarcolemma attachment sites. Cell Motil. *3*, 449–462.

Cros, D., Harnden, P., Pellissier, J.F., and Serratrice, G. (1989). Muscle hypertrophy in Duchenne muscular dystrophy. A pathological and morphometric study. J. Neurol. *236*, 43–47.

Deconinck, a E., Rafael, J. a, Skinner, J. a, Brown, S.C., Potter, a C., Metzinger, L., Watt, D.J., Dickson, J.G., Tinsley, J.M., and Davies, K.E. (1997). Utrophin-dystrophin-deficient mice as a model for Duchenne muscular dystrophy. Cell *90*, 717–727.

van Deutekom, J.C., Janson, A.A., Ginjaar, I.B., Frankhuizen, W.S., Aartsma-Rus, A., Bremmer-Bout, M., den Dunnen, J.T., Koop, K., van der Kooi, A.J., Goemans, N.M., et al. (2007). Local Dystrophin Restoration with Antisense Oligonucleotide PRO051. N. Engl. J. Med. *357*, 2677–2686.

DiMario, J.X., Uzman, A., and Strohman, R.C. (1991). Fiber regeneration is not persistent in dystrophic (MDX) mouse skeletal muscle. Dev. Biol. *148*, 314–321.

Dominguez, R., and Holmes, K.C. (2011). Actin Structure and Function. Annu. Rev. Biophys. *40*, 169–186.

Dowling, P., Culligan, K., and Ohlendieck, K. (2002). Distal mdx muscle groups exhibiting up-regulation of utrophin and rescue of dystrophin-associated glycoproteins exemplify a protected phenotype in muscular dystrophy. Naturwissenschaften *89*, 75–78.

Duan, R., and Gallagher, P.J. (2009). Dependence of myoblast fusion on a cortical actin wall and nonmuscle myosin IIA. Dev. Biol. *325*, 374–385.

Duchenne, G.B. (1855). De l'electrisation localisée et de son application a la physiologie, a la pathologie et a la thérapeutique (A Paris: Chez J.B. Bailliere).

Ebashi, S., and Endo, M. (1968). Calcium ion and muscle contraction. Prog. Biophys. Mol. Biol. *18*, 123–183.

Emery, A.E. (2002). The muscular dystrophies. Lancet *359*, 687–695.

Ervasti, J.M. (2003). Costameres: the Achilles' Heel of Herculean Muscle. J. Biol. Chem. *278*, 13591–13594.

Ervasti, J.M. (2007). Dystrophin, its interactions with other proteins, and implications for muscular dystrophy. Biochim. Biophys. Acta - Mol. Basis Dis. *1772*, 108–117.

Ervasti, J.M., and Campbell, K.P. (1991). Membrane organization of the

dystrophin-glycoprotein complex. Cell *66*, 1121–1131.

Ervasti, J.M., and Campbell, K.P. (1993). A role for the dystrophin-glycoprotein complex as a transmembrane linker between laminin and actin. J. Cell Biol. *122*, 809–823.

Ervasti, J.M., Ohlendieck, K., Kahl, S.D., Gaver, M.G., and Campbell, K.P. (1990). Deficiency of a glycoprotein component of the dystrophin complex in dystrophic muscle. Nature *345*, 315–319.

Farah, M.E., Sirotkin, V., Haarer, B., Kakhniashvili, D., and Amberg, D.C. (2011). Diverse protective roles of the actin cytoskeleton during oxidative stress. Cytoskeleton *68*, 340–354.

Faulkner, J.A. (2003). Terminology for contractions of muscles during shortening, while isometric, and during lengthening. J. Appl. Physiol. *95*, 455–459.

Fedorova, M., Kuleva, N., and Hoffmann, R. (2010). Identification of cysteine, methionine and tryptophan residues of actin oxidized in vivo during oxidative stress. J. Proteome Res. *9*, 1598–1609.

Ferreira, L.F., and Reid, M.B. (2008). Muscle-derived ROS and thiol regulation in muscle fatigue. J. Appl. Physiol. *104*, 853–860.

De Figueiredo, A.S.P., Salmon, A.B., Bruno, F., Jimenez, F., Martinez, H.G., Halade, G. V., Ahuja, S.S., Clark, R.A., DeFronzo, R.A., Abboud, H.E., et al. (2015). Nox2 mediates skeletal muscle insulin resistance induced by a high fat diet. J. Biol. Chem. *290*, 13427–13439.

Finkel, T. (2011). Signal transduction by reactive oxygen species. J. Cell Biol. *194*, 7–15.

Flanigan, K.M. (2014). Duchenne and Becker Muscular Dystrophies. Neurol. Clin. *32*, 671–688.

Fukada, S., Morikawa, D., Yamamoto, Y., Yoshida, T., Sumie, N., Yamaguchi, M., Ito, T., Miyagoe-Suzuki, Y., Takeda, S., Tsujikawa, K., et al. (2010). Genetic background affects properties of satellite cells and mdx phenotypes. Am. J. Pathol. *176*, 2414–2424.

Garry, D.J., Ordway, G. a, Lorenz, J.N., Radford, N.B., Chin, E.R., Grange, R.W., Bassel-Duby, R., and Williams, R.S. (1998). Mice without myoglobin. Nature *395*, 905–908.

Glesby, M.J., Rosenmann, E., Nylen, E.G., and Wrogemann, K. (1988). Serum CK, calcium, magnesium, and oxidative phosphorylation in mdx mouse muscular dystrophy. Muscle Nerve *11*, 852–856.

Godfrey, C., Foley, A.R., Clement, E., and Muntoni, F. (2011). Dystroglycanopathies: coming into focus. Curr. Opin. Genet. Dev. *21*, 278–285.

Gokhin, D.S., Lewis, R.A., McKeown, C.R., Nowak, R.B., Kim, N.E., Littlefield, R.S., Lieber, R.L., and Fowler, V.M. (2010). Tropomodulin isoforms regulate thin filament pointed-end capping and skeletal muscle physiology. J. Cell Biol. *189*, 95–109.

Górecki, D.C., Monaco, A.P., Derry, J.M., Walker, A.P., Barnard, E.A., and Barnard, P.J. (1992). Expression of four alternative dystrophin transcripts in brain regions regulated by different promoters. Hum. Mol. Genet. *1*, 505–510.

Gowers, W.R. (1886). A manual of diseases of the nervous system. 2 v.

Grady, R.M., Teng, H., Nichol, M.C., Cunningham, J.C., Wilkinson, R.S., and Sanes, J.R. (1997). Skeletal and cardiac myopathies in mice lacking utrophin and dystrophin: a model for Duchenne muscular dystrophy. Cell *90*, 729–738.

Grady, R.M., Grange, R.W., Lau, K.S., Maimone, M.M., Nichol, M.C., Stull, J.T., and Sanes, J.R. (1999). Role for α-dystrobrevin in the pathogenesis of dystrophin-dependent muscular dystrophies. Nat. Cell Biol. *1*, 215–220.

Gregorevic, P., Blankinship, M.J., Allen, J.M., Crawford, R.W., Meuse, L., Miller, D.G., Russell, D.W., and Chamberlain, J.S. (2004). Systemic delivery of genes to striated muscles using adeno-associated viral vectors. Nat. Med. *10*, 828–834.

Grounds, M.D., Radley, H.G., Lynch, G.S., Nagaraju, K., and De Luca, A. (2008). Towards developing standard operating procedures for pre-clinical testing in the mdx mouse model of Duchenne muscular dystrophy. Neurobiol. Dis. *31*, 1–19.

Guiraud, S., and Davies, K.E. (2017). Pharmacological advances for treatment in Duchenne muscular dystrophy. Curr. Opin. Pharmacol. *34*, 36–48.

Hall, Z.W., Lubit, B.W., and Schwartz, J.H. (1981). Cytoplasmic actin in postsynaptic structures at the neuromuscular junction. J. Cell Biol. *90*, 789–792.

Han, R., Rader, E.P., Levy, J.R., Bansal, D., and Campbell, K.P. (2011). Dystrophin deficiency exacerbates skeletal muscle pathology in dysferlin-null mice. Skelet. Muscle *1*, 35.

Hanft, L.M., Rybakova, I.N., Patel, J.R., Rafael-Fortney, J.A., and Ervasti, J.M. (2006). Cytoplasmic gamma-actin contributes to a compensatory remodeling response in dystrophin-deficient muscle. Proc. Natl. Acad. Sci. U. S. A. *103*, 5385–5390.

Hara, Y., Balci-Hayta, B., Yoshida-Moriguchi, T., Kanagawa, M., Beltrán-Valero de Bernabé, D., Gündeşli, H., Willer, T., Satz, J.S., Crawford, R.W., Burden, S.J., et al. (2011). A Dystroglycan Mutation Associated with Limb-Girdle Muscular Dystrophy. N. Engl. J. Med. *364*, 939–946.

Hnia, K., Zouiten, D., Cantel, S., Chazalette, D., Hugon, G., Fehrentz, J.-A., Masmoudi, A., Diment, A., Bramham, J., Mornet, D., et al. (2007). ZZ domain of dystrophin and utrophin: topology and mapping of a β-dystroglycan interaction site. Biochem. J. *401*, 667–677.

Hoffman, E.P., Brown, R.H., and Kunkel, L.M. (1987). Dystrophin: The protein product of the duchenne muscular dystrophy locus. Cell *51*, 919–928.

Hollinger, K., Yang, C.X., Montz, R.E., Nonneman, D., Ross, J.W., and Selsby, J.T. (2014). Dystrophin insufficiency causes selective muscle histopathology and loss of dystrophin-glycoprotein complex assembly in pig skeletal muscle. FASEB J. *28*, 1600–1609.

Huizinga, J.D. (1999). Gastrointestinal peristalsis: Joint action of enteric nerves, smooth muscle, and interstitial cells of Cajal. Microsc. Res. Tech. *47*, 239–247.

Ibraghimov-Beskrovnaya, O., Ervasti, J.M., Leveille, C.J., Slaughter, C.A., Sernett, S.W., and Campbell, K.P. (1992). Primary structure of dystrophin-associated glycoproteins linking dystrophin to the extracellular matrix. Nature *355*, 696–702.

Jaeger, M.A., Sonnemann, K.J., Fitzsimons, D.P., Prins, K.W., and Ervasti, J.M. (2009). Context-dependent functional substitution of alpha-skeletal actin by gamma-cytoplasmic actin. FASEB J. *23*, 2205–2214.

Janssen, I., Heymsfield, S.B., Wang, Z., and Ross, R. (2000). Skeletal muscle mass and distribution in 468 men and women aged 18–88 yr. J. Appl. Physiol. *89*, 81–88.

Johansson, M., and Lundberg, M. (2007). Glutathionylation of beta-actin via a cysteinyl sulfenic acid intermediary. BMC Biochem. *8*, 26.

Kameya, S., Miyagoe, Y., Nonaka, I., Ikemoto, T., Endo, M., Hanaoka, K., Nabeshima, Y., and Takeda, S. (1999). alpha1-syntrophin gene disruption results

in the absence of neuronal-type nitric-oxide synthase at the sarcolemma but does not induce muscle degeneration. J. Biol. Chem. *274*, 2193–2200.

Kang, D.H., Lee, D.J., Lee, K.W., Park, Y.S., Lee, J.Y., Lee, S.H., Koh, Y.J., Koh, G.Y., Choi, C., Yu, D.Y., et al. (2011). Peroxiredoxin II is an essential antioxidant enzyme that prevents the oxidative inactivation of VEGF receptor-2 in vascular endothelial cells. Mol. Cell *44*, 545–558.

Kee, A.J., Schevzov, G., Nair-Shalliker, V., Robinson, C.S., Vrhovski, B., Ghoddusi, M., Qiu, M.R., Lin, J.J.-C.C., Weinberger, R., Gunning, P.W., et al. (2004). Sorting of a nonmuscle tropomyosin to a novel cytoskeletal compartment in skeletal muscle results in muscular dystrophy. J. Cell Biol. *166*, 685–696.

Kerr, J.P., Robison, P., Shi, G., Bogush, A.I., Kempema, A.M., Hexum, J.K., Becerra, N., Harki, D.A., Martin, S.S., Raiteri, R., et al. (2015). Detyrosinated microtubules modulate mechanotransduction in heart and skeletal muscle. Nat. Commun. *6*, 1–14.

Khairallah, R.J., Shi, G., Sbrana, F., Prosser, B.L., Borroto, C., Mazaitis, M.J., Hoffman, E.P., Mahurkar, A., Sachs, F., Sun, Y., et al. (2012). Microtubules Underlie Dysfunction in Duchenne Muscular Dystrophy. Sci. Signal. *5*, ra56.

Kinali, M., Arechavala-Gomeza, V., Feng, L., Cirak, S., Hunt, D., Adkin, C., Guglieri, M., Ashton, E., Abbs, S., Nihoyannopoulos, P., et al. (2009). Local restoration of dystrophin expression with the morpholino oligomer AVI-4658 in Duchenne muscular dystrophy: a single-blind, placebo-controlled, dose-escalation, proof-of-concept study. Lancet Neurol. *8*, 918–928.

Klymiuk, N., Blutke, A., Graf, A., Krause, S., Burkhardt, K., Wuensch, A., Krebs, S., Kessler, B., Zakhartchenko, V., Kurome, M., et al. (2013). Dystrophin-deficient pigs provide new insights into the hierarchy of physiological derangements of dystrophic muscle. Hum. Mol. Genet. *22*, 4368–4382.

Kobayashi, Y.M., Rader, E.P., Crawford, R.W., Iyengar, N.K., Thedens, D.R., Faulkner, J.A., Parikh, S. V., Weiss, R.M., Chamberlain, J.S., Moore, S.A., et al. (2008). Sarcolemma-localized nNOS is required to maintain activity after mild exercise. Nature *456*, 511–515.

Koenig, M., and Kunkel, L.M. (1990). Detailed analysis of the repeat domain of dystrophin reveals four potential hinge segments that may confer flexibility. J. Biol. Chem. *265*, 4560–4566.

Koenig, M., Hoffman, E.P., Bertelson, C.J., Monaco, A.P., Feener, C., and Kunkel, L.M. (1987). Complete cloning of the duchenne muscular dystrophy

(DMD) cDNA and preliminary genomic organization of the DMD gene in normal and affected individuals. Cell *50*, 509–517.

Koenig, M., Monaco, A.P., and Kunkel, L.M. (1988). The complete sequence of dystrophin predicts a rod-shaped cytoskeletal protein. Cell *53*, 219–228.

Koenig, M., Beggs, A.H., Moyer, M., Scherpf, S., Heindrich, K., Bettecken, T., Meng, G., Müller, C.R., Lindlöf, M., Kaariainen, H., et al. (1989). The molecular basis for Duchenne versus Becker muscular dystrophy: correlation of severity with type of deletion. Am. J. Hum. Genet. *45*, 498–506.

Kornegay, J.N., Tuler, S.M., Miller, D.M., and Levesque, D.C. (1988). Muscular dystrophy in a litter of golden retriever dogs. Muscle Nerve *11*, 1056–1064.

Kunkel, L.M., Bachrach, E., Bennett, R.R., Guyon, J., and Steffen, L. (2006). Diagnosis and cell-based therapy for Duchenne muscular dystrophy in humans, mice, and zebrafish. J. Hum. Genet. *51*, 397–406.

Lai, Y., Thomas, G.D., Yue, Y., Yang, H.T., Li, D., Long, C., Judge, L., Bostick, B., Chamberlain, J.S., Terjung, R.L., et al. (2009). Dystrophins carrying spectrin-like repeats 16 and 17 anchor nNOS to the sarcolemma and enhance exercise performance in a mouse model of muscular dystrophy. J. Clin. Invest. *119*, 624–635.

Lai, Y., Zhao, J., Yue, Y., and Duan, D. (2013). α2 and α3 helices of dystrophin R16 and R17 frame a microdomain in the 1 helix of dystrophin R17 for neuronal NOS binding. Proc. Natl. Acad. Sci. *110*, 525–530.

Lamb, G.D., and Westerblad, H. (2011). Acute effects of reactive oxygen and nitrogen species on the contractile function of skeletal muscle. J. Physiol. *589*, 2119–2127.

Lassing, I., Schmitzberger, F., Björnstedt, M., Holmgren, A., Nordlund, P., Schutt, C.E., and Lindberg, U. (2007). Molecular and Structural Basis for Redox Regulation of β-Actin. J. Mol. Biol. *370*, 331–348.

Laval, S.H., and Bushby, K.M.D. (2004). Limb-girdle muscular dystrophies - from genetics to molecular pathology. Neuropathol. Appl. Neurobiol. *30*, 91–105.

Lebakken, C.S., Venzke, D.P., Hrstka, R.F., Consolino, C.M., Faulkner, J.A., Williamson, R.A., and Campbell, K.P. (2000). Sarcospan-deficient mice maintain normal muscle function. Mol. Cell. Biol. *20*, 1669–1677.

Lee, T.H., Kim, S.U., Yu, S.L., Kim, S.H., Park, D.S., Moon, H.B., Dho, S.H.,

Kwon, K.S., Kwon, H.J., Han, Y.H., et al. (2003). Peroxiredoxin II is essential for sustaining life span of erythrocytes in mice. Blood *101*, 5033–5038.

Levine, B.A., Moir, A.J., Patchell, V.B., and Perry, S. V (1990). The interaction of actin with dystrophin. FEBS Lett. *263*, 159–162.

Li, D., Bareja, A., Judge, L., Yue, Y., Lai, Y., Fairclough, R., Davies, K.E., Chamberlain, J.S., and Duan, D. (2010). Sarcolemmal nNOS anchoring reveals a qualitative difference between dystrophin and utrophin. J. Cell Sci. *123*, 2008–2013.

Lin-Moshier, Y., Sebastian, P.J., Higgins, L.A., Sampson, N.D., Hewitt, J.E., and Marchant, J.S. (2013). Re-evaluation of the role of Calcium Homeostasis Endoplasmic Reticulum Protein (CHERP) in cellular calcium signaling. J. Biol. Chem. *288*, 355–367.

Lloyd, T.E., and Taylor, J.P. (2010). Flightless flies: Drosophila models of neuromuscular disease. Ann. N. Y. Acad. Sci. *1184*, e1-20.

Lloyd, C., Schevzov, G., and Gunning, P. (1992). Transfection of nonmuscle beta- and gamma-actin genes into myoblasts elicits different feedback regulatory responses from endogenous actin genes. J. Cell Biol. *117*, 787–797.

Loehr, J.A., Stinnett, G.R., Hernández-Rivera, M., Roten, W.T., Wilson, L.J., Pautler, R.G., and Rodney, G.G. (2016). Eliminating Nox2 reactive oxygen species production protects dystrophic skeletal muscle from pathological calcium influx assessed in vivo by manganese-enhanced magnetic resonance imaging. J. Physiol. *594*, 6395–6405.

Long, C., Amoasii, L., Mireault, A.A., McAnally, J.R., Li, H., Sanchez-Ortiz, E., Bhattacharyya, S., Shelton, J.M., Bassel-Duby, R., and Olson, E.N. (2016). Postnatal genome editing partially restores dystrophin expression in a mouse model of muscular dystrophy. Science (80-.). *351*, 400–403.

Lovering, R.M., and Brooks, S. V (2014). Eccentric exercise in aging and diseased skeletal muscle: good or bad? J. Appl. Physiol. *116*, 1439–1445.

Lynch, G.S., Rafael, J.A., Chamberlain, J.S., and Faulkner, J.A. (2000). Contraction-induced injury to single permeabilized muscle fibers from mdx, transgenic mdx, and control mice. Am. J. Physiol. Cell Physiol. *279*, C1290-4.

Malik, V., Rodino-Klapac, L.R., Viollet, L., Wall, C., King, W., Al-Dahhak, R., Lewis, S., Shilling, C.J., Kota, J., Serrano-Munuera, C., et al. (2010). Gentamicin-induced readthrough of stop codons in Duchenne muscular dystrophy. Ann.

Neurol. *67*, NA-NA.

Matsuda, R., Nishikawa, A., and Tanaka, H. (1995). Visualization of dystrophic muscle fibers in mdx mouse by vital staining with Evans blue: evidence of apoptosis in dystrophin-deficient muscle. J. Biochem. *118*, 959–964.

Matsumura, K., Ervasti, J.M., Ohlendieck, K., Kahl, S.D., and Campbell, K.P. (1992). Association of dystrophin-related protein with dystrophin-associated proteins in mdx mouse muscle. Nature *360*, 588–591.

Mázala, D.A.G., Pratt, S.J.P., Chen, D., Molkentin, J.D., Lovering, R.M., and Chin, E.R. (2015). SERCA1 overexpression minimizes skeletal muscle damage in dystrophic mouse models. Am. J. Physiol. - Cell Physiol. *308*, C699–C709.

McDonagh, B., Sakellariou, G.K., Smith, N.T., Brownridge, P., and Jackson, M.J. (2014). Differential Cysteine Labeling and Global Label-Free Proteomics Reveals an Altered Metabolic State in Skeletal Muscle Aging. J. Proteome Res. *13*, 5008–5021.

Mendell, J.R., and Rodino-Klapac, L.R. (2016). Duchenne muscular dystrophy: CRISPR/Cas9 treatment. Cell Res. *26*, 513–514.

Mendell, J.R., Campbell, K., Rodino-Klapac, L., Sahenk, Z., Shilling, C., Lewis, S., Bowles, D., Gray, S., Li, C., Galloway, G., et al. (2010). Dystrophin Immunity in Duchenne's Muscular Dystrophy. N. Engl. J. Med. *363*, 1429–1437.

Mendell, J.R., Shilling, C., Leslie, N.D., Flanigan, K.M., Al-Dahhak, R., Gastier-Foster, J., Kneile, K., Dunn, D.M., Duval, B., Aoyagi, A., et al. (2012). Evidence-based path to newborn screening for duchenne muscular dystrophy. Ann. Neurol. *71*, 304–313.

Michele, D.E., Barresi, R., Kanagawa, M., Saito, F., Cohn, R.D., Satz, J.S., Dollar, J., Nishino, I., Kelley, R.I., Somer, H., et al. (2002). Post-translational disruption of dystroglycan–ligand interactions in congenital muscular dystrophies. Nature *418*, 417–421.

Millay, D.P., Goonasekera, S.A., Sargent, M.A., Maillet, M., Aronow, B.J., and Molkentin, J.D. (2009). Calcium influx is sufficient to induce muscular dystrophy through a TRPC-dependent mechanism. Proc. Natl. Acad. Sci. U. S. A. *106*, 19023–19028.

Moens, P., Baatsen, P., Maréchal, G., and Marechal, G. (1993). Increased susceptibility of EDL muscles from mdx mice to damage induced by contraction with stretch. J. Muscle Res. Cell Motil. *14*, 446–451.

Monaco, A.P., Bertelson, C.J., Liechti-Gallati, S., Moser, H., and Kunkel, L.M. (1988). An explanation for the phenotypic differences between patients bearing partial deletions of the DMD locus. Genomics *2*, 90–95.

Moran, A.L., Warren, G.L., and Lowe, D.A. (2005). Soleus and EDL muscle contractility across the lifespan of female C57BL/6 mice. Exp. Gerontol. *40*, 966–975.

Morine, K.J., Sleeper, M.M., Barton, E.R., and Sweeney, H.L. (2010). Overexpression of SERCA1a in the *mdx* Diaphragm Reduces Susceptibility to Contraction-Induced Damage. Hum. Gene Ther. *21*, 1735–1739.

Munnamalai, V., Weaver, C.J., Weisheit, C.E., Venkatraman, P., Agim, Z.S., Quinn, M.T., and Suter, D.M. (2014). Bidirectional interactions between NOX2-type NADPH oxidase and the F-actin cytoskeleton in neuronal growth cones. J. Neurochem. *130*, 526–540.

Muntoni, F., Torelli, S., and Ferlini, A. (2003). Dystrophin and mutations: one gene, several proteins, multiple phenotypes. Lancet. Neurol. *2*, 731–740.

Murphy, R.M., Dutka, T.L., and Lamb, G.D. (2008). Hydroxyl radical and glutathione interactions alter calcium sensitivity and maximum force of the contractile apparatus in rat skeletal muscle fibres. J. Physiol. *586*, 2203–2216.

Muthu, M., Richardson, K.A., and Sutherland-Smith, A.J. (2012). The Crystal Structures of Dystrophin and Utrophin Spectrin Repeats: Implications for Domain Boundaries. PLoS One *7*, e40066.

Nakamura, K., Fujii, W., Tsuboi, M., Tanihata, J., Teramoto, N., Takeuchi, S., Naito, K., Yamanouchi, K., and Nishihara, M. (2015). Generation of muscular dystrophy model rats with a CRISPR/Cas system. Sci. Rep. *4*, 5635.

Nelson, C.E., Hakim, C.H., Ousterout, D.G., Thakore, P.I., Moreb, E.A., Rivera, R.M.C., Madhavan, S., Pan, X., Ran, F.A., Yan, W.X., et al. (2016). In vivo genome editing improves muscle function in a mouse model of Duchenne muscular dystrophy. Science (80-.). *351*, 403–407.

Norwood, F.L., Sutherland-Smith, A.J., Keep, N.H., and Kendrick-Jones, J. (2000). The structure of the N-terminal actin-binding domain of human dystrophin and how mutations in this domain may cause Duchenne or Becker muscular dystrophy. Structure *8*, 481–491.

Nowak, K.J., Ravenscroft, G., Jackaman, C., Filipovska, A., Davies, S.M., Lim, E.M., Squire, S.E., Potter, A.C., Baker, E., Clément, S., et al. (2009a). Rescue of

skeletal muscle α-actin-null mice by cardiac (fetal) α-actin. J. Cell Biol. *185*, 903–915.

Nowak, S.J., Nahirney, P.C., Hadjantonakis, A.-K., and Baylies, M.K. (2009b). Nap1-mediated actin remodeling is essential for mammalian myoblast fusion. J. Cell Sci. *122*, 3282–3293.

Nudel, U., Zuk, D., Einat, P., Zeelon, E., Levy, Z., Neuman, S., and Yaffe, D. (1989). Duchenne muscular dystrophy gene product is not identical in muscle and brain. Nature *337*, 76–78.

Ohlendieck, K., and Campbell, K.P. (1991). Dystrophin-associated proteins are greatly reduced in skeletal muscle from mdx mice. J. Cell Biol. *115*, 1685–1694.

Oliva Chávez, A.S., Fairman, J.W., Felsheim, R.F., Nelson, C.M., Herron, M.J., Higgins, L.A., Burkhardt, N.Y., Oliver, J.D., Markowski, T.W., Kurtti, T.J., et al. (2015). An O-Methyltransferase Is Required for Infection of Tick Cells by Anaplasma phagocytophilum. PLoS Pathog. *11*, 1–40.

Otey, C.A., Kalnoski, M.H., and Bulinski, J.C. (1988). Immunolocalization of muscle and nonmuscle isoforms of actin in myogenic cells and adult skeletal muscle. Cell Motil. Cytoskeleton *9*, 337–348.

Ozawa, E., Mizuno, Y., Hagiwara, Y., Sasaoka, T., and Yoshida, M. (2005). Molecular and cell biology of the sarcoglycan complex. Muscle Nerve *32*, 563–576.

Pal, R., Palmieri, M., Loehr, J.A., Li, S., Abo-Zahrah, R., Monroe, T.O., Thakur, P.B., Sardiello, M., and Rodney, G.G. (2014). Src-dependent impairment of autophagy by oxidative stress in a mouse model of Duchenne muscular dystrophy. Nat. Commun. *5*, 4425.

Palmer, E., Wilhelm, J.M., and Sherman, F. (1979). Phenotypic suppression of nonsense mutants in yeast by aminoglycoside antibiotics. Nature *277*, 148–150.

Papponen, H., Kaisto, T., Leinonen, S., Kaakinen, M., and Metsikkö, K. (2009). Evidence for γ-actin as a Z disc component in skeletal myofibers. Exp. Cell Res. *315*, 218–225.

Partridge, T.A. (2013). The mdx mouse model as a surrogate for Duchenne muscular dystrophy. FEBS J. *280*, 4177–4186.

Pascual, J., Pfuhl, M., Walther, D., Saraste, M., and Nilges, M. (1997). Solution structure of the spectrin repeat: a left-handed antiparallel triple-helical coiled-coil

1 1Edited by P. E. Wright. J. Mol. Biol. *273*, 740–751.

Pastoret, C., and Sebille, A. (1995). mdx mice show progressive weakness and muscle deterioration with age. J. Neurol. Sci. *129*, 97–105.

Patrinostro, X., O'Rourke, A.R., Chamberlain, C.M., Moriarity, B.S., Perrin, B.J., and Ervasti, J.M. (2017). Relative importance of β cyto - and γ cyto -actin in primary mouse embryonic fibroblasts. Mol. Biol. Cell *28*, 771–782.

Peckham, M. (2008). Engineering a multi-nucleated myotube, the role of the actin cytoskeleton. J. Microsc. *231*, 486–493.

Percy, M.E., Chang, L.S., Murphy, E.G., Oss, I., Verellen-Dumoulin, C., and Thompson, M.W. (1979). Serum creatine kinase and pyruvate kinase in duchenne muscular dystrophy carrier detection. Muscle Nerve *2*, 329–339.

Perrin, B.J., and Ervasti, J.M. (2010). The actin gene family: function follows isoform. Cytoskeleton (Hoboken). *67*, 630–634.

Perrin, B.J., Strandjord, D.M., Narayanan, P., Henderson, D.M., Johnson, K.R., and Ervasti, J.M. (2013). Actin and Fascin-2 Cooperate to Maintain Stereocilia Length. J. Neurosci. *33*, 8114–8121.

Petrof, B.J., Shrager, J.B., Stedman, H.H., Kelly, A.M., and Sweeney, H.L. (1993). Dystrophin protects the sarcolemma from stresses developed during muscle contraction. Proc. Natl. Acad. Sci. U. S. A. *90*, 3710–3714.

Pillers, D.-A.M., Bulman, D.E., Weleber, R.G., Sigesmund, D.A., Musarella, M.A., Powell, B.R., Murphey, W.H., Westall, C., Panton, C., Becker, L.E., et al. (1993). Dystrophin expression in the human retina is required for normal function as defined by electroretinography. Nat. Genet. *4*, 82–86.

Pollard, T.D., and Borisy, G.G. (2003). Cellular motility driven by assembly and disassembly of actin filaments. Cell *112*, 453–465.

Pollard, T.D., and Cooper, J.A. (2009). Actin, a Central Player in Cell Shape and Movement. Science (80-.). *326*, 1208–1212.

Pollard, T.D., Blanchoin, L., and Mullins, R.D. (2000). Molecular Mechanisms Controlling Actin Filament Dynamics in Nonmuscle Cells. Annu. Rev. Biophys. Biomol. Struct. *29*, 545–576.

Ponting, C.P., Blake, D.J., Davies, K.E., Kendrick-Jones, J., and Winder, S.J. (1996). ZZ and TAZ: new putative zinc fingers in dystrophin and other proteins.

Trends Biochem. Sci. *21*, 11–13.

Porter, G.A., Dmytrenko, G.M., Winkelmann, J.C., and Bloch, R.J. (1992). Dystrophin colocalizes with beta-spectrin in distinct subsarcolemmal domains in mammalian skeletal muscle. J. Cell Biol. *117*, 997–1005.

Powers, S., and Jackson, M. (2008a). Exercise-induced oxidative stress: cellular mechanisms and impact on muscle force production. Physiol. Rev. *88*, 1243–1276.

Powers, S.K.S., and Jackson, M.M.J. (2008b). Exercise-Induced Oxidative Stress : Cellular Mechanisms and Impact on Muscle Force Production. Physiol. Rev. *88*, 1243–1276.

Powers, S.K., Ji, L.L., Kavazis, A.N., and Jackson, M.J. (2011). Reactive oxygen species: impact on skeletal muscle. Compr. Physiol. *1*, 941–969.

Pratt, S.J.P., Shah, S.B., Ward, C.W., Inacio, M.P., Stains, J.P., and Lovering, R.M. (2013). Effects of *in vivo* injury on the neuromuscular junction in healthy and dystrophic muscles. J. Physiol. *591*, 559–570.

Prins, K.W., Lowe, D.A., and Ervasti, J.M. (2008). Skeletal muscle-specific ablation of gamma(cyto)-actin does not exacerbate the mdx phenotype. PLoS One *3*, e2419.

Prins, K.W., Call, J. a, Lowe, D. a, and Ervasti, J.M. (2011). Quadriceps myopathy caused by skeletal muscle-specific ablation of β(cyto)-actin. J. Cell Sci. *124*, 951–957.

Rahimov, F., and Kunkel, L.M. (2013). The cell biology of disease: cellular and molecular mechanisms underlying muscular dystrophy. J. Cell Biol. *201*, 499–510.

Rall, S., and Grimm, T. (2012). Survival in Duchenne muscular dystrophy. Acta Myol. *31*, 117–120.

Rayment, I., Holden, H.M., Whittaker, M., Yohn, C.B., Lorenz, M., Holmes, K.C., and Milligan, R.A. (1993). Structure of the actin-myosin complex and its implications for muscle contraction. Science. *261*, 58–65.

Rebolledo, D.L., Kim, M.J., Whitehead, N.P., Adams, M.E., and Froehner, S.C. (2016). Sarcolemmal targeting of nNOSμ improves contractile function of mdx muscle. Hum. Mol. Genet. *25*, 158–166.

Reinig, A.M., Mirzaei, S., and Berlau, D.J. (2017). Advances in the Treatment of Duchenne Muscular Dystrophy: New and Emerging Pharmacotherapies. Pharmacother. J. Hum. Pharmacol. Drug Ther. *37*, 492–499.

Rhee, S.G. (2016). Overview on Peroxiredoxin. Mol. Cells *39*, 1–5.

Rhee, S.G., Kang, S.W., Jeong, W., Chang, T.S., Yang, K.S., and Woo, H.A. (2005). Intracellular messenger function of hydrogen peroxide and its regulation by peroxiredoxins. Curr. Opin. Cell Biol. *17*, 183–189.

Rhee, S.G., Jeong, W., Chang, T.-S., and Woo, H. a (2007). Sulfiredoxin, the cysteine sulfinic acid reductase specific to 2-Cys peroxiredoxin: its discovery, mechanism of action, and biological significance. Kidney Int. Suppl. S3-8.

Ricotti, V., Ridout, D.A., Scott, E., Quinlivan, R., Robb, S.A., Manzur, A.Y., Muntoni, F., Manzur, A., Muntoni, F., Robb, S., et al. (2013). Long-term benefits and adverse effects of intermittent versus daily glucocorticoids in boys with Duchenne muscular dystrophy. J. Neurol. Neurosurg. Psychiatry *84*, 698–705.

Ricotti, V., Spinty, S., Roper, H., Hughes, I., Tejura, B., Robinson, N., Layton, G., Davies, K., Muntoni, F., and Tinsley, J. (2016). Safety, Tolerability, and Pharmacokinetics of SMT C1100, a 2-Arylbenzoxazole Utrophin Modulator, following Single- and Multiple-Dose Administration to Pediatric Patients with Duchenne Muscular Dystrophy. PLoS One *11*, e0152840.

Rodrigues, M., Echigoya, Y., Maruyama, R., Lim, K.R.Q., Fukada, S., and Yokota, T. (2016). Impaired regenerative capacity and lower revertant fibre expansion in dystrophin-deficient mdx muscles on DBA/2 background. Sci. Rep. *6*, 38371.

Roy, P., Rau, F., Ochala, J., Messéant, J., Fraysse, B., Lainé, J., Agbulut, O., Butler-Browne, G., Furling, D., and Ferry, A. (2016). Dystrophin restoration therapy improves both the reduced excitability and the force drop induced by lengthening contractions in dystrophic mdx skeletal muscle. Skelet. Muscle *6*, 1–17.

Rubenstein, P.A. (1990). The functional importance of multiple actin isoforms. BioEssays *12*, 309–315.

Rybakova, I.N., Amann, K.J., and Ervasti, J.M. (1996). A new model for the interaction of dystrophin with F-actin. J. Cell Biol. *135*, 661–672.

Rybakova, I.N., Patel, J.R., and Ervasti, J.M. (2000). The Dystrophin Complex Forms a Mechanically Strong Link between the Sarcolemma and Costameric

Actin. J. Cell Biol. *150*, 1209–1214.

Rybakova, I.N., Patel, J.R., Davies, K.E., Yurchenco, P.D., and Ervasti, J.M. (2002). Utrophin Binds Laterally along Actin Filaments and Can Couple Costameric Actin with Sarcolemma When Overexpressed in Dystrophin-deficient Muscle. Mol. Biol. Cell *13*, 1512–1521.

Schwartz, R.J., and Rothblum, K.N. (1981). Gene switching in myogenesis: differential expression of the chicken actin multigene family. Biochemistry *20*, 4122–4129.

Selden, L.A., Estes, J.E., and Gershman, L.C. (1983). The tightly bound divalent cation regulates actin polymerization. Biochem. Biophys. Res. Commun. *116*, 478–485.

Selsby, J.T. (2011). Increased catalase expression improves muscle function in *mdx* mice. Exp. Physiol. *96*, 194–202.

Sethuraman, M., McComb, M.E., Huang, H., Huang, S., Heibeck, T., Costello, C.E., and Cohen, R.A. (2004). Isotope-Coded Affinity Tag (ICAT) Approach to Redox Proteomics: Identification and Quantitation of Oxidant-Sensitive Cysteine Thiols in Complex Protein Mixtures. J. Proteome Res. *3*, 1228–1233.

Shkryl, V.M., Martins, A.S., Ullrich, N.D., Nowycky, M.C., Niggli, E., and Shirokova, N. (2009). Reciprocal amplification of ROS and Ca2+ signals in stressed mdx dystrophic skeletal muscle fibers. Pflugers Arch. Eur. J. Physiol. *458*, 915–928.

Sicinski, P., Geng, Y., Ryder-Cook, A.S., Barnard, E.A., Darlison, M.G., and Barnard, P.J. (1989). The molecular basis of muscular dystrophy in the mdx mouse: a point mutation. Science *244*, 1578–1580.

Sobotta, M.C., Liou, W., Stöcker, S., Talwar, D., Oehler, M., Ruppert, T., Scharf, A.N.D., and Dick, T.P. (2015). Peroxiredoxin-2 and STAT3 form a redox relay for H2O2 signaling. Nat. Chem. Biol. *11*, 64–70.

Song, M.Y., Makino, A., and Yuan, J.X.J. (2011). Role of Reactive Oxygen Species and Redox in Regulating the Function of Transient Receptor Potential Channels. Antioxid. Redox Signal. *15*, 1549–1565.

Sonnemann, K.J., Fitzsimons, D.P., Patel, J.R., Liu, Y., Schneider, M.F.F., Moss, R.L., and Ervasti, J.M.M. (2006). Cytoplasmic γ-Actin Is Not Required for Skeletal Muscle Development but Its Absence Leads to a Progressive Myopathy. Dev. Cell *11*, 387–397.

Sonnemann, K.J., Heun-Johnson, H., Turner, A.J., Baltgalvis, K.A., Lowe, D.A., and Ervasti, J.M. (2009). Functional Substitution by TAT-Utrophin in Dystrophin-Deficient Mice. PLoS Med. *6*, e1000083.

Straub, V., Bittner, R.E., Léger, J.J., and Voit, T. (1992). Direct visualization of the dystrophin network on skeletal muscle fiber membrane. J. Cell Biol. *119*, 1183–1191.

Sudo, M., and Kano, Y. (2009). Myofiber apoptosis occurs in the inflammation and regeneration phase following eccentric contractions in rats. J. Physiol. Sci. *59*, 405–412.

Suzuki, A., Yoshida, M., Yamamoto, H., and Ozawa, E. (1992). Glycoprotein-binding site of dystrophin is confined to the cysteine-rich domain and the first half of the carboxy-terminal domain. FEBS Lett. *308*, 154–160.

Tabebordbar, M., Zhu, K., Cheng, J.K.W., Chew, W.L., Widrick, J.J., Yan, W.X., Maesner, C., Wu, E.Y., Xiao, R., Ran, F.A., et al. (2016). In vivo gene editing in dystrophic mouse muscle and muscle stem cells. Science (80-.). *351*, 407–411.

Tamura, M., Kai, T., Tsunawaki, S., Lambeth, J.D., and Kameda, K. (2000). Direct interaction of actin with p47(phox) of neutrophil NADPH oxidase. Biochem. Biophys. Res. Commun. *276*, 1186–1190.

Tamura, M., Itoh, K., Akita, H., Takano, K., and Oku, S. (2006). Identification of an actin-binding site in p47phox an organizer protein of NADPH oxidase. FEBS Lett. *580*, 261–267.

Tanabe, Y., Esaki, K., and Nomura, T. (1986). Skeletal muscle pathology in X chromosome-linked muscular dystrophy (mdx) mouse. Acta Neuropathol. *69*, 91–95.

Tang, W.H., Shilov, I. V., and Seymour, S.L. (2008). Nonlinear fitting method for determining local false discovery rates from decoy database searches. J. Proteome Res. *7*, 3661–3667.

Tinsley, J., Deconinck, N., Fisher, R., Kahn, D., Phelps, S., Gillis, J.-M., and Davies, K. (1998). Expression of full-length utrophin prevents muscular dystrophy in mdx mice. Nat. Med. *4*, 1441–1444.

Tinsley, J.M., Blake, D.J., Roche, A., Fairbrother, U., Riss, J., Byth, B.C., Knight, A.E., Kendrick-Jones, J., Suthers, G.K., Love, D.R., et al. (1992). Primary structure of dystrophin-related protein. Nature *360*, 591–593.

Tinsley, J.M., Potter, A.C., Phelps, S.R., Fisher, R., Trickett, J.I., and Davies, K.E. (1996). Amelioration of the dystrophic phenotype of mdx mice using a truncated utrophin transgene. Nature *384*, 349–353.

Tinsley, J.M., Fairclough, R.J., Storer, R., Wilkes, F.J., Potter, A.C., Squire, S.E., Powell, D.S., Cozzoli, A., Capogrosso, R.F., Lambert, A., et al. (2011). Daily Treatment with SMTC1100, a Novel Small Molecule Utrophin Upregulator, Dramatically Reduces the Dystrophic Symptoms in the mdx Mouse. PLoS One *6*, e19189.

Tondeleir, D., Lambrechts, A., Müller, M., Jonckheere, V., Doll, T., Vandamme, D., Bakkali, K., Waterschoot, D., Lemaistre, M., Debeir, O., et al. (2012). Cells lacking β-actin are genetically reprogrammed and maintain conditional migratory capacity. Mol. Cell. Proteomics *11*, 255–271.

Touyz, R.M., Yao, G., Quinn, M.T., Pagano, P.J., and Schiffrin, E.L. (2005). p47phox associates with the cytoskeleton through cortactin in human vascular smooth muscle cells role in NAD(P)H oxidase regulation by angiotensin II. Arterioscler. Thromb. Vasc. Biol. *25*, 512–518.

Valentine, B.A., Cooper, B.J., Cummings, J.F., and deLahunta, A. (1986). Progressive muscular dystrophy in a golden retriever dog: light microscope and ultrastructural features at 4 and 8 months. Acta Neuropathol. *71*, 301–310.

Verma, S., Anziska, Y., and Cracco, J. (2010). Review of Duchenne Muscular Dystrophy (DMD) for the Pediatricians in the Community. Clin. Pediatr. (Phila). *49*, 1011–1017.

Wang, B., Li, J., and Xiao, X. (2000). Adeno-associated virus vector carrying human minidystrophin genes effectively ameliorates muscular dystrophy in mdx mouse model. Proc. Natl. Acad. Sci. U. S. A. *97*, 13714–13719.

Wang, Z., Kuhr, C.S., Allen, J.M., Blankinship, M., Gregorevic, P., Chamberlain, J.S., Tapscott, S.J., and Storb, R. (2007). Sustained AAV-mediated Dystrophin Expression in a Canine Model of Duchenne Muscular Dystrophy with a Brief Course of Immunosuppression. Mol. Ther. *15*, 1160–1166.

Ward, C.W., Prosser, B.L., and Lederer, W.J. (2014). Mechanical Stretch-Induced Activation of ROS/RNS Signaling in Striated Muscle. Antioxid. Redox Signal. *20*, 929–936.

Watchko, J., O'Day, T., Wang, B., Zhou, L., Tang, Y., Li, J., and Xiao, X. (2002). Adeno-Associated Virus Vector-Mediated Minidystrophin Gene Therapy Improves Dystrophic Muscle Contractile Function in *mdx* Mice. Hum. Gene Ther.

13, 1451–1460.

Whitehead, N.P., Pham, C., Gervasio, O.L., and Allen, D.G. (2008). N-Acetylcysteine ameliorates skeletal muscle pathophysiology in mdx mice. J. Physiol. *586*, 2003–2014.

Whitehead, N.P., Yeung, E.W., Froehner, S.C., and Allen, D.G. (2010). Skeletal muscle NADPH oxidase is increased and triggers stretch-induced damage in the mdx mouse. PLoS One *5*, e15354.

Wiese, S., Reidegeld, K.A., Meyer, H.E., and Warscheid, B. (2007). Protein labeling by iTRAQ: A new tool for quantitative mass spectrometry in proteome research. Proteomics *7*, 340–350.

Willmann, R., De Luca, A., Benatar, M., Grounds, M., Dubach, J., Raymackers, J.M., and Nagaraju, K. (2012). Enhancing translation: Guidelines for standard pre-clinical experiments in mdx mice. Neuromuscul. Disord. *22*, 43–49.

Woledge, R.C., Curtin, N.A., and Homsher, E. (1985). Energetic aspects of muscle contraction. Monogr. Physiol. Soc. *41*, 1–357.

Woo, H.A., Kang, S.W., Kim, H.K., Yang, K.S., Chae, H.Z., and Rhee, S.G. (2003). Reversible oxidation of the active site cysteine of peroxiredoxins to cysteine sulfinic acid. Immunoblot detection with antibodies specific for the hyperoxidized cysteine-containing sequence. J. Biol. Chem. *278*, 47361–47364.

Xu, L., Park, K.H., Zhao, L., Xu, J., El Refaey, M., Gao, Y., Zhu, H., Ma, J., and Han, R. (2016). CRISPR-mediated Genome Editing Restores Dystrophin Expression and Function in mdx Mice. Mol. Ther. *24*, 564–569.

Yeung, E.W., Whitehead, N.P., Suchyna, T.M., Gottlieb, P.A., Sachs, F., and Allen, D.G. (2005). Effects of stretch-activated channel blockers on [Ca2+]i and muscle damage in the mdx mouse. J. Physiol. *562*, 367–380.

Yin, H., Moulton, H.M., Betts, C., Seow, Y., Boutilier, J., Iverson, P.L., and Wood, M.J.A. (2009). A fusion peptide directs enhanced systemic dystrophin exon skipping and functional restoration in dystrophin-deficient mdx mice. Hum. Mol. Genet. *18*, 4405–4414.

Young, C.S., Hicks, M.R., Ermolova, N.V., Nakano, H., Jan, M., Younesi, S., Karumbayaram, S., Kumagai-Cresse, C., Wang, D., Zack, J.A., et al. (2016). A Single CRISPR-Cas9 Deletion Strategy that Targets the Majority of DMD Patients Restores Dystrophin Function in hiPSC-Derived Muscle Cells. Cell Stem Cell *18*, 533–540.

Zanou, N., Iwata, Y., Schakman, O., Lebacq, J., Wakabayashi, S., and Gailly, P. (2009). Essential role of TRPV2 ion channel in the sensitivity of dystrophic muscle to eccentric contractions. FEBS Lett. *583*, 3600–3604.

Zhu, H., Santo, A., and Li, Y. (2012). The antioxidant enzyme peroxiredoxin and its protective role in neurological disorders. Exp. Biol. Med. (Maywood). *237*, 143–149.

Zubrzycka-Gaarn, E.E., Bulman, D.E., Karpati, G., Burghes, A.H.M., Belfall, B., Klamut, H.J., Talbot, J., Hodges, R.S., Ray, P.N., and Worton, R.G. (1988). The Duchenne muscular dystrophy gene product is localized in sarcolemma of human skeletal muscle. Nature *333*, 466–469.